NAVAL POSTGRADUATE SCHOOL
MONTEREY, CALIFORNIA

THESIS

THE REMOTE IMPACTS OF A WESTERN PACIFIC TROPICAL CYCLONE

by

CRAIG E. JAKUS

September, 1995

Thesis Advisor: Tom Murphree

Approved for public release; distribution is unlimited.

DISCLAIMER NOTICE

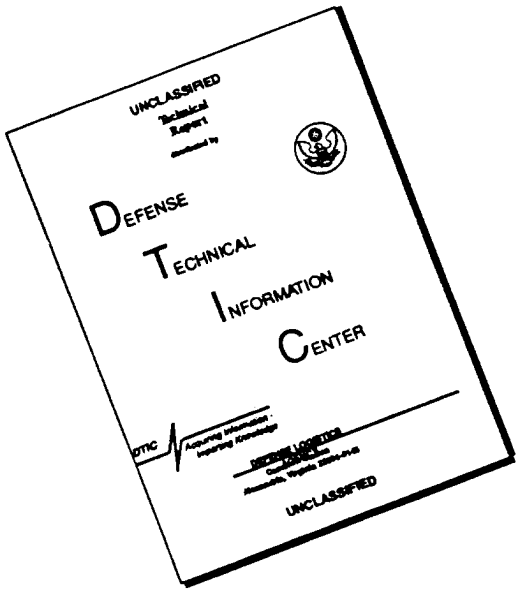

THIS DOCUMENT IS BEST QUALITY AVAILABLE. THE COPY FURNISHED TO DTIC CONTAINED A SIGNIFICANT NUMBER OF PAGES WHICH DO NOT REPRODUCE LEGIBLY.

DISCLAIMER NOTICE

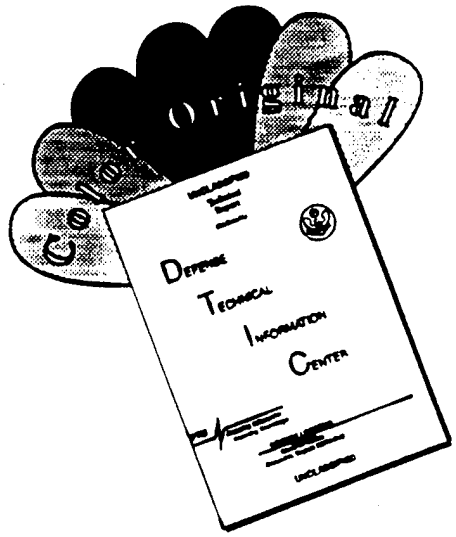

THIS DOCUMENT IS BEST QUALITY AVAILABLE. THE COPY FURNISHED TO DTIC CONTAINED A SIGNIFICANT NUMBER OF COLOR PAGES WHICH DO NOT REPRODUCE LEGIBLY ON BLACK AND WHITE MICROFICHE.

REPORT DOCUMENTATION PAGE

Form Approved OMB No. 0704-0188

1. AGENCY USE ONLY *(Leave blank)*	2. REPORT DATE	3. REPORT TYPE AND DATES COVERED
	September 1995	Master's Thesis

4. TITLE AND SUBTITLE *THE REMOTE IMPACTS OF A WESTERN PACIFIC TROPICAL CYCLONE

5. FUNDING NUMBERS

6. AUTHOR(S) Craig E. Jakus

7. PERFORMING ORGANIZATION NAME(S) AND ADDRESS(ES)
Naval Postgraduate School Monterey CA 93943-5000

8. PERFORMING ORGANIZATION REPORT NUMBER

9. SPONSORING/MONITORING AGENCY NAME(S) AND ADDRESS(ES)

10. SPONSORING/MONITORING AGENCY REPORT NUMBER

11. SUPPLEMENTARY NOTES The views expressed in this thesis are those of the author and do not reflect the official policy or position of the Department of Defense or the U.S. Government.

12a. DISTRIBUTION/AVAILABILITY STATEMENT
Approved for public release; distribution is unlimited.

12b. DISTRIBUTION CODE

13. ABSTRACT *(maximum 200 words)*

The short term teleconnections arising from an individual tropical cyclone in the western Pacific (typhoon Seth, October 1994) were examined using an operational global data assimilation system and numerical weather prediction model. During the data assimilation, the model's initial conditions were modified using a tropical cyclone bogusing procedure that either maintained or eliminated the individual storm. These different initial conditions were used in six extended-range forecasts of about 3.5 weeks duration. Three of these forecasts simulated the atmosphere with the tropical cyclone and three without the storm. The ensemble average differences between the forecasts with the storm and those without it were used to infer the global teleconnection response to the tropical cyclone.

This response was dominated by a strong and persistent Rossby wave train that extended from east Asia across the North Pacific into North America. This wave train was initiated when an anticyclonic circulation formed near Japan as the tropical cyclone approached the east Asian jet. The anticyclone formation was primarily the result of two factors: (1) vortex stretching; and (2) absolute vorticity advection as divergent outflow from the tropical cyclone crossed the large absolute vorticity gradient of the east Asian jet.

The wave response was quasi-stationary. However, the basic wave train (i.e., the teleconnection pattern) developed within a week due to a relatively rapid eastward propagation of wave energy across the North Pacific and North America. In regions of strong jet flow, this propagation tended to parallel the flow while in regions of weaker flow, the propagation had stronger poleward or equatorward components. The wave train intensified well after the tropical cyclone and the initial wave formation process had dissipated. This growth appeared to be greater near areas of potential barotropic instability along the east Asian - North Pacific jet. The model atmosphere *with* the tropical cyclone showed a midlatitude jet and storm track that were markedly different from the jet and storm track seen in the model atmosphere *without* the tropical cyclone.

14. SUBJECT TERMS Teleconnections; Tropical Cyclones; Tropical Cyclone Bogusing; Jet Stream; Extended-Range Forecasting; Rossby Wave Train

15. NUMBER OF PAGES 136

16. PRICE CODE

17. SECURITY CLASSIFICATION OF REPORT	18. SECURITY CLASSIFICATION OF THIS PAGE	19. SECURITY CLASSIFICATION OF ABSTRACT	20. LIMITATION OF ABSTRACT
Unclassified	Unclassified	Unclassified	UL

NSN 7540-01-280-5500

Standard Form 298 (Rev. 2-89)
Prescribed by ANSI Std. 239-18

Approved for public release; distribution is unlimited

THE REMOTE IMPACTS OF A

WESTERN PACIFIC TROPICAL CYCLONE

Craig E. Jakus
Lieutenant Commander, United States Navy
B.S., Texas A & M University, 1984

Submitted in partial fulfillment

of the requirements for the degree of

MASTERS OF SCIENCE IN METEOROLOGY AND PHYSICAL OCEANOGRAPHY

from the

NAVAL POSTGRADUATE SCHOOL

September 1995

Author: 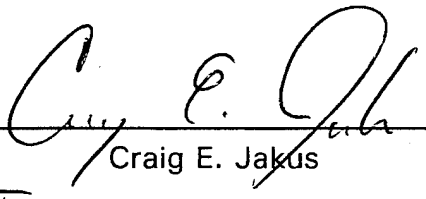

Craig E. Jakus

Approved by: 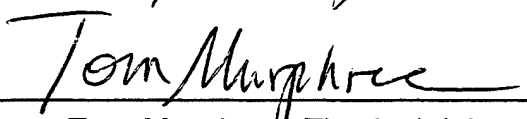

Tom Murphree, Thesis Advisor

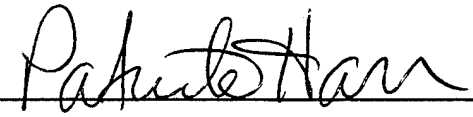

Patrick Harr, Second Reader

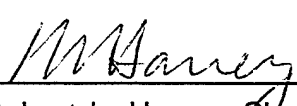

Robert L. Haney, Chairman
Department of Meteorology

ABSTRACT

The short term teleconnections arising from an individual tropical cyclone in the western Pacific (typhoon Seth, October 1994) were examined using an operational global data assimilation system and numerical weather prediction model. During the data assimilation, the model's initial conditions were modified using a tropical cyclone bogusing procedure that either maintained or eliminated the individual storm. These different initial conditions were used in six extended-range forecasts of about 3.5 weeks duration. Three of these forecasts simulated the atmosphere with the tropical cyclone and three without the storm. The ensemble average differences between the forecasts with the storm and those without it were used to infer the global teleconnection response to the tropical cyclone.

This response was dominated by a strong and persistent Rossby wave train that extended from east Asia across the North Pacific into North America. This wave train was initiated when an anticyclonic circulation formed near Japan as the tropical cyclone approached the east Asian jet. The anticyclone formation was primarily the result of two factors: (1) vortex stretching; and (2) absolute vorticity advection as divergent outflow from the tropical cyclone crossed the large absolute vorticity gradient of the east Asian jet.

The wave response was quasi-stationary. However, the basic wave

train (i.e., the teleconnection pattern) developed within a week due to a relatively rapid eastward propagation of wave energy across the North Pacific and North America. In regions of strong jet flow, this propagation tended to parallel the flow while in regions of weaker flow, the propagation had stronger poleward or equatorward components. The wave train intensified well after the tropical cyclone and the initial wave formation process had dissipated. This growth appeared to be greater near areas of potential barotropic instability along the east Asian - North Pacific jet. The model atmosphere *with* the tropical cyclone showed a midlatitude jet and storm track that were markedly different from the jet and storm track seen in the model atmosphere *without* the tropical cyclone.

The views expressed in this thesis are those of the author and do not reflect the official policy or position of the Department of Defense or the U.S. Government.

TABLE OF CONTENTS

LIST OF ACRONYMS AND SYMBOLS

ADVDIV	advection of absolute vorticity by the divergent part of the wind
ADVROT	advection of absolute vorticity by the rotational part of the wind
β	total derivative of the Coriolis parameter, $\frac{df}{dy}$
BTI	barotropic instability
EA	ensemble average
F1	Forecast 1: 26 day NOGAPS model run started from 12Z, 06 October 1994 initial conditions for typhoon Seth
F2	Forecast 2: 25 day NOGAPS model run started from 00Z, 08 October 1994 initial conditions for typhoon Seth
F3	Forecast 3: 23 day NOGAPS model run started from 12Z, 09 October 1994 initial conditions for typhoon Seth
FNMOC	Fleet Numerical Meteorology and Oceanography Center
gpm	geopotential meter
H1/2/3/4	first/second/third/forth major positive 200 mb height response to Seth
IDEA Lab	Interactive Digital Environmental Analysis Laboratory
JTWC	Joint Typhoon Warning Center
L1/2/3	first/second/third major negative 200 mb height response to Seth
m	meter
mb	millibar

NEGATIVE	synthetic tropical cyclone data assimilation (bogusing) procedure applied to the NOGAPS initial conditions that has the affect of removing the storm from the model's initial conditions
NOGAPS	Navy Operational Global Atmospheric Prediction System
NPNA	North Pacific-North America
NRL	Naval Research Laboratory
POSITIVE	the standard synthetic tropical cyclone data assimilation (bogusing) procedure applied to the NOGAPS initial conditions that has the affect of improving the atmospheric circulation around the cyclone in the model's initial conditions
Q_L	atmospheric Latent Heating
Q_S	atmospheric Sensible Heating
QG	quasi-geostrophic
S	Rossby wave source
s	second
SLP	sea level pressure
T79	triangular 79 wave truncation
T159	triangular 159 wave truncation
u_χ	zonal component of the divergent wind
u_ψ	zonal component of the rotational wind
V_{1000}	1000 mb horizontal wind vector
V_{200}	200 mb horizontal wind vector

V_χ	divergent horizontal wind vector
V_ψ	rotational horizontal wind vector
v_χ	meridional component of the divergent wind
v_ψ	meridional component of the rotational wind
χ_{200}	200 mb velocity potential
ψ_{200}	200 mb stream function
ζ_{200}	200 mb relative vorticity
Φ_{1000}	1000 mb geopotential height
Φ_{200}	200 mb geopotential height
Z	Zulu time (Greenwich Mean Time)

ACKNOWLEDGEMENTS

I thank Professor Tom Murphree for his many hours answering questions, providing historical reference, and pointing the direction to go. I also thank Dr. Jim Goerss, Naval Research Laboratory Monterey, for providing the assimilated data, the model runs, and the computer code to read it, and Pat Harr for highlighting areas needing further analysis. I also deeply appreciate the computer expertise provided by Mike Cook, NPS Oceanography Department. His MATLAB knowledge and numerous locally produced computer programs saved me countless hours of programming. Lastly, I thank my wife, Anne, for her patience during the year it took to complete this project.

I. INTRODUCTION

A. MOTIVATION FOR THIS STUDY

Numerical weather prediction models are relatively skillful in the short-range (less than about five days). But the skill of these models diminishes rapidly when they are used for medium-range (five to ten days) or long-range (greater than ten days) forecasts. Midlatitude weather systems, such as cold fronts, are embedded in and steered by large-scale quasistationary systems (Carlson 1991). These large, slowly evolving background systems may be significantly affected by remote tropical processes, such as tropical cyclones (Chang and Lum 1985) and El Nino events (Tribbia 1991). Thus, accurate medium-range and extended-range midlatitude forecasts depend, in part, on accurate forecasting of tropical events and of the interaction of these events with the midlatitudes.

The impacts of a disturbance in one part of the atmosphere on another distant part of the atmosphere are described by the term *teleconnections* (Wallace and Gutzler 1981). Teleconnections have become a central concept in the scientific search for an improved understanding of long distance linkages between weather and climate anomalies (Glantz, et al. 1991). The purpose of this study is to explore how individual tropical cyclones in the western Pacific may generate short term (one to three week) teleconnections. This study continues the work of Woll (1993) and Springer

(1994).

B. TELECONNECTIONS

1. Interannual teleconnections

Large-scale, low-frequency weather phenomena were first described by Sir Gilbert Walker. He observed correlations between the interannual fluctuations in sea-level pressure, surface air temperature, and precipitation in Darwin, Australia and Tahiti (Trenberth 1991).

Bjerknes (1966) showed that weak or non-existent equatorial easterly winds over the eastern and central Pacific in late 1957 and early 1958 brought about a brief cessation of equatorial upwelling. This caused above-normal sea surface temperatures in the tropical Pacific from the American coast westward to the dateline. This anomalous heat source for the atmosphere intensified the Hadley circulation, especially in the wintertime (northern) hemisphere.

Bjerknes (1972) showed that during periods of reduced upwelling, between 1962 and 1967, in the equatorial eastern Pacific, a feedback from the unusually warm ocean led to a reduction in atmospheric stability and an increase in precipitation. He noted that a side effect of the widespread warming of the tropical atmosphere was an increased exchange of angular momentum with the subtropics. As a result, the subtropical westerly jet strengthened from the central Pacific to the eastern Mediterranean.

2. Intraseasonal teleconnections

Kurihara and Tsuyuki (1987) found several occasions of intensified convection near the northern Philippines that were followed by eastward propagation, at about 10-12 m/s, of middle- and upper-tropospheric geopotential height anomalies across the North Pacific to North America. Using a linear barotropic vorticity model, they simulated these height anomalies as a barotropic Rossby wave train excited by tropical western Pacific forcing.

Nitta (1987) correlated 5-day mean tropical cloud amounts and 500 mb geopotential heights during the northern summers of 1978-1984. He found that intense convective heating fluctuations near the Philippines that were strongly modulated by the intraseasonal variations were linked to a wavetrain-like pattern of mid-tropospheric height anomalies over the North Pacific.

3. Short term teleconnections

Chang and Lum (1985) examined cold surges and tropical cyclones during the northern hemisphere winter and the response of the midlatitude jet to variations in tropical convection. They found that the strengthening of upper-tropospheric divergence from a tropical heating source was associated with the strengthening of the nearby midlatitude westerly jet. The response of the westerly jet to the tropical forcing showed no

discernable time lag. These episodes of increases jet strength tended to be followed by a downstream propagation of the jet, which was apparently the result of self advection of the zonal wind since the tropical divergence center did not move significantly during the episodes. Chang and Lum concluded that these short-term intensifications of the midlatitude jet were more likely the result, and not the cause, of tropical-extratropical interaction. They also inferred that large-scale tropical convective events in regions outside their normal locations may cause a significant longitudinal displacement of the east Asian jet streak, and therefore the downstream weather.

Hurrell and Vincent (1990) studied the correlation between low-latitude heating and the strength of the subtropical westerly jet near Australia during January-March 1979. They found that episodes of strong divergent outflow associated with tropical convection correlated with the strengthening and eastward propagation of westerly wind maxima in the subtropical jet. The response time between the upper-level tropical outflow and subtropical westerly enhancement was about 12 hours.

Hurrell and Vincent (1990) found that these westerly enhancements were driven mainly by the Coriolis force acting on the diabatically driven meridional circulation. The largest positive tendencies due to this term were found in the entrance regions of the subtropical westerly jet. Divergent

circulations accounted for nearly all of the total ageostrophic flow and that nearly all of the divergent kinetic energy was converted to zonal kinetic energy. They concluded that transient tropical heating events enhance local meridional overturning in the atmosphere, which in turn strengthens the summer subtropical westerly jet stream.

Harr and Elsberry (1991) found that western Pacific tropical cyclones may be associated with distinct large-scale flow anomalies. Furthermore, Harr and Elsberry (1995) found that the large-scale anomalies over the tropical western Pacific that were associated with an active monsoon trough were also associated with a wave train-like pattern of anomalous cyclonic and anticyclonic circulations at the 200 mb and 700 mb levels that stretched eastward from east Asia to western North America (Figure 1). Periods during which there were few or no tropical cyclones had very different anomaly patterns (Figure 2). Their findings suggest that short term tropical disturbances, such as tropical cyclones, may have far-reaching effects on large-scale midlatitude circulations.

Springer (1994) showed that data assimilation and modeling procedures can be successfully used to produce realistic simulations of the global atmosphere with and without an individual typhoon. He showed that a typhoon may trigger an upper-tropospheric height response across the North Pacific - North American (NPNA) region that is strong and persistent,

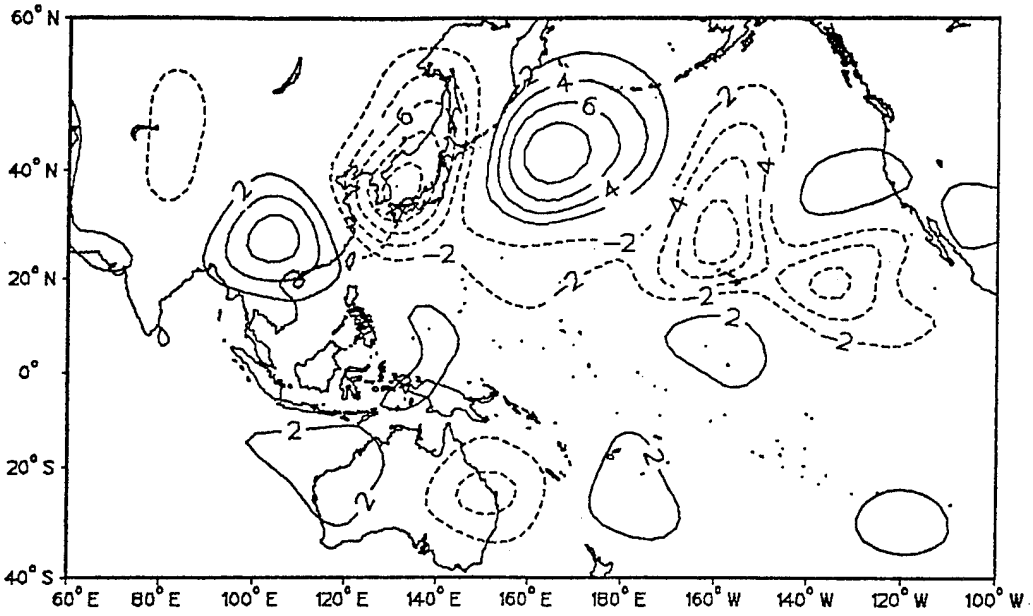

Figure 1. Composite of 200 mb streamfunction anomalies associated with an active monsoon trough and numerous recurving tropical cyclones in the western Pacific. The contour interval is 2.0 x 10^6 m^2 s^{-1}. Negative contours are dashed. (from Harr and Elsberry 1995)

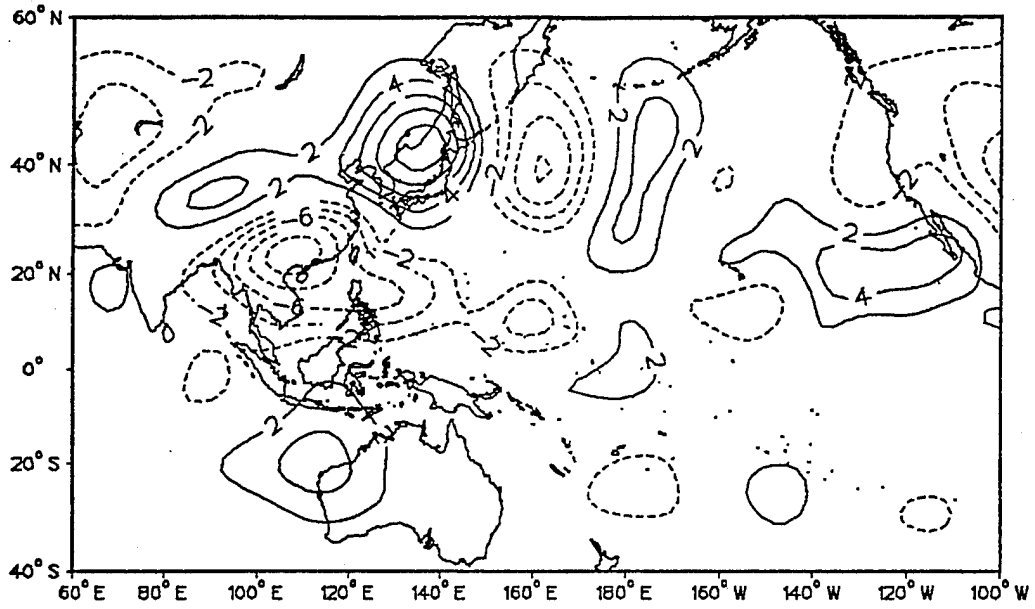

Figure 2. Composite of 200 mb streamfunction anomalies during periods associated with few or no tropical cyclones in the western Pacific. The contour interval is 2.0 x 10^6 m^2 s^{-1}. Negative contours are dashed. (from Harr and Elsberry 1995)

lasting several days to more than a week. This response showed distinct Rossby-wave train characteristics with eastward group velocities exceeding relatively slow eastward phase velocities. He found that advection of relative vorticity by the upper-level divergent wind from the typhoon was important in initiating the wave response. He also found that subsequent growth and propagation of the wave response was not directly affected by the typhoon but was influenced by the extratropical jets, which acted to guide and amplify the response.

C. DESIGN OF THIS STUDY

This study builds on the methodology and analysis used by Woll (1993) and Springer (1994) to examine the impacts of a single typhoon on the global atmosphere. Woll (1993) studied typhoon Yuri (November-December 1991) while Springer (1994) examined typhoon Robyn (August 1993). In this study, we examined the impacts of Typhoon Seth (October 1994).

In this study, we investigated three main hypotheses.

- **Hypothesis 1**: Individual tropical cyclones can produce strong teleconnections.

- **Hypothesis 2**: The development of the teleconnection is strongly influenced by the waveguiding and amplification effects of the midlatitude westerly jet.

- **Hypothesis 3**: The flux of ambient absolute vorticity associated with the divergent outflow from a tropical cyclone located near a jet may be an important mechanism for initiating a teleconnection response to the tropical cyclone.

Our basic strategy was to use a data assimilation procedure to modify the representation of an individual tropical cyclone in the initial conditions of a global operational forecast model. The model was then run for two to three weeks to simulate the global impacts of the tropical cyclone. The data assimilation process was used to:

1. retain the tropical cyclone in the model atmosphere, or
2. remove the tropical cyclone from the model atmosphere.

The methods used are described in Chapter II. The results are presented in Chapter III. Conclusions and recommendations are given in Chapter IV.

D. SUMMARY

Teleconnections play an important role in modifying weather and climate. Understanding and forecasting their far field impacts will help improve medium-range and long-range weather forecasts. This study, like those of Woll (1993) and Springer (1994), focuses on the short-term (one to two weeks) teleconnections associated with individual tropical cyclones.

II. DATA AND PROCEDURES

Our work is a continuation of the studies of Woll (1993) and Springer (1994). In particular, we used similar data assimilation and modeling procedures to conduct an additional case study of the remote effects of an individual typhoon. This chapter summarizes the data assimilation and modeling procedures. More detailed explanations of these procedures can be found in Woll's and Springer's papers.

A. TROPICAL CYCLONE SELECTION

Woll (1993) and Springer (1994) discussed several factors which affect the ability of an individual tropical cyclone to generate a strong teleconnection response. These factors led them and us to select for our studies a tropical cyclone that was:

- strong during and soon after recurvature into the extratropics,
- located within or near the extratropical westerlies, especially the midlatitude jet,
- relatively isolated from other tropical disturbances,
- accurately simulated by the forecast model.

Using these criteria, we selected for our study typhoon Seth, which occurred in the western Pacific in October 1994. Figure 3 shows the maximum sustained winds at selected positions along the Joint Typhoon Warning Center's (JTWC) best track for typhoon Seth.

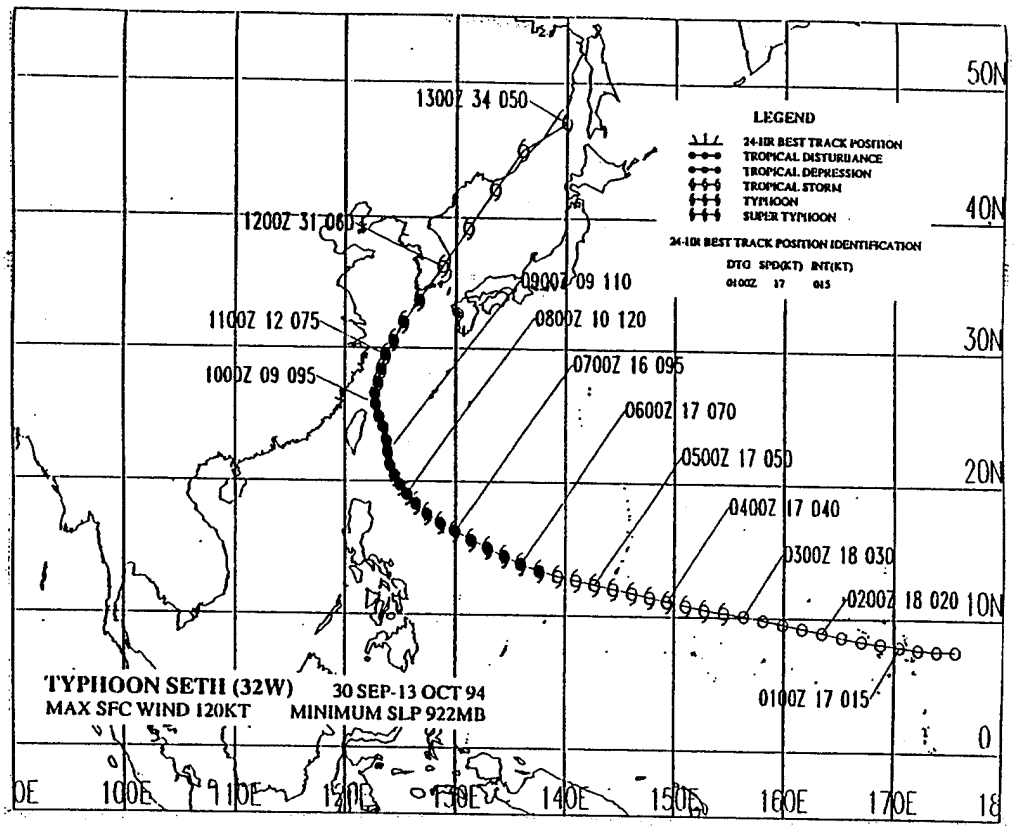

Figure 3. The JTWC best track for typhoon Seth based on Seth's positions at six-hour intervals. At selected times and locations, Seth's propagation speed and maximum sustained wind speeds (in nautical miles/hour) are shown.

B. ATMOSPHERIC MODEL DESCRIPTION

Our numerical weather prediction model was the U.S. Navy Global Atmospheric Prediction System (NOGAPS) Version 3.2. NOGAPS is a full physics spectral model that uses a triangular 79 (T79) truncation, which corresponds to a 1.5 degree latitude-longitude transform grid. It has 18 vertical levels and a time step of 30 minutes. NOGAPS uses the Arakawa-Schubert cumulus parameterization that includes the effects of downdrafts, latent heat of fusion, and evaporation of falling precipitation. The model equations are formulated in spherical coordinates and a hybrid vertical coordinate, η, is used. An in-depth description of NOGAPS is contained in Hogan and Rosmond (1991). NOGAPS Version 3.2 was, until recently, the U.S. Navy's operational model for worldwide weather prediction. The current operational model is a higher resolution (T159) version.

All of our model runs were conducted by Dr. J. Goerss at the Naval Research Laboratory (NRL) in Monterey, California using the computing facilities at the Fleet Numerical Meteorology and Oceanography Center (FNMOC) in Monterey. Postprocessing of the model output was done in the Interactive Digital Environmental Analysis (IDEA) Laboratory at the Naval Postgraduate School in Monterey.

C. MODEL OUTPUT FIELDS

A number of standard NOGAPS global output fields were analyzed in this study. These fields were provided on a 1.0 degree latitude - longitude grid, with output provided at 00Z and 12Z of each model day. The model runs lasted from 23 to 26 days. Our investigations focused on the following NOGAPS fields.

1. Sea level pressure

The sea-level pressure (SLP), in millibars (mb), provided information on the initial conditions at the start of each model run and was used to represent the model's prediction of the tropical cyclone track.

2. 1000 mb geopotential height

The 1000 mb geopotential heights (Φ_{1000}), in geopotential meters (gpm), represent the structure of the lower troposphere.

3. 1000 mb winds

The 1000 mb horizontal wind fields (V_{1000}), in m s^{-1}, were used to represent the circulation of the lower troposphere.

4. Atmospheric latent heating

The atmospheric heating (Q_L), in Watts m^{-2}, is the latent heating of the model's atmosphere, representing areas of convective systems.

5. **Atmospheric sensible heating**

The atmospheric heating (Q_S), in Watts m^{-2}, is the sensible heating of the model's atmosphere.

6. **200 mb geopotential height**

The 200 mb geopotential heights (Φ_{200}), in geopotential meters, were used to identify upper-tropospheric teleconnections and quasi-geostrophic wave dynamics.

7. **200 mb wind**

The 200 mb total horizontal wind field (V_{200}), in m s^{-1}, was used to represent the circulation of the upper troposphere.

8. **200 mb velocity potential**

The 200 mb velocity potential (χ_{200}) fields, in m^2 s^{-1}, were used to obtain the divergent wind (V_χ). The total horizontal wind is the sum of the divergent and rotational winds ($V = V_\chi + V_\psi$). The divergent wind was used in the Rossby wave source calculations. It also provided an indicator of the tropical cyclone's location in the upper troposphere.

9. **200 mb streamfunction**

The 200 mb stream function (ψ_{200}) fields, in m^2 s^{-1}, were used to calculate the rotational wind ($V_\psi = k \times \nabla\psi$)., which is then used to calculate the Rossby wave source.

10. 200 mb relative vorticity

The 200 mb relative vorticity fields (ζ_{200}) in $m^2\ s^{-1}$, represent the relative cyclonic or anticyclonic flow of the atmosphere. They were used in the Rossby wave source calculations.

D. TROPICAL CYCLONE BOGUSING PROCEDURES

The spatial resolution of operational forecast models is too coarse to accurately depict the mesoscale characteristics of individual tropical cyclones. To improve the representation of the tropical cyclone in the forecast model initial conditions, synthetic data assimilation (bogusing) procedures have been added to some operational weather prediction systems. Goerss and Jeffries (1994) described the operational NOGAPS tropical cyclone bogusing procedure and evaluated its impacts on forecasts of western Pacific tropical cyclones. They showed that NOGAPS with tropical cyclone bogusing generally does quite well at predicting storm intensity and track when the cyclone is at or above tropical storm strength.

In this study, we used the tropical cyclone bogusing procedure as an experimental tool to selectively alter the initial conditions for Seth in runs of the NOGAPS model. We used two types of bogusing techniques.

1. POSITIVE bogus

In the POSITIVE bogus procedure, synthetic data were introduced to give a more realistic representation of the storm than would otherwise be

possible. This POSITIVE bogus procedure is the operational procedure described by Goerss and Jeffries (1994). We used the model runs that were started from the POSITIVE bogus initial conditions as our control representation of the atmosphere's development with the tropical cyclone included.

2. NEGATIVE bogus

The second bogusing procedure, referred to as the NEGATIVE bogus, removed the tropical cyclone from the NOGAPS initial conditions. This procedure is described more fully in Woll (1993). Our model runs using the NEGATIVE bogus initial conditions represent how the atmosphere might have evolved if the tropical cyclone had never occurred. The differences between the output from the model runs using the POSITIVE and NEGATIVE bogusing procedures allowed us to infer the impact of the tropical cyclone on the atmosphere. We refer to these differences as the model *response* to the presence of the tropical cyclone. Table 1 provides descriptions and explanations of these differences.

E. MODEL RUNS AND ANALYSES

We conducted a total of six forecast runs in our study of Seth. These six runs represent the two bogus types described above, and three different initial times. For each initial time, two forecast runs were done: one using initial conditions from the POSITIVE bogus procedure and one using initial

Model Run	What it does	What it describes
POSITIVE	simulates the global atmosphere with tropical cyclone standard NOGAPS bogusing in the data assimilation	the tropical cyclone, the global circulation, and their interactions
NEGATIVE	simulates the global atmosphere after the tropical cyclone has been removed during the data assimilation	the global circulation without the tropical cyclone
POSITIVE-NEGATIVE	displays the difference between the POSITIVE and the NEGATIVE	the features in the global circulation that result from the presence of the tropical cyclone in the POSITIVE runs

Table 1. Overview of the model runs, according to the tropical cyclone bogusing procedure used to develop the model initial conditions (first two rows of table). Overview of the model differences, according to the bogusing procedures (bottom row).

conditions from the NEGATIVE bogus procedure. This gave a total of six forecast runs.

The initial times were near the time when Seth reached its maximum intensity and were defined to be 36 hours apart, at 12Z, 6 October 1994; 00Z, 8 October 1994; and 12Z, 9 October 1994.

The following naming convention is used to distinguish the runs.

- The two runs started at 12Z, 6 October were called the Forecast 1 (F1) runs.
- The two runs started at 00Z, 8 October were called the Forecast 2 (F2) runs.
- The two runs started at 12Z, 9 October were called the Forecast 3 (F3) runs.

Each of the six model runs is identified by its initialization time and its bogusing procedure. For example, the run started at 12Z, 6 October 1994 from the initial conditions developed from the POSITIVE bogusing procedure is called the Forecast 1 POSITIVE run -- or the F1 POSITIVE run, for short. Note that the six model runs differed only in their initial conditions. These initial condition differences represented three different start times and two different treatments of typhoon Seth during the data assimilation. The same NOGAPS model was used for all six runs.

Each of the six forecasts were run out to 00Z, 1 November 1994,

with model fields being output at 00Z and 12Z of each model day. Figure 4 is a schematic of the data assimilation procedures and the six model runs.

F. ENSEMBLE AVERAGING OF MODEL OUTPUT

For many analyses of the model results, the model fields were first ensemble averaged (EA). This procedure averaged together the results from runs that involved the same bogusing procedure but had different initial times. This averaging was done only at corresponding forecast times and dates from the different runs. Figure 5 gives a schematic description of the ensemble averaging process.

The net effect of ensemble averaging was a relative enhancement of the features that were common to all the forecasts being averaged, and a relative reduction of the features that were different between the forecasts being averaged. The ensemble averaging procedure is explained more fully in Woll (1993).

G. WAVE ENERGY AND INSTABILITY CALCULATIONS

Hypothesis 2 proposes that the development of the teleconnection is strongly influenced by the waveguiding and amplification effects of the extratropical westerly jets. To test this hypothesis and identify the mechanisms of the model's teleconnections, the following diagnostic quantities were calculated using the model's 200 mb height and wind fields.

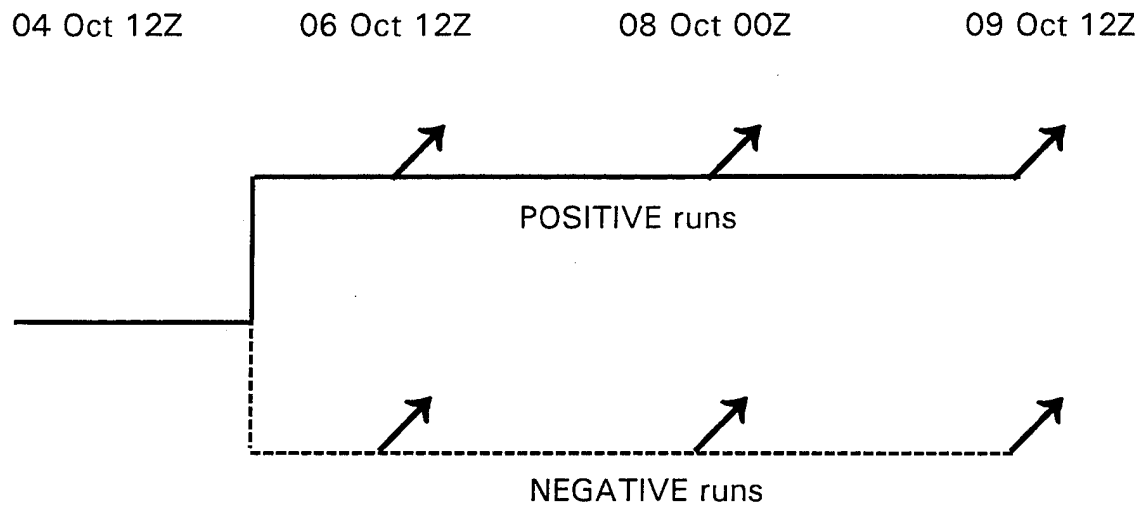

Figure 4. Schematic of the data assimilation and tropical cyclone bogusing procedures for the six model runs. Bogusing started when Seth's wind reached 18 m/s. Bogusing continued until the start of each model run.

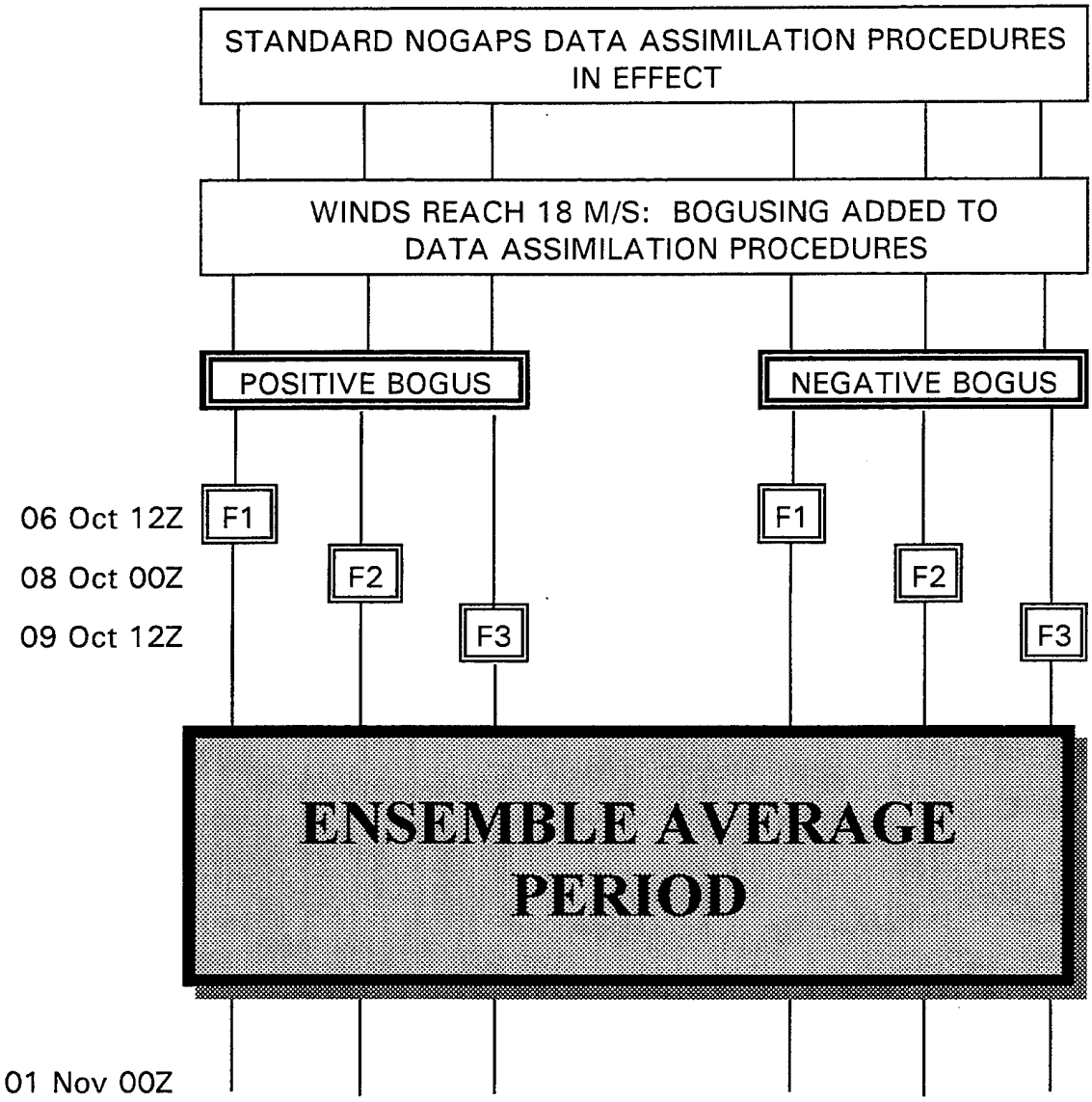

SYMBOLS USED: F1 = FORECAST 1
F2 = FORECAST 2
F3 = FORECAST 3

Figure 5. Schematic of six model runs conducted, showing standard data assimilation periods, modified data assimilation (i.e., bogusing) periods, forecast periods, and ensemble averaging periods.

1. Quasi-geostrophic wave activity flux vectors

Quasi-geostrophic (QG) wave activity flux vectors (Plumb 1985), were used to track the quasi-geostrophic wave energy as it propagated through the model's upper-troposphere. These flux vectors are parallel to the wave energy propagation, and their magnitude is proportional to the amount of propagating energy. Converging flux vectors indicate a wave energy sink, while diverging vectors denote a wave energy source.

2. 200 mb potential barotropic instability

Barotropic instability (BTI) has been suggested as a probable mechanism in tropical to midlatitude teleconnections (Simmons et al. 1983, Woll 1993). Woll (1993) concluded that areas of potential barotropic instability contributed energy to the teleconnection response to Yuri. In our study, as in Woll (1993) and Springer (1994), areas of potential barotropic instability in the model were identified using the Rayleigh-Kuo criterion (Kuo 1949):

$$\beta - \frac{\partial^2 u}{\partial y^2} = 0 \qquad (1)$$

Where β is the total derivative of the Coriolis parameter, $\frac{df}{dy}$, and $\frac{\partial^2 u}{\partial y^2}$ is the second meridional derivative of the 200 mb zonal wind. Note that (1) is not exactly the Rayleigh-Kuo condition since the wind is not zonally symmetric. However, this asymmetry should not significantly alter the implications of the condition, if the wind changes relatively slowly in the zonal direction

(Branstator 1983). As in Woll (1993), we have smoothed the $\beta - \frac{\partial^2 u}{\partial y^2}$ fields with a weighted nine-point horizontal smoother before plotting them.

It is important to note that (1) is a necessary, but not a sufficient, condition for barotropic instability. Thus (1) denotes possible wave energy source areas, where barotropic instability mechanisms might provide energy to the waves, but it does not guarantee that these are actually wave energy source areas.

H. ROSSBY WAVE SOURCE

1. Motivation

Many modeling and theoretical studies have indicated that it is very difficult, or impossible, for Rossby waves generated in the tropics to propagate through the tropical easterlies and impact the extratropics (e.g., Tribbia 1991). However, many studies have also shown that tropical disturbances do have extratropical impacts that appear as Rossby wave trains. Sardeshmukh and Hoskins (1988) noted that in many modeling and theoretical studies, the divergent portion of the horizontal wind, V_χ, had been ignored. Past studies assumed that V_χ was insignificant in the teleconnection process because, on large scales, V_χ usually is much smaller than V_ψ, the rotational portion of the horizontal wind.

Sardeshmukh and Hoskins (1988) showed that, near an extratropical jet, the advection of absolute vorticity by the divergent component of the

horizontal wind can be quite significant in generating Rossby waves. They defined a Rossby wave source in the absolute vorticity equation as the sum of two terms: the advection of absolute vorticity by the divergent horizontal wind term and the stretching term. They showed that the effects of a Rossby wave source caused by a localized tropical disturbance can extend well beyond the disturbance and into the region of the extratropical jet (Figure 6). Figure 7 shows an example of a Rossby wave source computed by Sardeshmukh and Hoskins (1988). Thus, they concluded that tropical disturbances may have an extratropical influence by indirectly generating Rossby waves at an extratropical jet, rather than by directly propagating Rossby waves out of the tropics.

Springer (1993) found that for typhoons Yuri and Robyn the advection of absolute vorticity by the divergent horizontal wind (ADVDIV) appeared to initiate upper tropospheric wave train responses to these storms. In particular, ADVDIV produced a negative source that was associated with the development of an area of negative relative vorticity north of the storms and on the flank of the East Asian - North Pacific jet. This negative vorticity region marked the southwestern end of the wave train responses. Springer (1994) suggested that the phasing of these wave train responses may have been determined, at least initially, by the sign of the Rossby wave source difference.

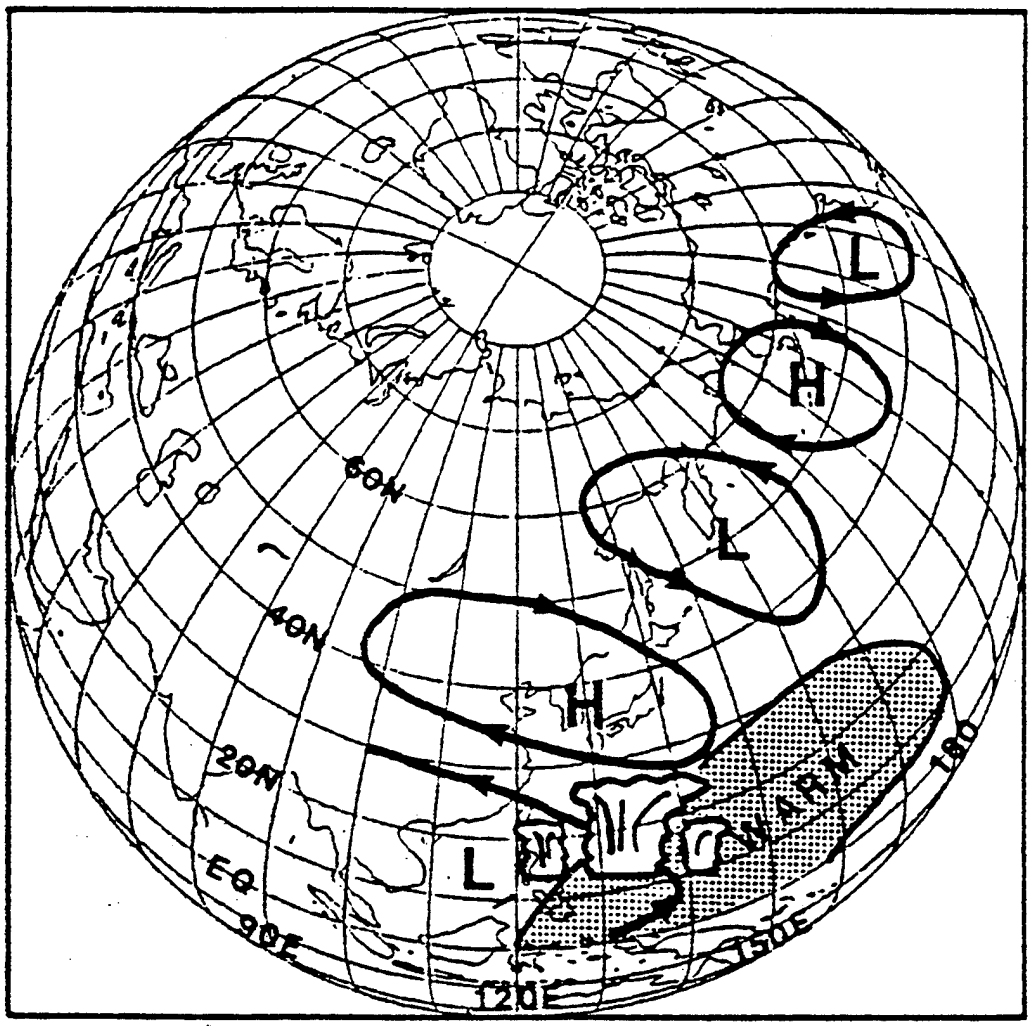

Figure 6. Schematic of northern summer 500 mb height anomalies associated with increased convection over warmer than normal SST in the tropical western Pacific. H denotes a positive height anomaly, L denotes a negative height anomaly (from Nitta 1987).

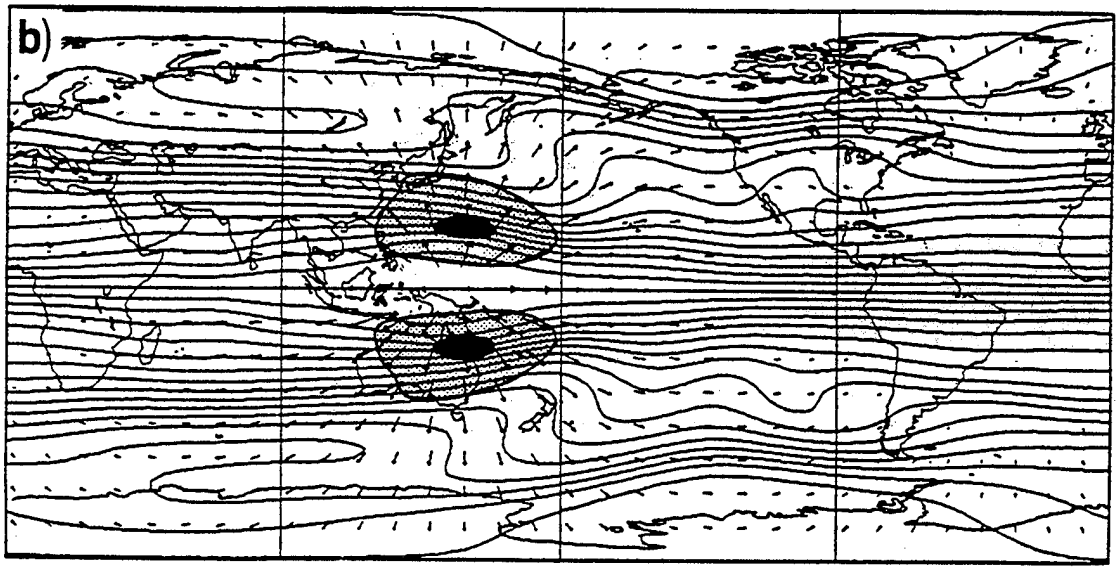

Figure 7. Schematic of upper tropospheric Rossby wave sources due to advection of absolute vorticity by steady divergent winds emanating from the equatorial western Pacific. Wavy contours indicate upper tropospheric stream function. Vectors indicate divergent wind (maximum wind is about 5 m/s) Shading along subtropical western Pacific jets indicates negative Rossby wave sources (from Sardeshmukh and Hoskins 1988).

2. Formulation of the Rossby wave source

The Rossby wave source is contained in the absolute vorticity equation, shown below in isobaric coordinate form:

$$(\frac{\partial}{\partial t} + \boldsymbol{V}_\psi \bullet \nabla)(\zeta + f) = S \qquad (2)$$

where $(\zeta + f)$ is the absolute vorticity and S is the Rossby wave source, defined as:

$$S = -\nabla \bullet [\boldsymbol{V}_\chi (\zeta + f)] \qquad (3)$$

Expanding (3) gives:

$$S = -[\boldsymbol{V}_\chi \bullet \nabla(\zeta + f) + (\zeta + f)\nabla \bullet \boldsymbol{V}_\chi] \qquad (4)$$

Further expansion gives:

$$S = -[u_\chi \frac{\partial \zeta}{\partial x} + v_\chi \frac{\partial \zeta}{\partial y} + v_\chi \beta + (\zeta + f)(\frac{\partial u_\chi}{\partial x} + \frac{\partial v_\chi}{\partial y})] \qquad (5)$$

The first three terms on the right-hand side of (5) represent ADVDIV. The last term in (5) is the vortex stretching (or divergence) term. Rearranging (2) gives:

$$\frac{\partial \zeta}{\partial t} = -\boldsymbol{V}_\psi \bullet \nabla(\zeta + f) + S \qquad (6)$$

The left-hand term is the relative vorticity tendency and $-\boldsymbol{V}_\psi \bullet \nabla(\zeta + f)$ is the advection of absolute vorticity by the rotational part of the horizontal wind (ADVROT). In component form, ADVROT is:

$$-\left(u_\psi \frac{\partial \zeta}{\partial x} + v_\psi \frac{\partial \zeta}{\partial y} + v_\psi \beta\right) \qquad (7)$$

Notice that this is similar in form to ADVDIV, except that the rotational

horizontal wind is used in (7).

The terms in (5) were calculated from the output fields for the Seth model runs. These calculations were made using finite difference approximations to the derivatives in (5).

III. RESULTS

A. OVERVIEW

The value of the results found in any study are dependent upon the quality of the raw data and methods used in the study. The raw data used in this study were the forecast results from the six different model runs and the methods are those described in Chapter II.

To assess these data and methods, we applied the four prerequisites used by Woll (1993) and Springer (1994):

Prerequisite 1: The bogusing procedure used during the data assimilation must have a significant effect on the model's initial conditions only in the vicinity of the tropical cyclone.

Prerequisite 2: The model runs that attempt to simulate the tropical cyclone (i.e., those for which the POSITIVE bogus procedure was used) must give a relatively accurate simulation of the typhoon's track and strength. The model runs that attempt to remove the tropical cyclone from the model atmosphere (i.e., those for which the NEGATIVE bogus was used) must show, at most, only a very weak tropical cyclone.

Prerequisite 3: All the model runs, regardless of the bogus procedure used, must provide a realistic representation of basic climatological features.

Prerequisite 4: When ensemble averaging is done, the major features of the individual forecasts being averaged must be preserved in the average.

B. PREREQUISITE 1 - BOGUSING AND THE INITIAL CONDITIONS

A POSITIVE and NEGATIVE bogusing procedure was used in developing the initial conditions for each of the model runs. The purpose of the POSITIVE bogus was to enhance the initial conditions for Seth. This was done to improve the model's ability to correctly forecast Seth's strength and track. The purpose of the NEGATIVE bogus was to remove Seth from the initial conditions so that the model forecasts would represent the evolution of the global atmosphere without Seth.

1. SLP initial condition

Figure 8 shows the sea-level pressure initial conditions for the F2 POSITIVE, NEGATIVE, and POSITIVE - NEGATIVE runs. Figure 8a and Figure 8b are very similar except for the area in the tropical west Pacific, east of China. In this area, Figure 8a shows a well developed low, while Figure 8b shows a much weaker low. Figure 8c highlights this difference and indicates that the NEGATIVE bogusing procedure largely succeeded in removing Seth from the initial conditions.

Figure 8c also shows a small SLP difference in the southern hemisphere at approximately 70S, 150E. Woll (1993) and Springer (1994) found similar weak SLP differences in the southern hemisphere, and

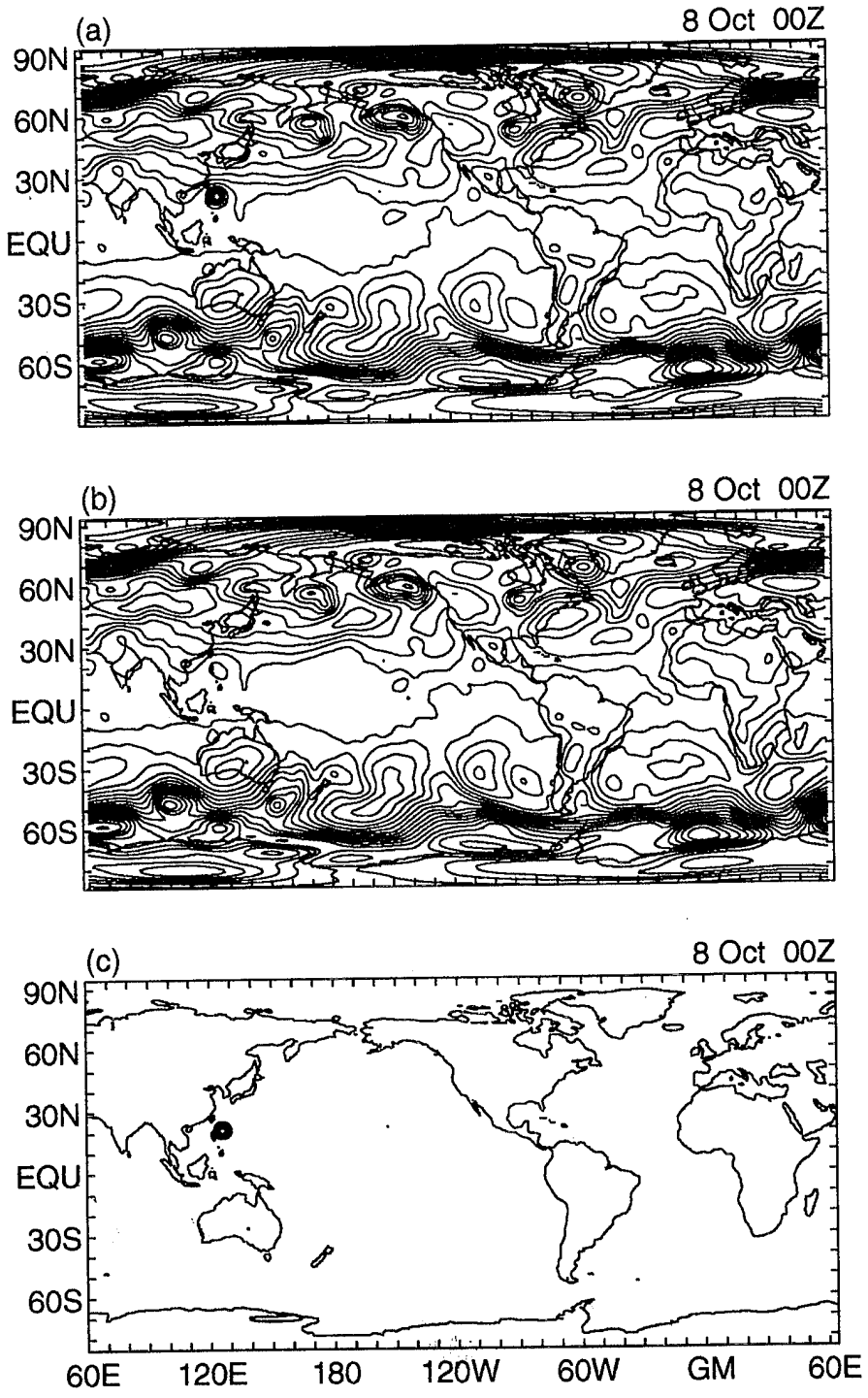

Figure 8. Sea level pressure initial conditions for Forecast 2: (a) Positive Bogus, (b) Negative Bogus, (c) Positive - Negative Bogus. Contour interval is 4 mb. Zero contour omitted.

suggested that these remote differences might be an artifact of the horizontal truncation.

The SLP difference fields for F1 and F3 runs also show a clear POSITIVE - NEGATIVE difference at the location of Seth with no remote differences.

2. Conclusion for prerequisite 1

The main SLP differences for F1, F2, and F3 were centered on Seth's location. Remote SLP differences were much weaker. Thus, we conclude that prerequisite 1 was met.

C. PREREQUISITE 2 - TYPHOON TRACK AND INTENSITY

In order to test our hypotheses, our data assimilation and modeling methods needed to give a reasonably accurate prediction of Seth's track and intensity in the POSITIVE runs. In addition, our methods needed to eliminate Seth from the NEGATIVE runs. Thus, we compared the track and minimum SLP for Seth in the POSITIVE runs with the analyzed track and SLP provided by JTWC. We also examined the western North Pacific SLP in the NEGATIVE runs for indications of a residual Seth.

1. Typhoon track

The position of the SLP minima at selected times for the F3 POSITIVE and NEGATIVE runs are shown in Figures 9 and 10. The JTWC best track

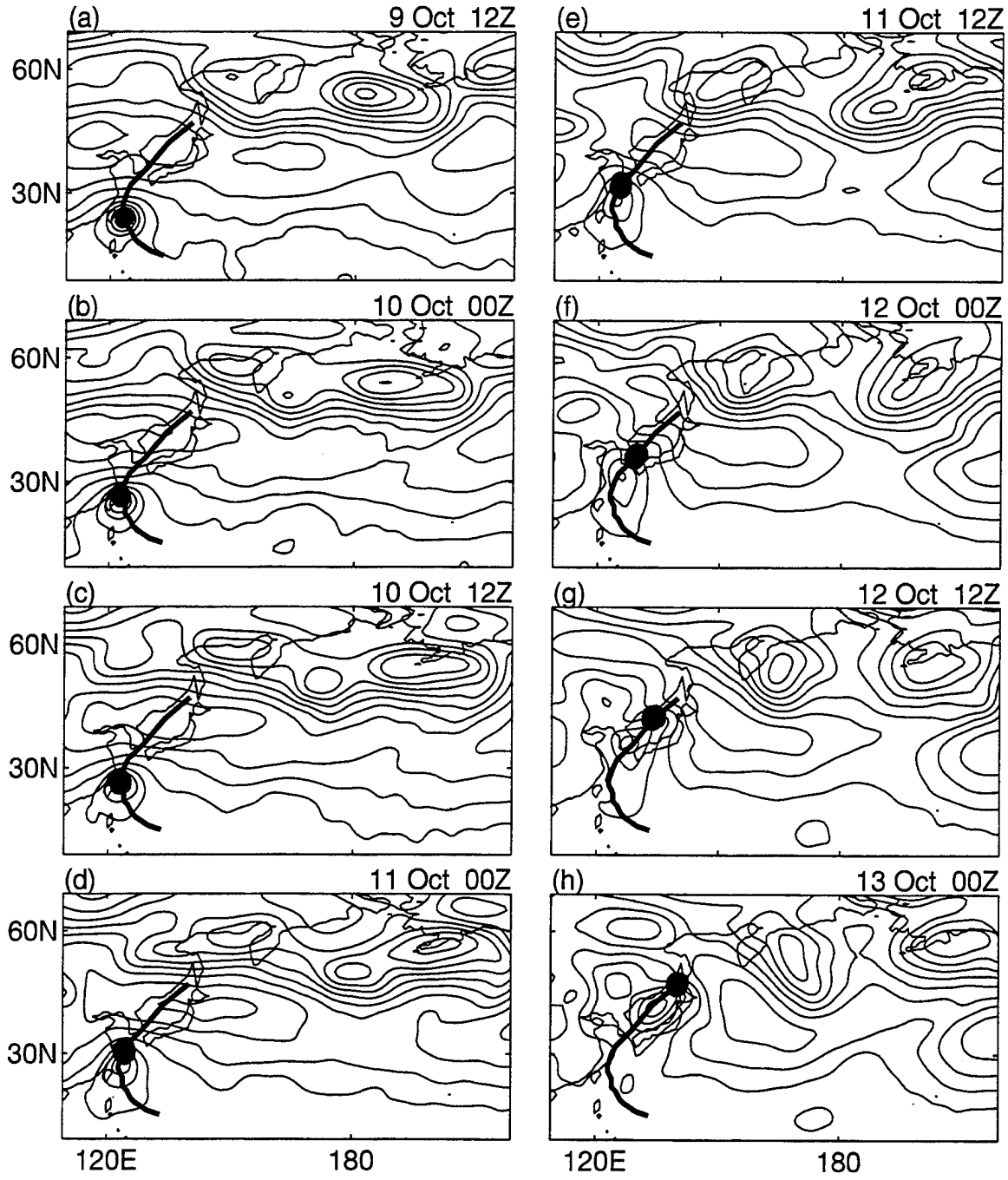

Figure 9. Sea-level pressures in the western Pacific at selected times for Forecast 3 POSITIVE run. Contour interval is 4 mb. Bold **line** is the recurving portion of the JTWC best track. The bold **dot** is the JTWC best track position for that date and time.

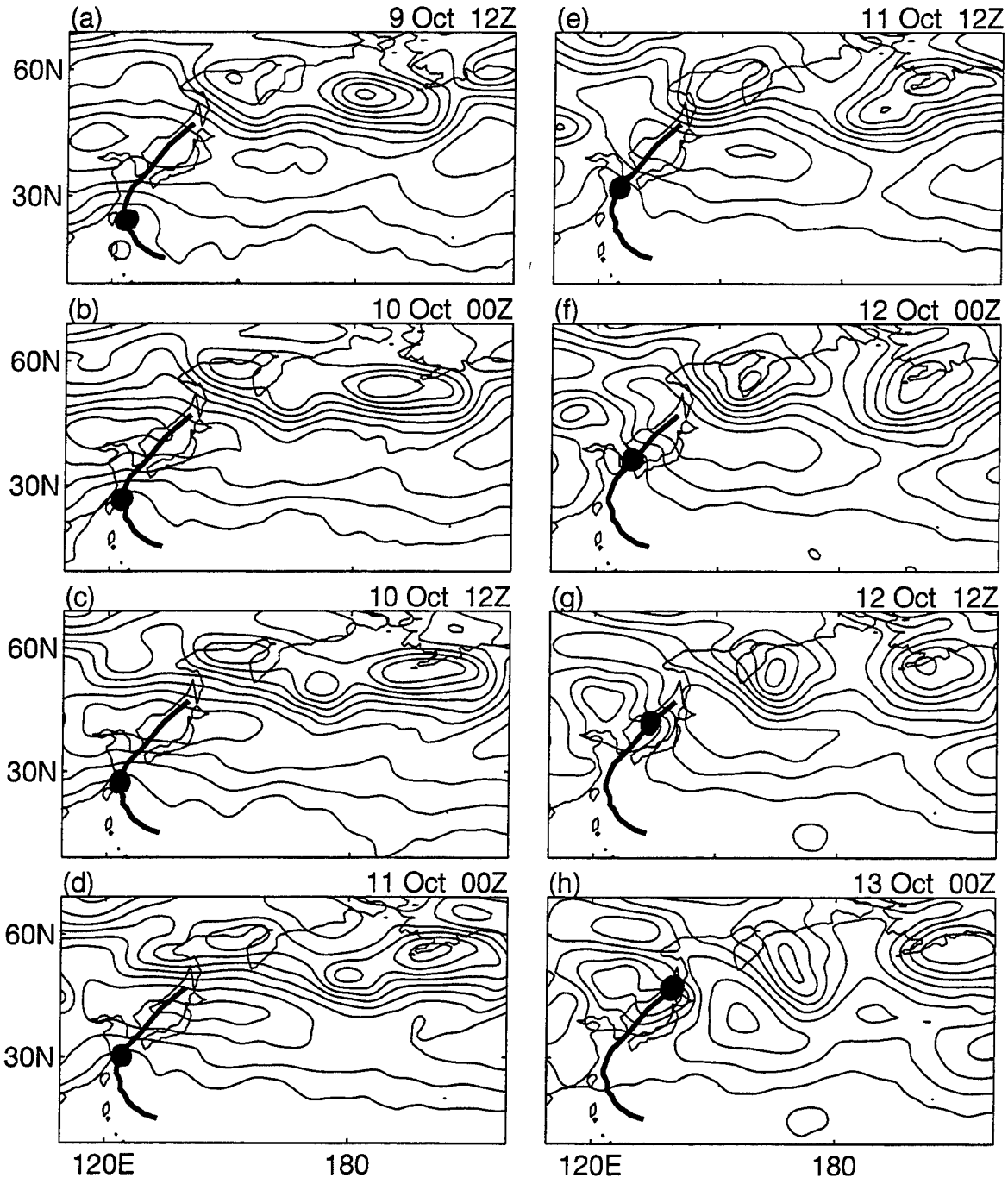

Figure 10. Sea-level pressures in the western Pacific at selected times for Forecast 3 NEGATIVE run. Contour interval is 4 mb. Bold **line** is the recurving portion of the JTWC best track. The bold **dot** is the JTWC best track position for that date and time.

for Seth is superimposed in these figures as a bold curved line, with Seth's position at the indicated time shown by a **bold** dot.

The SLP minima corresponding to Seth in the F3 POSITIVE run was well defined and traced a track that was very similar to the JTWC best track during most of Seth's existence (Figure 9). However, the model Seth's track speed was less than that of the actual Seth, so that by 00Z, 13 October 1994, there was a considerable lag between the two (Figure 9h).

The SLP minima for the F1 and F2 POSITIVE runs (not shown) were less successful in tracking Seth than those for the F3 POSITIVE run. These two runs generated tracking speeds that were too slow. The F1 POSITIVE run did not recurve. In the F2 POSITIVE run, the recurvature occurred several days too late.

The SLP minima for the F3 NEGATIVE run (Figure 10) clearly showed the effects of bogusing out Seth in the model initial conditions. At 12Z, 9 October 1994, the model had a weak low in the vicinity of the actual Seth position (Figure 10a). During 10-12 October 1994, the model generated a weak trough near the position of the actual Seth (Figure 10b-f). This trough merged with a midlatitude low on about 12Z October 1994 (Figure 10g). Figure 10 shows that in the F3 NEGATIVE run, Seth was largely, but not entirely, eliminated.

The SLP minima for the F1 and F2 NEGATIVE runs (not shown) were similar to those for the F3 NEGATIVE run (Figure 10). However, for these two runs the initial low near the position of the actual Seth location did not extend itself into the subtropics and midlatitudes.

2. **Typhoon intensity**

We also used the SLP minima as a measure of the model storm's intensity. Table 2 lists the SLP minima from the F3 POSITIVE and NEGATIVE bogus runs. Table 2 also lists the best track minimum SLP calculated using JTWC maximum sustained surface winds and the Atkinson and Holliday (1977) method for calculating the minimum SLP from those winds.

The SLP minima for the F3 POSITIVE run were notably higher than the best track SLP. This probably occurred for two main reasons. First, NOGAPS, like other numerical weather prediction models, has problems deepening a typhoon's central SLP without adversely affecting other, more pertinent, physical variables. Second, NOGAPS has limited resolution which makes it difficult to resolve the small scale central low pressure area. The SLP minima for the F3 NEGATIVE bogus were higher than for the corresponding POSITIVE run and the JTWC-based values. Similar results were found for the minima SLP's for the F1 and F2 POSITIVE and NEGATIVE runs (not shown).

Date Time (1994)	POSITIVE	JTWC
09 Oct 12Z	991 24N 123E	938 24N144E
10 Oct 00Z	993 25N 123E	948 26N 123E
10 Oct 12Z	996 26N 123E	958 27N 123E
11 Oct 00Z	997 27N 124E	967 30N 124E
11 Oct 12Z	1000 28N 124E	976 32N 125E
12 Oct 00Z	1000 32N 126E	980 36N 129E
12 Oct 12Z	998 36N 128E	984 42N 134E
13 Oct 00Z	995 41N 133E	987 47N 140E

Table 2. Strength and location of the typhoon Seth minimum sea level pressure (SLP minima), in mb, for the Forecast 3 POSITIVE run and the JTWC best estimates of minimum SLP at the specified times. SLP were derived from JTWC Maximum Sustained Surface Winds and equivalent minimum SLP (Alkinson and Holliday 1977).

3. Conclusion for prerequisite 2

The F3 POSITIVE runs gave relatively accurate depictions of Seth's track and intensity. The F1 and F2 POSITIVE runs did not do nearly as well as the F3 POSITIVE run in predicting the typhoon track, although they did as well as F3 in predicting the minimum SLP. Thus, we concluded that, overall, prerequisite 2 was essentially met. This is discussed further in section E.

D. PREREQUISITE 3 - COMPARISONS WITH CLIMATOLOGY

To estimate the overall accuracy of the NOGAPS forecasts, we took the models ensemble averaged forecasts from 00Z, 10 October to 00Z, 30 October, averaged them together, then compared this result with the corresponding observed monthly mean fields for October 1994.

1. 200 mb geopotential heights

The 20-day average 200 mb heights for the F3 POSITIVE and NEGATIVE runs are shown in Figure 11. The major features to note in both the POSITIVE and NEGATIVE runs are the strong jets over the northwest Pacific and the area of difluence just east of these jets. The other major features are the jet and diffluent regions over the North Atlantic and much of the southern hemisphere. These features are similar to those observed during October 1994 (cf. Kousky 1994). In the North Pacific - North American (NPNA) region, the POSITIVE results are noticeably more realistic

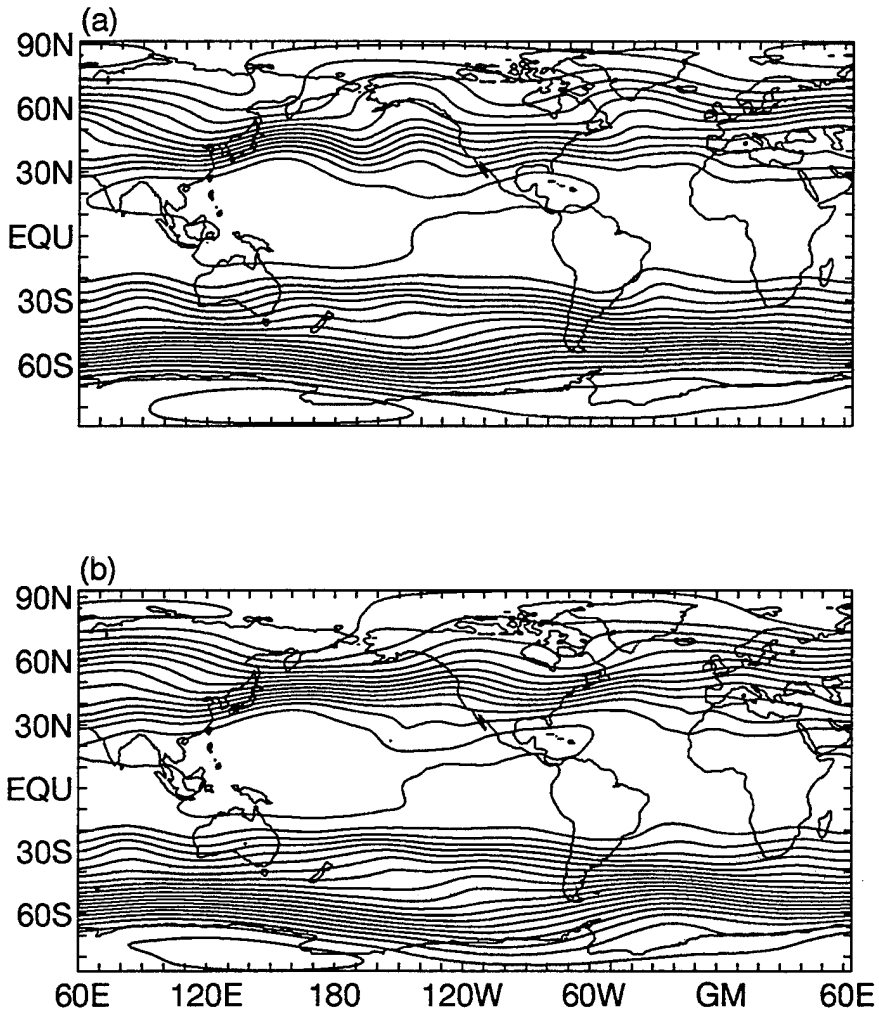

Figure 11. 20-day average 200 mb geopotential heights for Forecast 3 POSITIVE (a), and NEGATIVE (b) bogus. Contour interval is 100 gpm.

than the NEGATIVE results (cf. Kousky 1995). The corresponding heights from the F1 and F2 runs (not shown) were quite similar to those shown for the F3 runs.

2. Conclusion for prerequisite 3

Both POSITIVE and NEGATIVE 200 mb geopotential 20-day averages portrayed reasonable mean flows when compared to observed values. Thus, we concluded that prerequisite 3 was met.

E. PREREQUISITE 4 - EFFECTS OF ENSEMBLE AVERAGING

Ensemble averaging of the three POISITIVE runs and of the three NEGATIVE runs was used to minimize transient features and accentuate the more persistent features associated with significant teleconnections. However, to check that this averaging did not eliminate important features in the individual runs or create spurious features, we reviewed the individual 200 mb height forecasts from the POSITIVE and NEGATIVE runs and compared these with their respective ensemble average 200 mb heights. The first common time between the F1, F2, and F3 runs was 00Z, 10 October 1994. We review first the heights from the three POSITIVE runs and the POSITIVE ensemble average, and then the heights from the NEGATIVE runs and the NEGATIVE ensemble average. The features we are most interested in are the series of troughs and ridges in the NPNA region.

These features are related to the expected teleconnections (cf. Nitta 1987, Harr and Elsberry 1994, Woll 1993, Springer 1994).

1. **Positive 200 mb heights**

The discussion in this section of the POSITIVE 200 mb heights and their ensemble average refers to the following set of figures:

F1: Figure 12

F2: Figure 13

F3: Figure 14

Ensemble Average: Figure 15

00Z, 10 October 1994: All three POSITIVE runs showed a series of ridges and troughs across the NPNA region. These included a ridge over Asia, a flat trough extending across the central Pacific, and a ridge over central North America.

00Z, 12 October 1994: The west Pacific ridge and the central Pacific tough have moved eastward. The North American ridge has weakened considerably. A new ridge was developing in the east Pacific. This ridge was most noticeable in the F2 and F3 runs.

00Z, 14 October 1994: The west Pacific ridge has moved to Kamchatka, the central Pacific trough has become considerably deeper and more localized, and the east Pacific ridge has amplified.

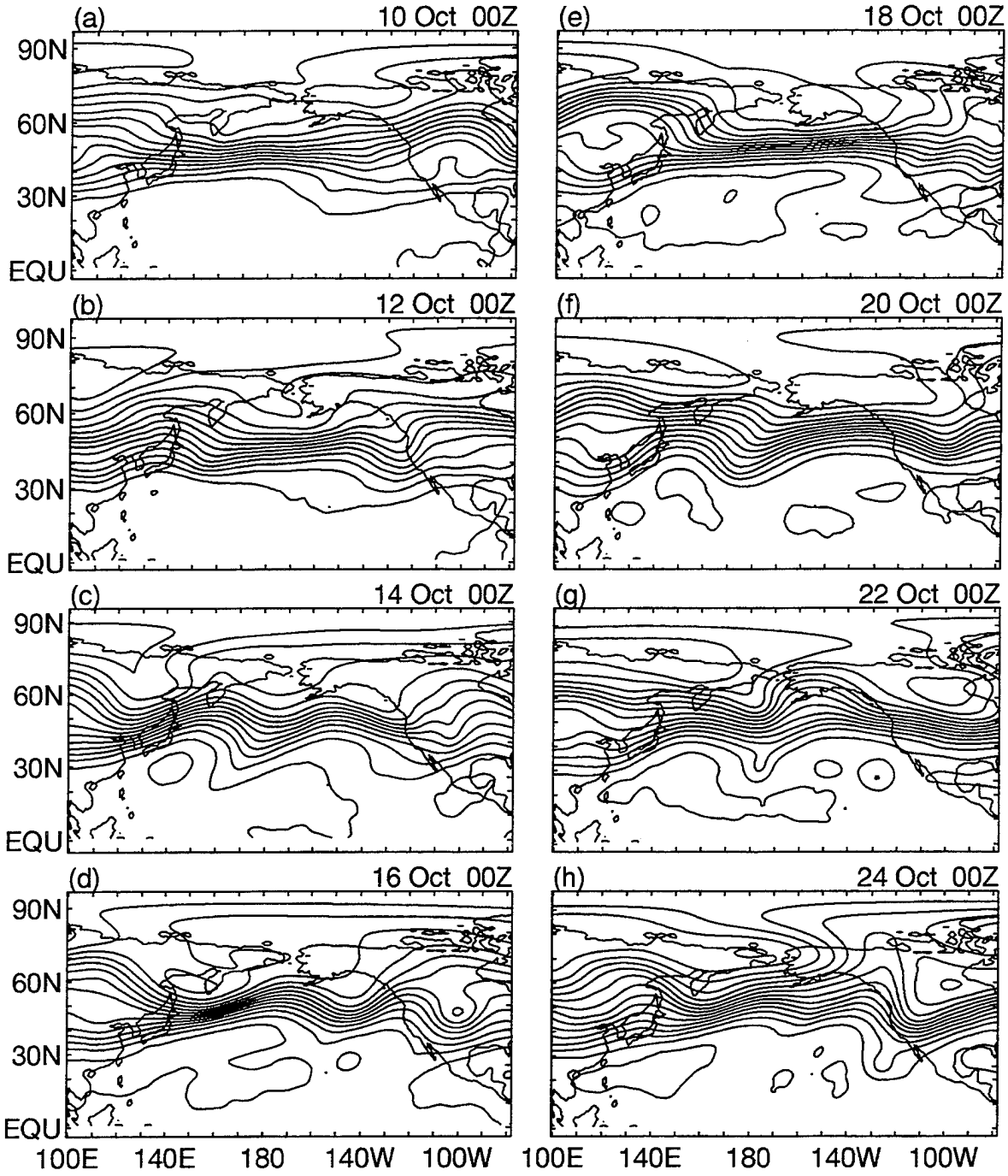

Figure 12. 200 mb geopotential heights at selected times for Forecast 1 POSITIVE run. Contour Interval is 100 gpm. Zero contour omitted.

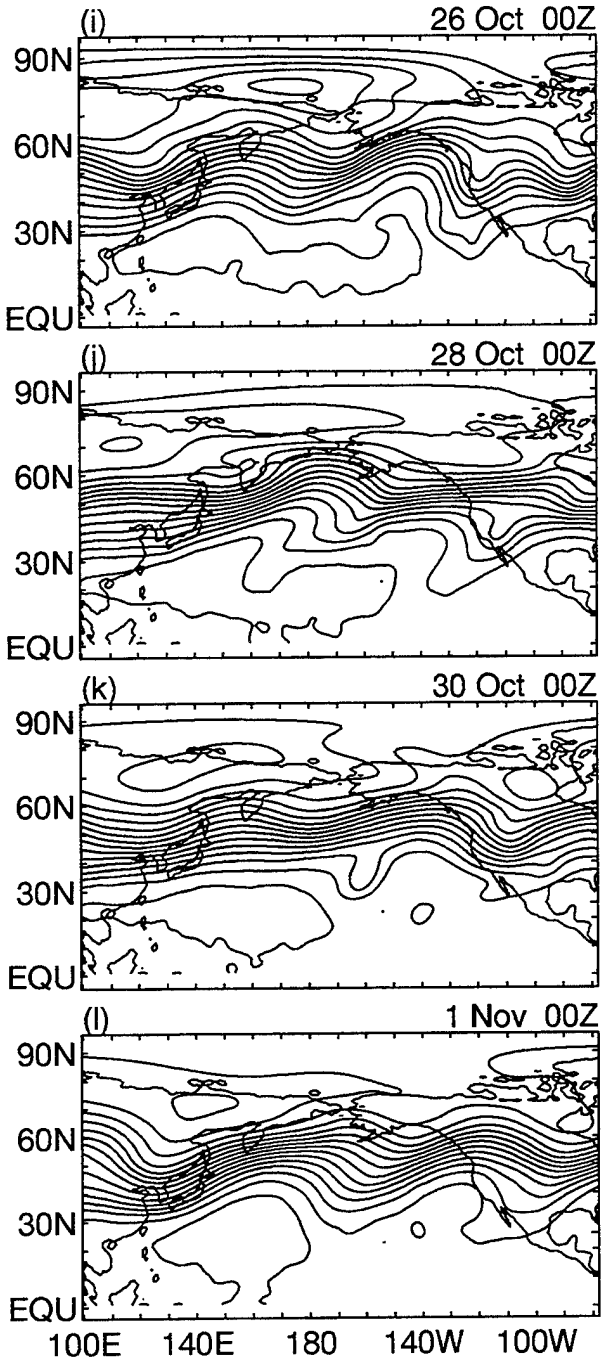

Figure 12. (Continued).

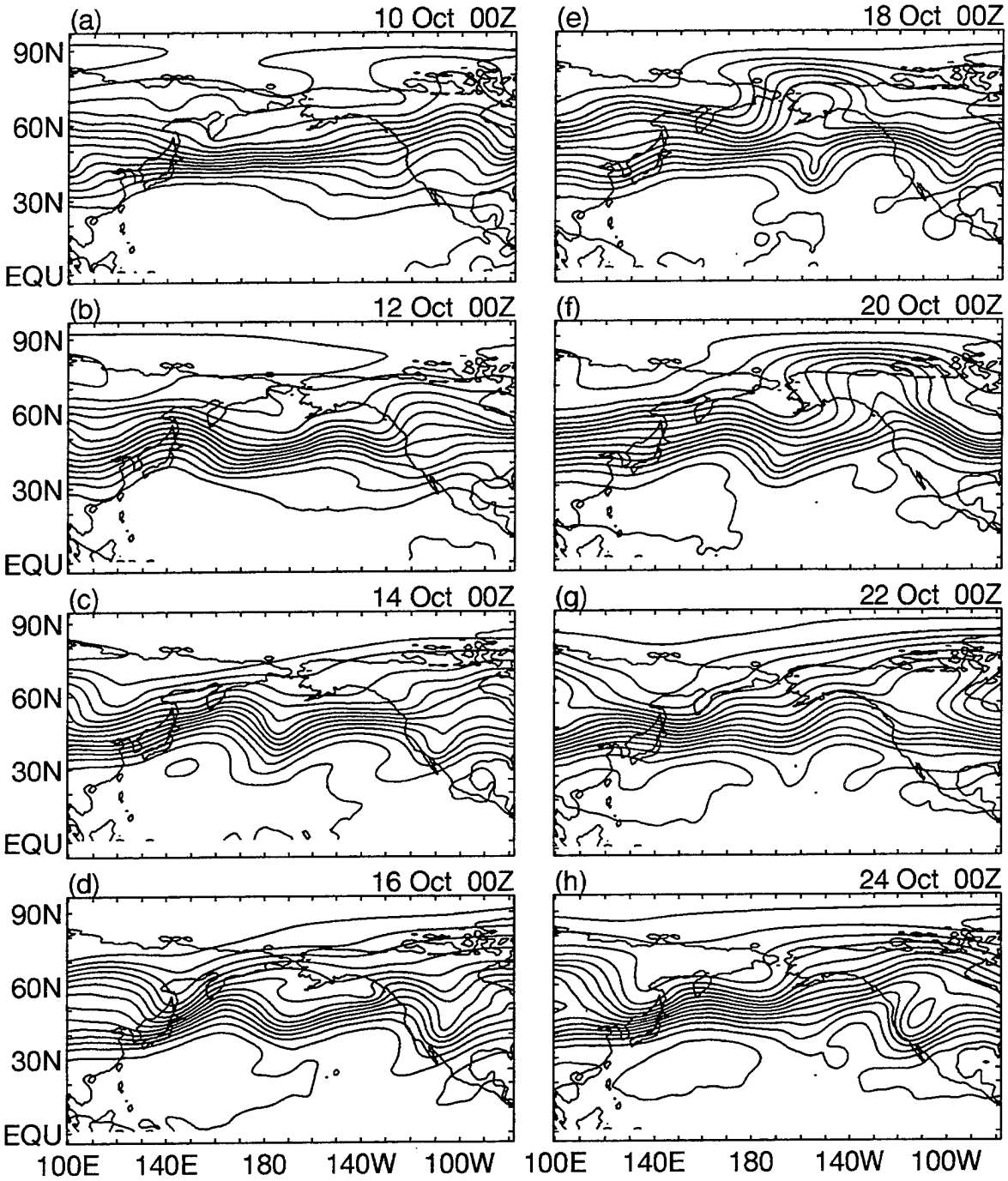

Figure 13. 200 mb geopotential heights at selected times for Forecast 2 POSITIVE run. Contour Interval is 100 gpm. Zero contour omitted.

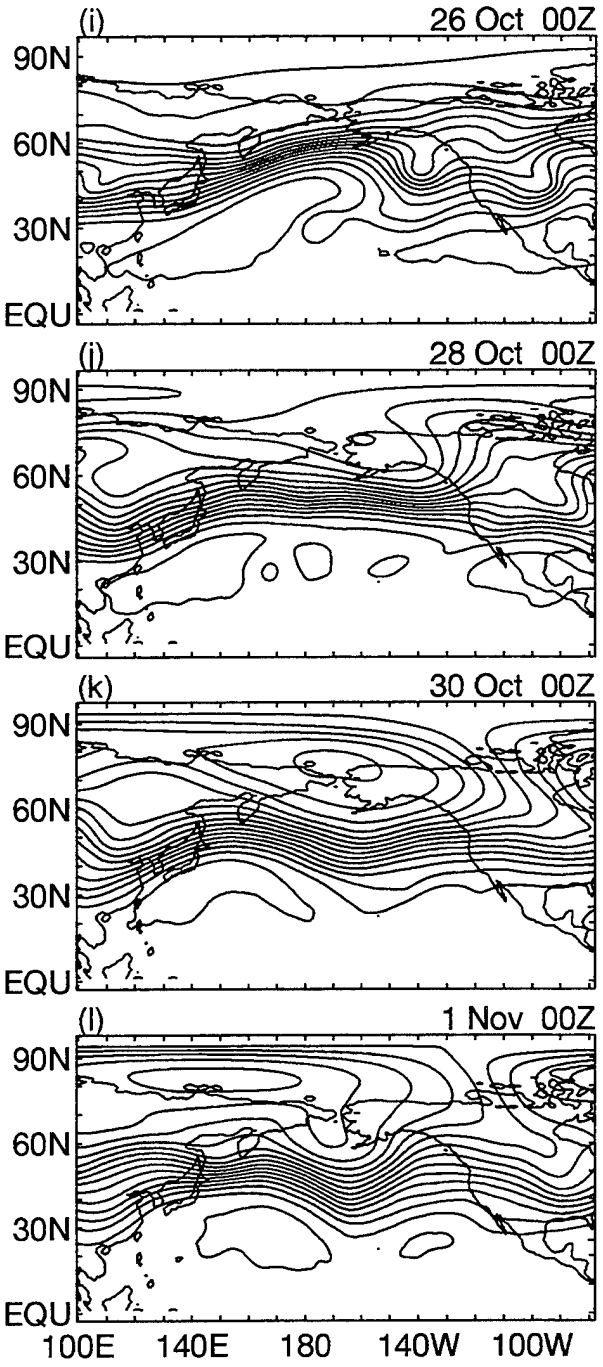

Figure 13. (Continued).

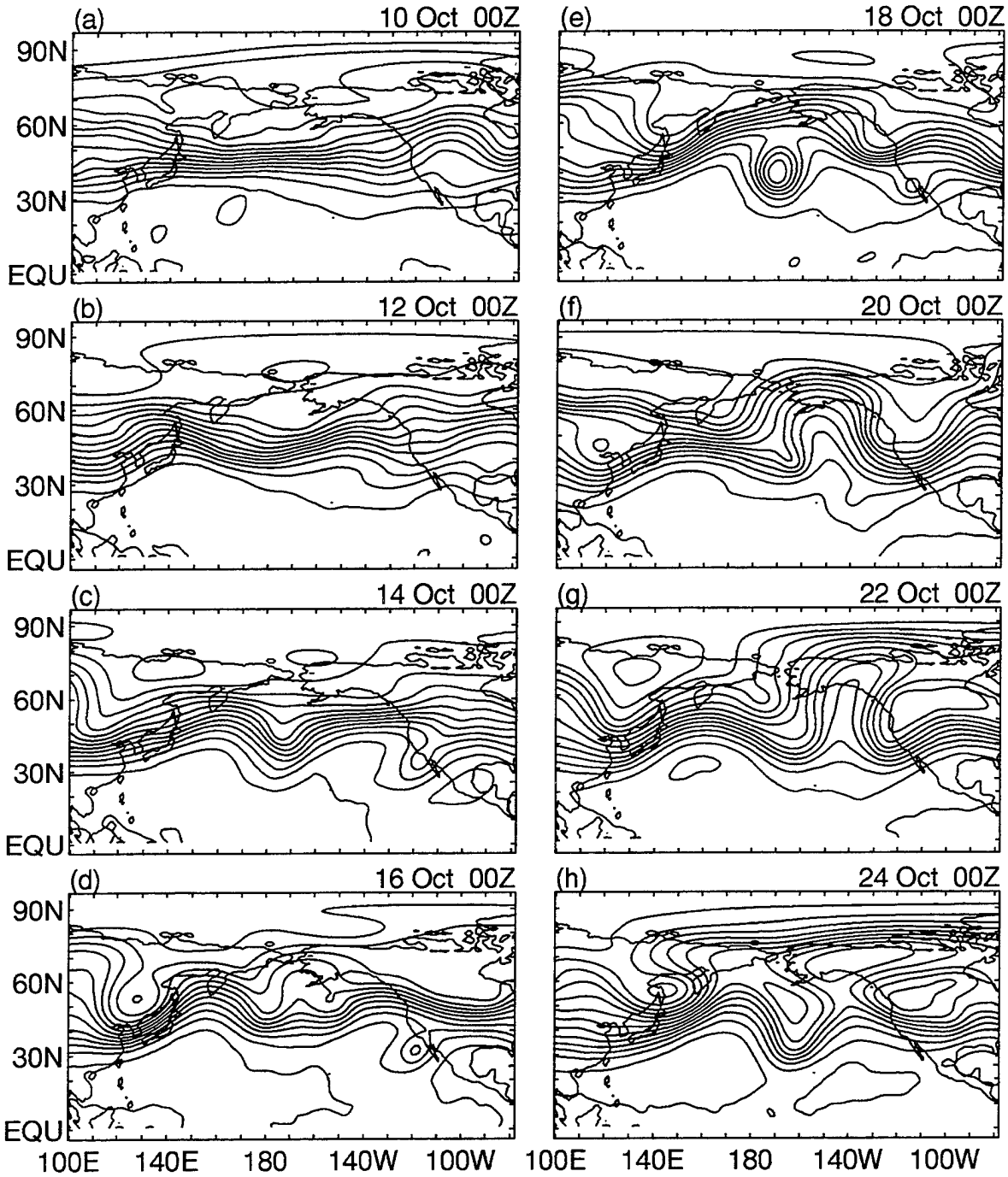

Figure 14. 200 mb geopotential heights at selected times for Forecast 3 POSITIVE run. Contour Interval is 100 gpm. Zero contour omitted.

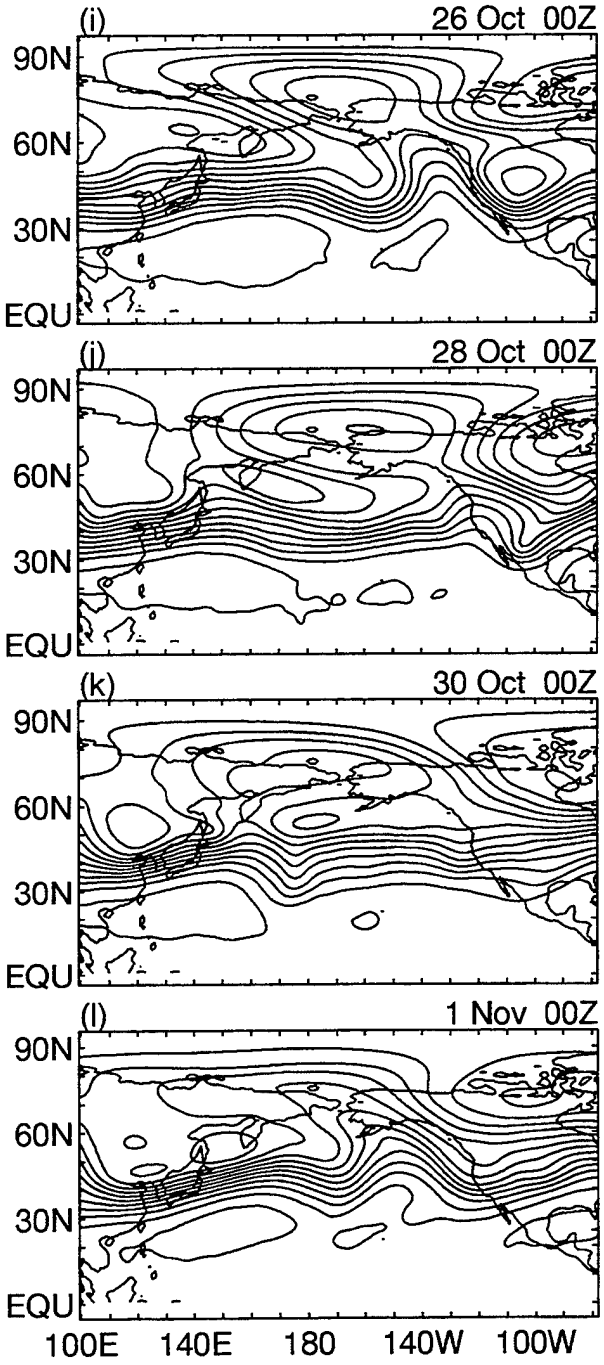

Figure 14. (Continued).

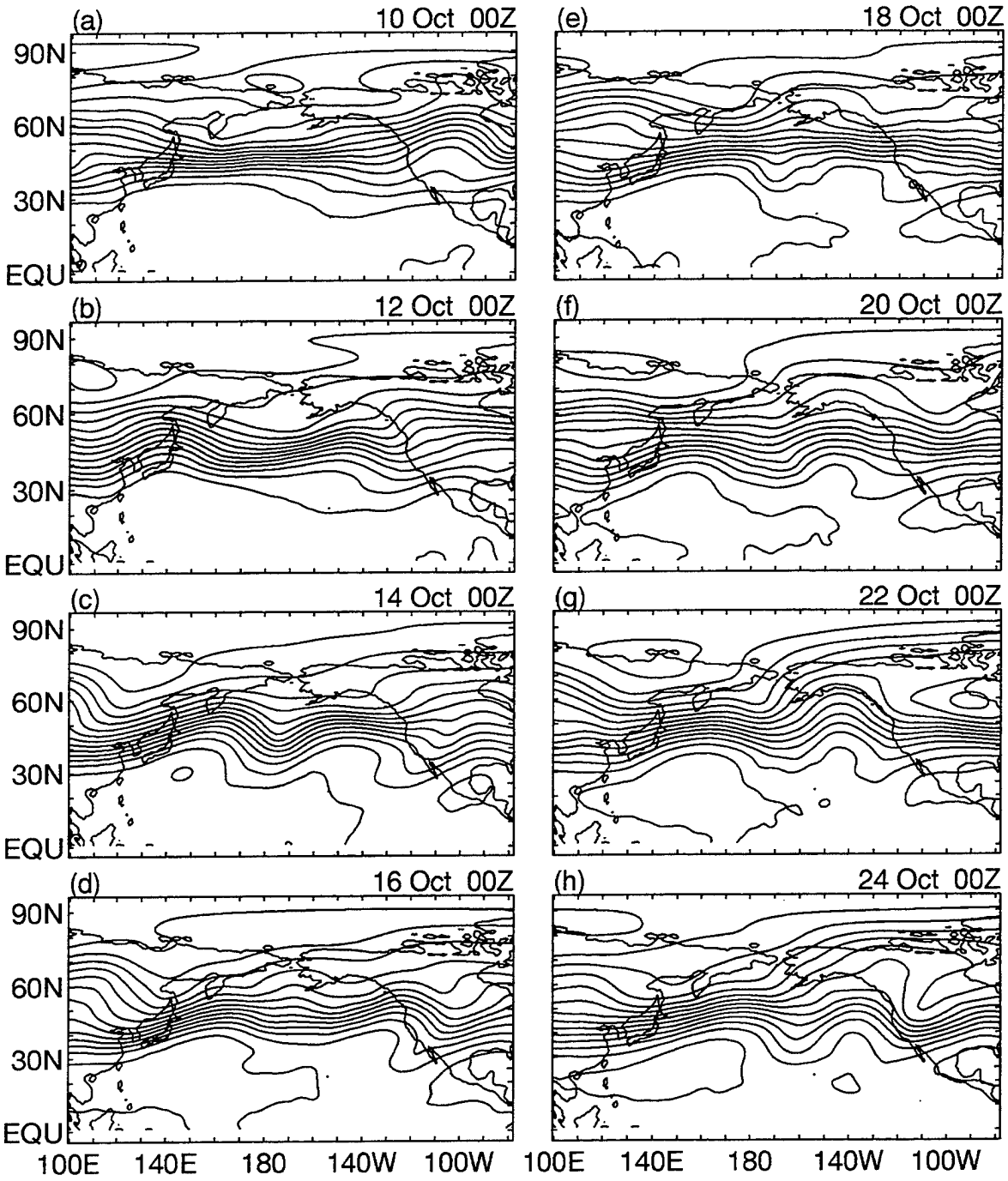

Figure 15. 200 mb geopotential heights at selected times for Ensemble Average POSITIVE run. Contour Interval is 100 gpm. Zero contour omitted.

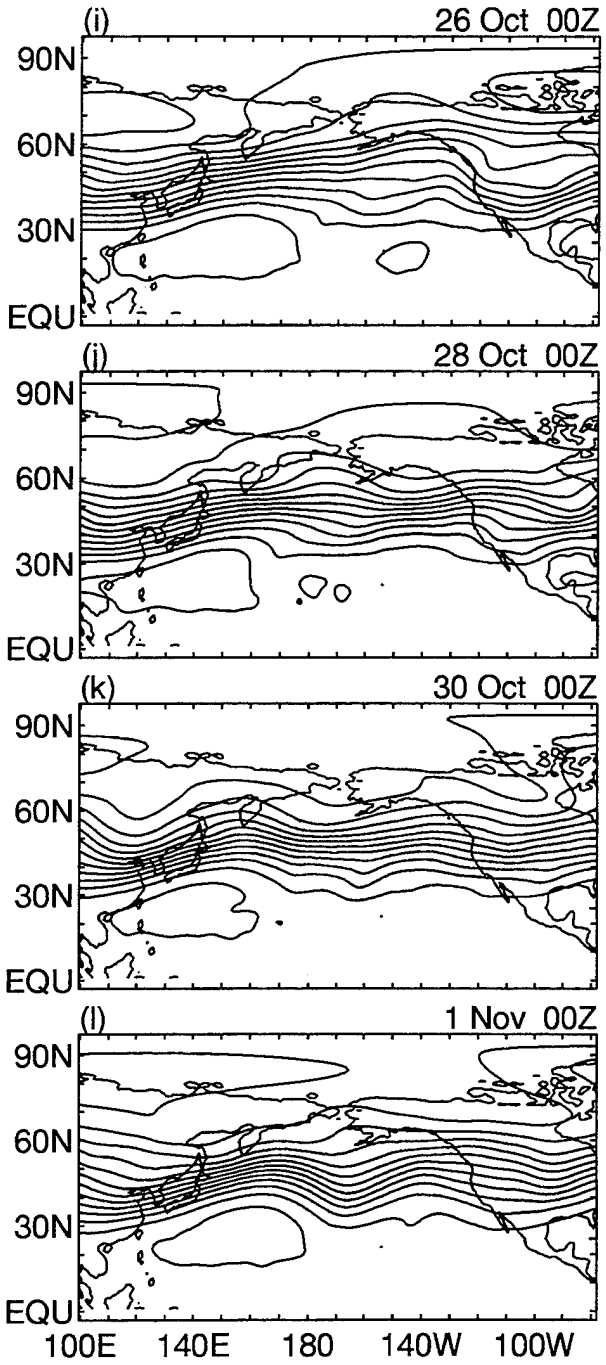

Figure 15. (Continued).

Through 14 October 1994, the differences between F1, F2, and F3 POSITIVE runs were very small. However, after this, the differences grew. This growth in the differences may have been partially the result of the differences in the tracking of Seth by the three POSITIVE runs.

00Z, 16 October 1994: The west Pacific ridge in the F1 run has moved to the central Pacific, while it is still in the west Pacific in the F2 and F3 runs. The F1 central Pacific trough and east Pacific ridge have also moved ahead of those in F2 and F3.

00Z 18 October 1994: The F1 ridge-trough-ridge system has moved further east than in F2 and F3. The F1 trough is not as long as those in F2 and F3. The F3 trough has been replaced by a ridge extending northward over Alaska. The F2 and F3 runs developed a short trough in the central North Pacific south of Alaska that was not present io the F1 run.

The eastward movement of the troughs and ridges continued throughout the remainder of the three forecast periods. Differences between the F1, F2, and F3 runs were apparent through the end of the ensemble average period on 1 November, especially on 24 and 28 October. However, there were many similarities between the large scale features in the three runs which were well represented in the ensemble average (e.g., the trough-ridge-trough-ridge-trough pattern that extended eastward from east Asia into North America on 1 November).

2. Standard deviation of the POSITIVE runs

To summarize the similarities and differences between the individual runs and their ensemble average, we calculated the standard deviation of the POSITIVE 200 mb runs with respect to their ensemble average. This standard deviation was then averaged over the NPNA area (20N-70N, 120E-80W) to give an area average standard deviation for each forecast output time:

$$SD = \left(\sum_{I} \sum_{J} \frac{\sum_{k=1}^{n} (F(k)_{IJ} - EA_{IJ})^2}{(n-1)} \right)^{1/2} \qquad (8)$$

In this equation: i and j are zonal and meridional indices, respectively; k is the forecast number index; n is the total number of forecast runs; F(k) is the 200 mb height for the kth forecast; and EA is the ensemble average 200 mb height.

As expected from the results shown in Figures 12-15, the standard deviation of the POSITIVE runs was small through 14 October increased sharply during 16-20 October and then leveled off at about 170 gpm (Figure 16). Plots of the differences between the individual forecasts and the ensemble average (not shown) indicate that that the F2 run was the most

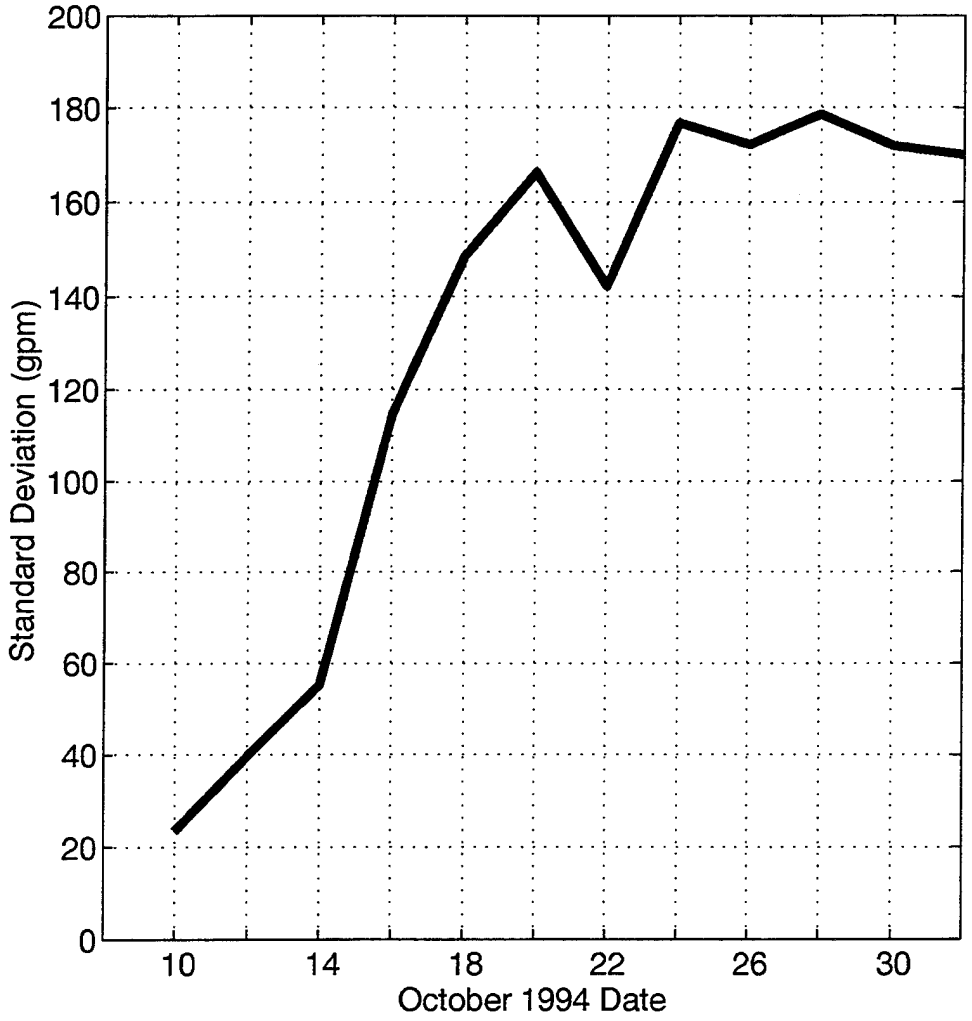

Figure 16. Standard deviation of the POSITIVE runs in the NPNA region (20N - 70N, 120E - 80W).

similar to the ensemble average, while the F1 (F3) run tended to be the least similar during the early (later) part of the averaging period.

3. Summary of POSITIVE ensemble averages

In summary, all three of the POSITIVE runs showed clear and similar 200 mb heights patterns across the NPNA region during most of the ensemble averaging period (Figures 12-14). These common patterns were captured in the ensemble average 200 mb heights (Figure 15). However, some strong and persistent features in the individual runs were only weakly represented in the ensemble average (e.g., the high amplitude ridge over the northeastern Pacific and northwestern North America in the F3 run during 20-26 October). This suggests that the individual runs may contain some information about the response to Seth that is not well represented in the ensemble average. This issue is examined in more detail in Chapter IV.

4. Negative 200 mb heights

The discussion in this section of the NEGATIVE 200 mb heights and their ensemble average refers to the following set of figures:

F1:	Figure 17
F2:	Figure 18
F3:	Figure 19
Ensemble Average:	Figure 20

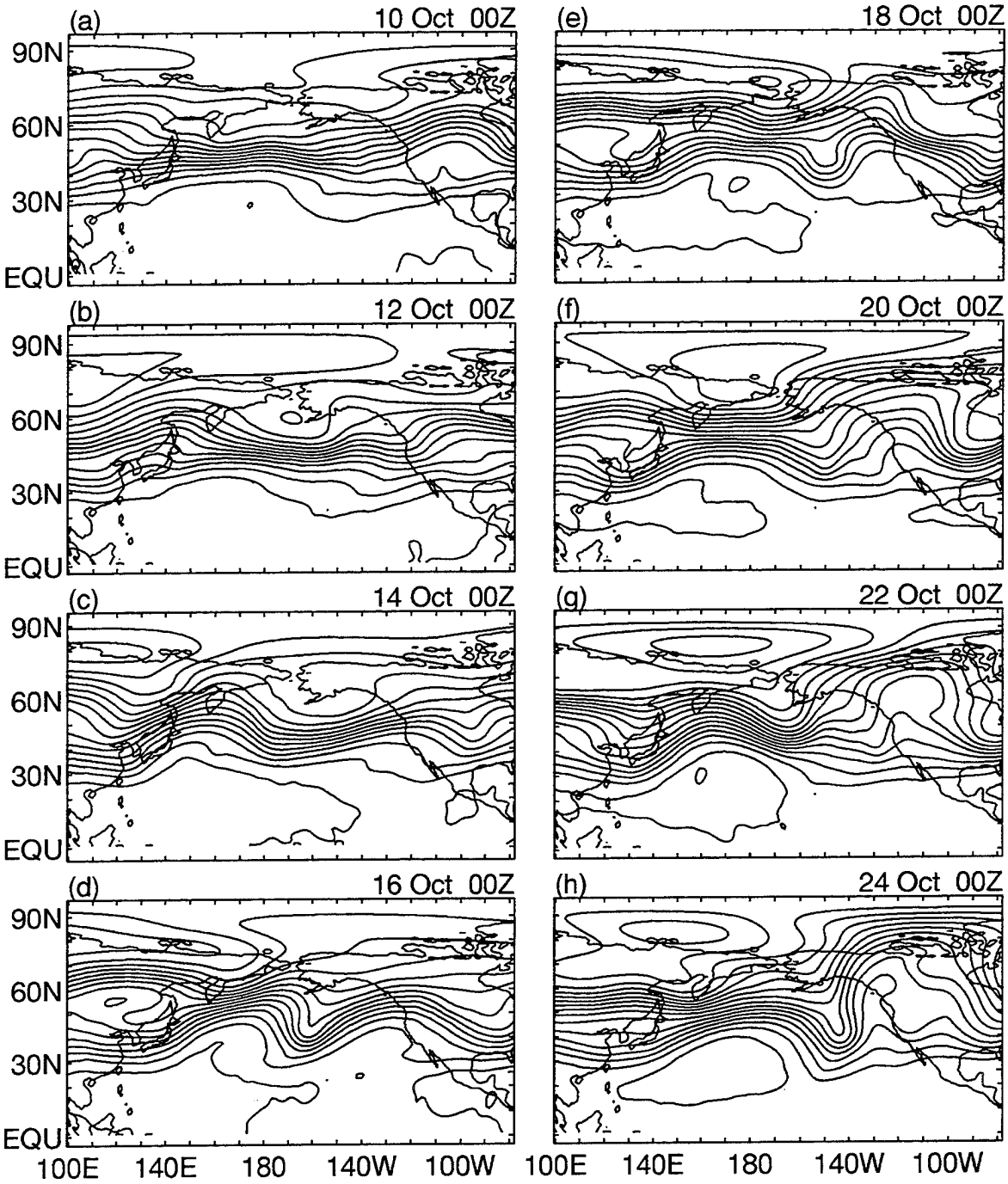

Figure 17. 200 mb geopotential heights at selected times for Forecast 1 NEGATIVE run. Contour Interval is 100 gpm. Zero contour omitted.

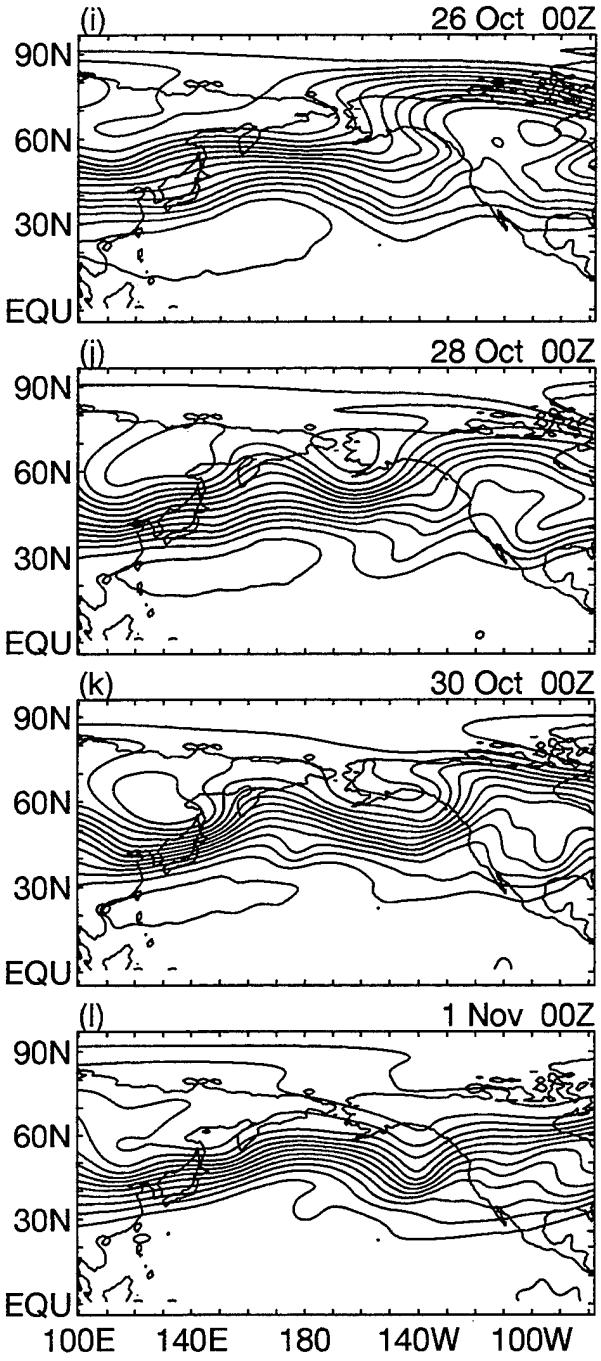

Figure 17. (Continued).

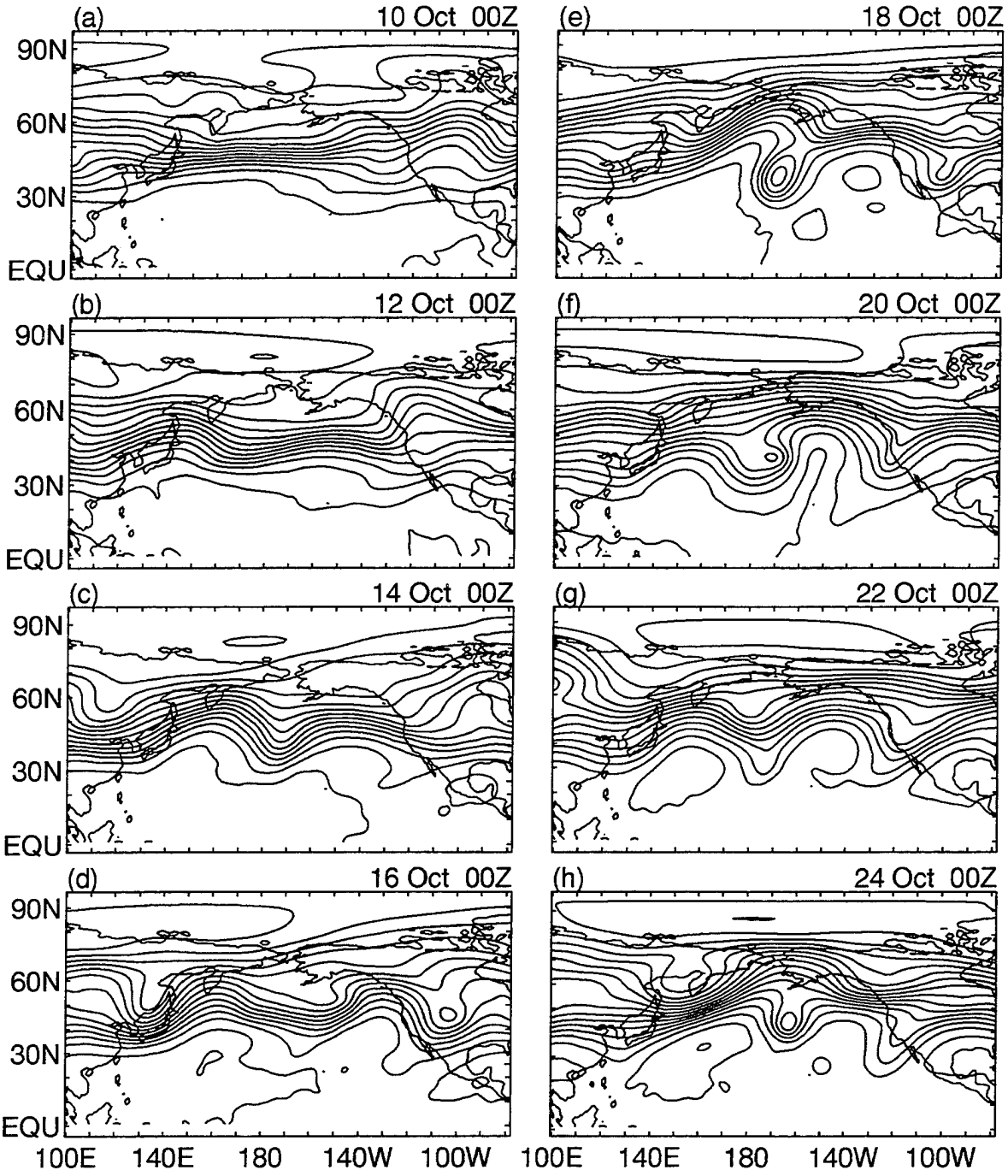

Figure 18. 200 mb geopotential heights at selected times for Forecast 2 NEGATIVE run. Contour Interval is 100 gpm. Zero contour omitted.

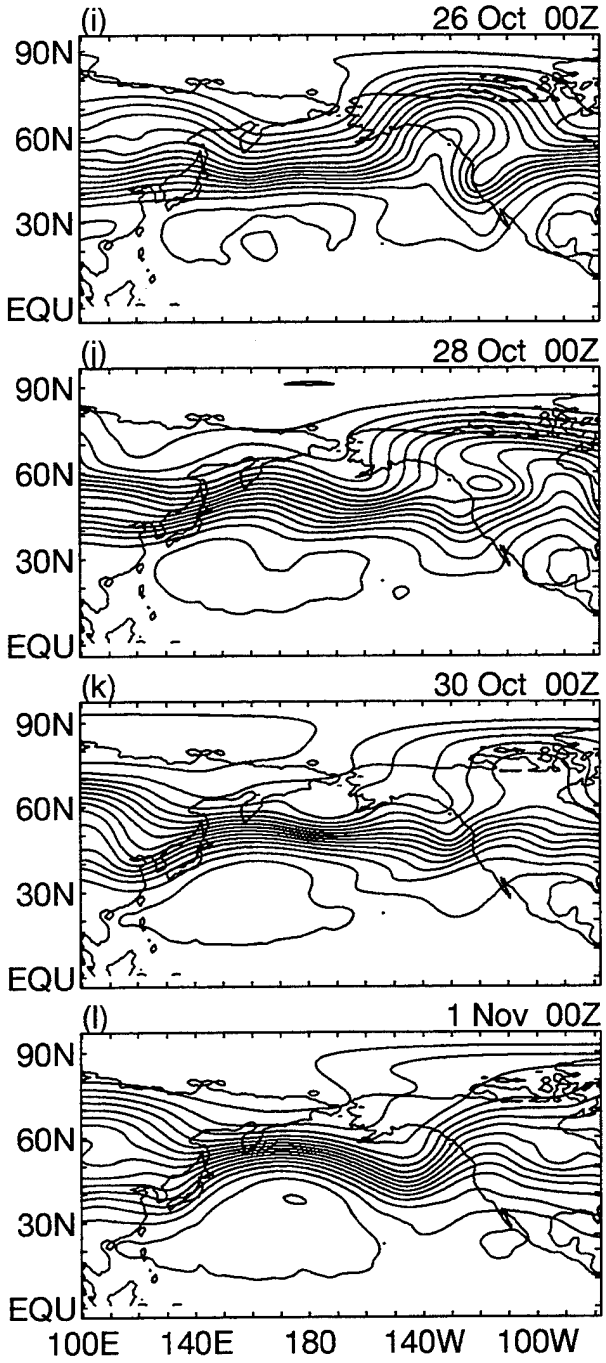

Figure 18. (Continued).

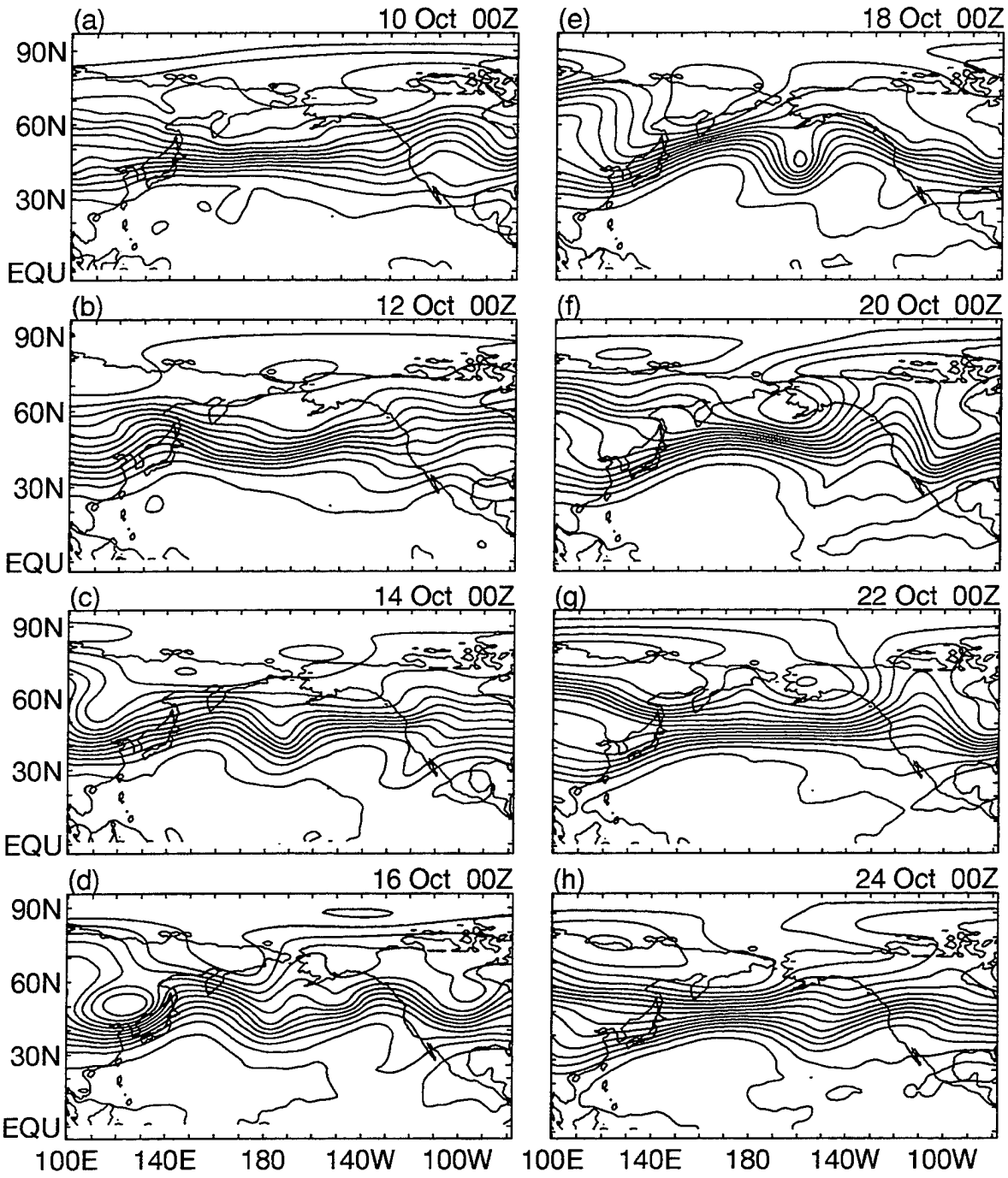

Figure 19. 200 mb geopotential heights at selected times for Forecast 3 NEGATIVE run. Contour Interval is 100 gpm. Zero contour omitted.

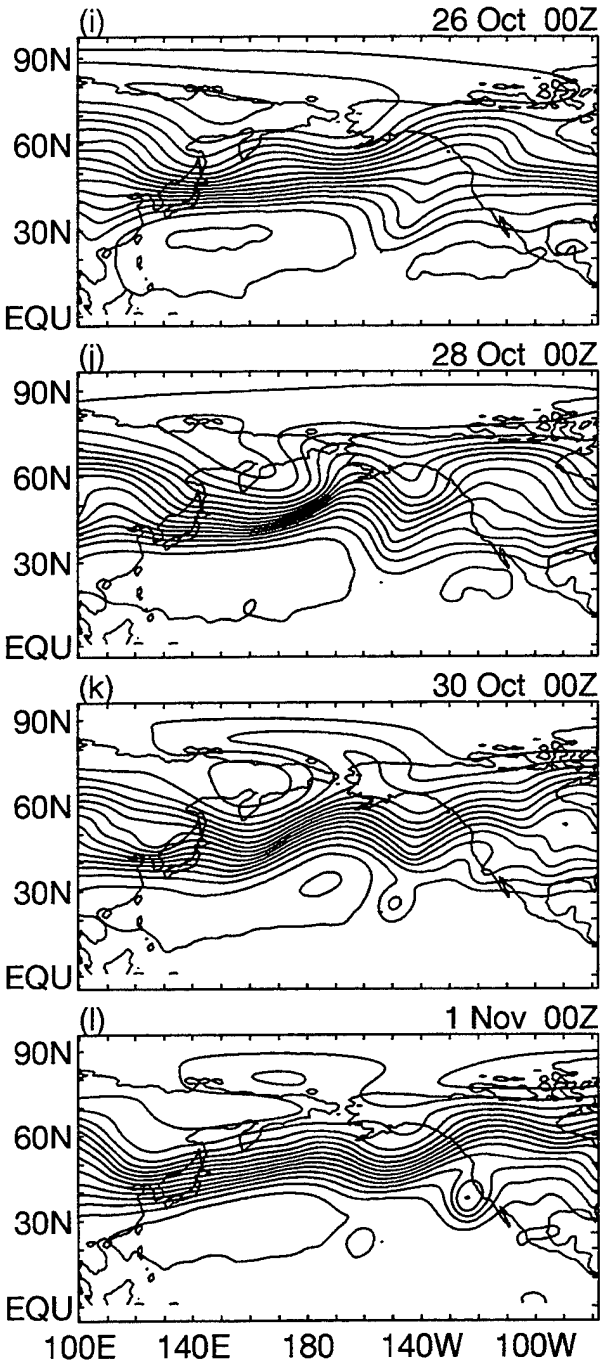

Figure 19. (Continued).

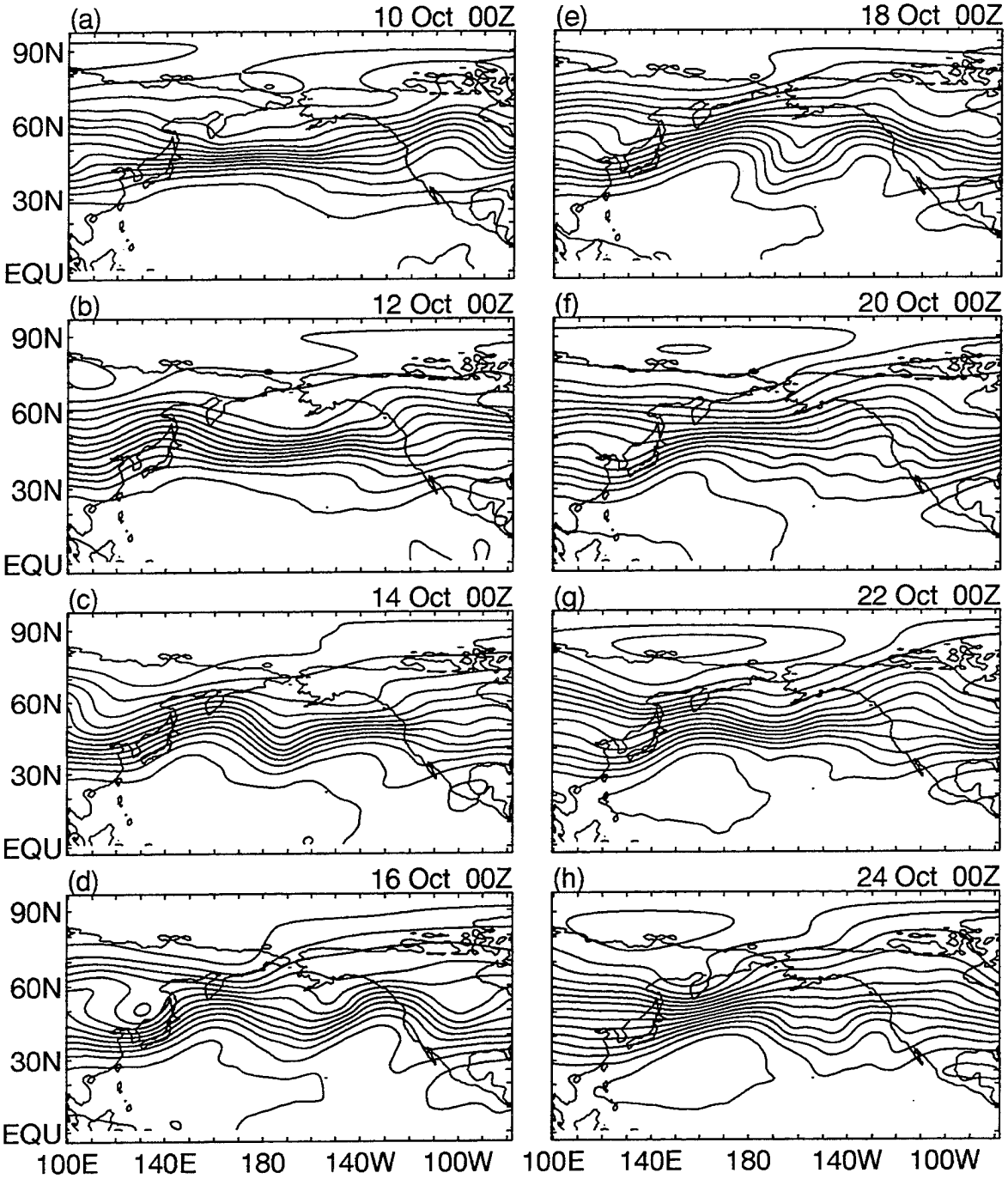

Figure 20. 200 mb geopotential heights at selected times for Ensemble Average NEGATIVE run. Contour Interval is 100 gpm. Zero contour omitted.

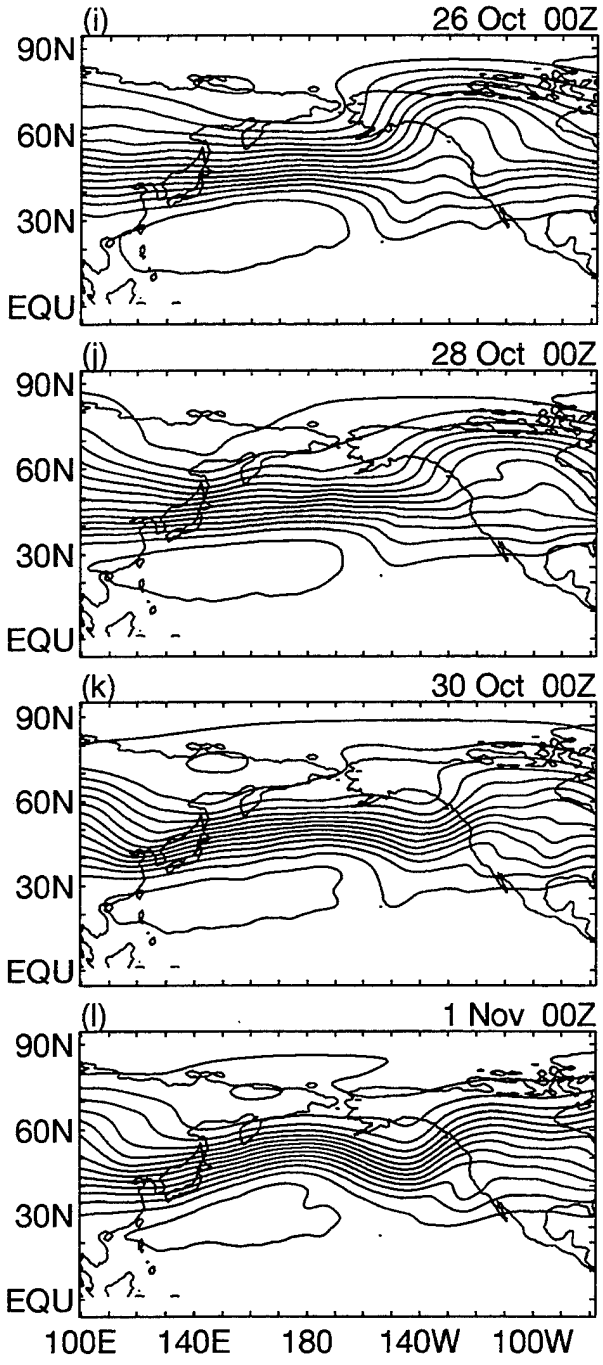

Figure 20. (Continued).

00Z, 10 October 1994: The ridges and troughs in all three NEGATIVE runs were very similar to those in the POSITIVE runs (Figures 12a, 13a, 14a). The F3 NEGATIVE run was slightly different in the central Pacific where there was a weak trough compared to a closed low in the same area in F3 POSITIVE run (Figure 14a).

00Z, 12 October 1994: A ridge had developed in the western Pacific, the shallow extended trough filled the central Pacific, and a ridge overlay western Canada. The three NEGATIVE forecasts had a similar trough-ridge pattern which was roughly similar to that in the corresponding POSITIVE runs.

00Z, 14 October 1994: All three NEGATIVE runs had a trough in the mid-Pacific, as in the POSITIVE runs. The troughs in the F1 POSITIVE and F1 NEGATIVE runs were more spread out than in the corresponding F2 and F3 runs.

00Z, 16 October 1994: The differences between the F1, F2, and F3 NEGATIVE runs were more noticeable. F1 had a well defined ridge tilted southwest to northeast in the western Pacific, a sharp trough in the central Pacific, and a broad ridge over western North America. F2 and F3 also had western Pacific ridges but with tilts opposite to that in F1.

After 14 October, these ridge-trough patterns in the three NEGATIVE runs became increasingly different from each other, primarily due to the

phase differences. For example, on 22 October 1994, the ridge that was over the northeastern Pacific - western North America region on 16 October in all three runs was about 15 degrees of longitude further to the east (west) in the F1 and F3 (F2) runs on 22 October. By the end of the runs on 2 November, all three NEGATIVE runs had developed some type of ridge in the central Pacific, a tough in the eastern Pacific, and a ridge over western North America.

5. Standard deviation of the NEGATIVE Runs

Figure 21 summarizes the results shown in Figures 17-19 by showing the standard deviation of the NEGATIVE runs with respect to their ensemble average for the NPNA region (20N-70N, 120E-80W). As expected from the results shown in Figures 17-20, the standard deviation of the NEGATIVE runs was small through 14 October increased sharply during 16-20 October and then leveled off at about 130 gpm. These results are very similar to the standard deviation of the POSITIVE runs (Figure 16).

6. Summary of NEGATIVE ensemble averages

In summary, the three NEGATIVE runs showed similar initial patterns of zonal and ridge-trough features across the NPNA region. The differences between the individual NEGATIVE runs were small initially, grew during 14-20 October and then leveled off or even declined during 20 October 2 November. Comparisons of the individual results (Figures 17-19) and the

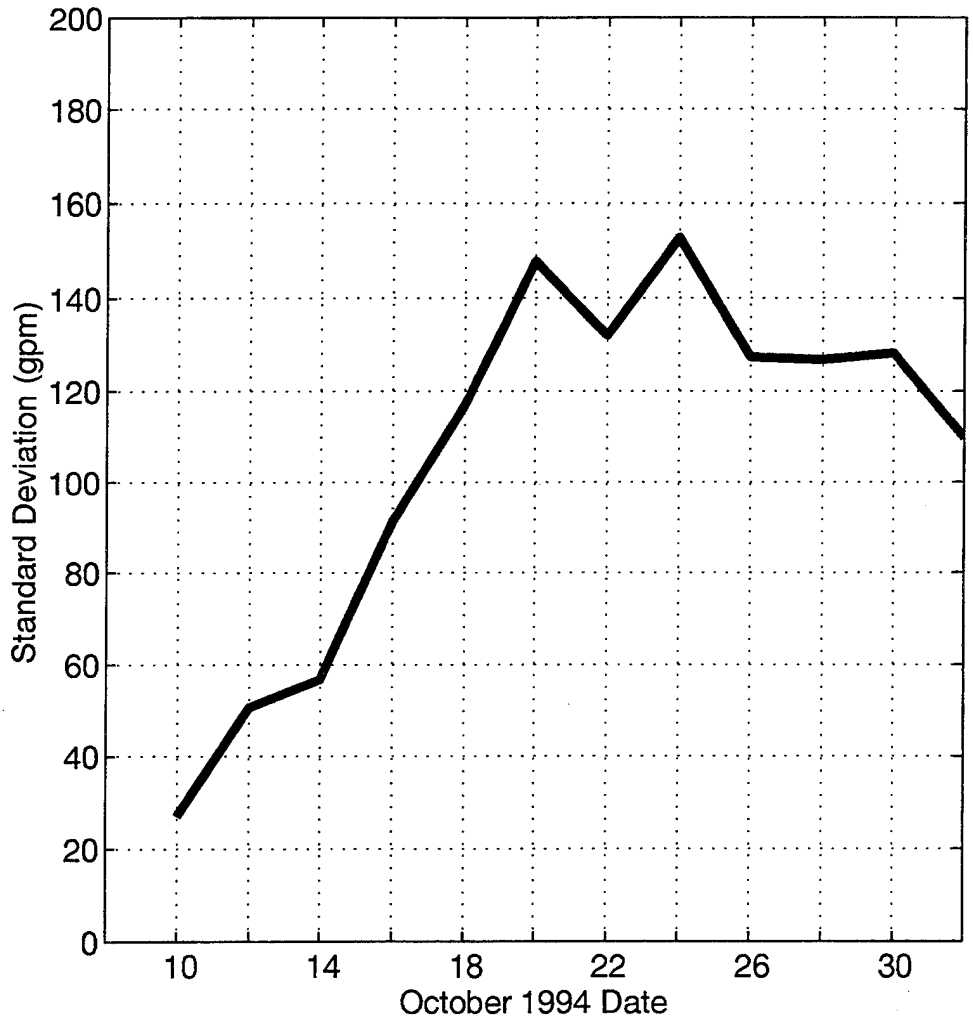

Figure 21. Standard deviation of the NEGATIVE runs in the NPNA region (20N - 70N, 120E - 80W).

ensemble average results (Figure 20) show that the ensemble average generally gives a good representation of the major NPNA features. The same is true for other regions of the world (not shown). Comparisons of the POSITIVE and NEGATIVE runs show that the results were initially similar but developed quite differently after a few days. These differences are discussed further later in this chapter.

7. Conclusion for prerequisite 4

Ensemble averaging the three forecast POSITIVE and NEGATIVE runs produced results that were very similar to the individual runs until about 16 October 1994. From then on, the ensemble averaging procedure averaged features that were, at times, out of phase or that existed in only one or two of the runs. However, the ensemble average still contained the common major features of the individual runs, although in a somewhat weakened form. The standard deviations of the POSITIVE and NEGATIVE runs in the NPNA region show that the F1, F2, and F3 runs diverged from each other, as expected for forecasts starting from quite different intial conditions. However, these standard deviations leveled off at moderate levels by the middle of the ensemble averaging period. In addition, the standard deviations tended to be several times smaller than the differences between the POSITIVE and NEGATIVE runs in the NPNA region, as will be shown in

the following section. Thus, we concluded that the ensemble averaged fields were useful representations of the individual forecast fields.

The POSITIVE ensemble averaged 200 mb height fields represent, in part, the effects of the model's representation of Seth on the upper-troposphere in the NPNA region. However, as discussed earlier in this chapter, Seth evolved differently in the three POSITIVE runs, with the simulation of Seth being least realistic in the F1 POSITIVE run and most realistic in the F3 POSITIVE run. This suggests that the ensemble average representation of Seth's remote effects may be less realistic than the effects derived from the most realistic run, F3 POSITIVE. This issue is discussed further in Chapter IV. However, the overall similarity of the ensemble average to the individual results led us to use the ensemble average results when estimating the teleconnections due to Seth. The remaining results, which examine the hypotheses described in Chapter I, will primarily be derived from the ensemble averaged forecasts.

F. HYPOTHESIS 1 - TELECONNECTIONS ASSOCIATED WITH SETH

Comparison of Figures 12-14 with Figures 17-19, or of Figure 15 with Figure 21, shows that the 200 mb height fields for the POSITIVE and NEGATIVE runs became increasingly different as the forecast time increased. These differences represent the teleconnection impacts of Seth. They are more clearly seen by calculating the ensemble average 200 mb

height response, which is the POSITIVE ensemble average height for a particular time minus the NEGATIVE ensemble average height for that time. As in the previous section, and as in Woll (1993) and Springer (1994), our analysis of the model's response to Seth is focused on the NPNA region.

1. Ensemble average differences in 200 mb geopotential height

Figure 22 shows the POSITIVE - NEGATIVE ensemble average differences in the 200 mb height fields. We tracked the evolution of the height differences in Figure 22 by identifying the major difference features, labeling them with the symbols H and L (for highs and lows), and numbering them according to the order in which they first appeared. When a major difference feature split into two features, or when two major difference features merged, the two parent, or daughter, features were labeled "a" and "b" (e.g., L1a and L1b). The five major height difference features of interest in Figure 22 are listed below in the order of their appearance.

H1, the first major positive difference, which appeared just south of southern Japan on 10 October 1994 (Figure 22a);

L1, the first major negative difference, which appeared southeast of Kamchatka on 11 October 1994 (cf. Figure 22b);

H2, the second major positive difference, appeared south of Alaska on 11 October 1994 (cf. Figure 22b);

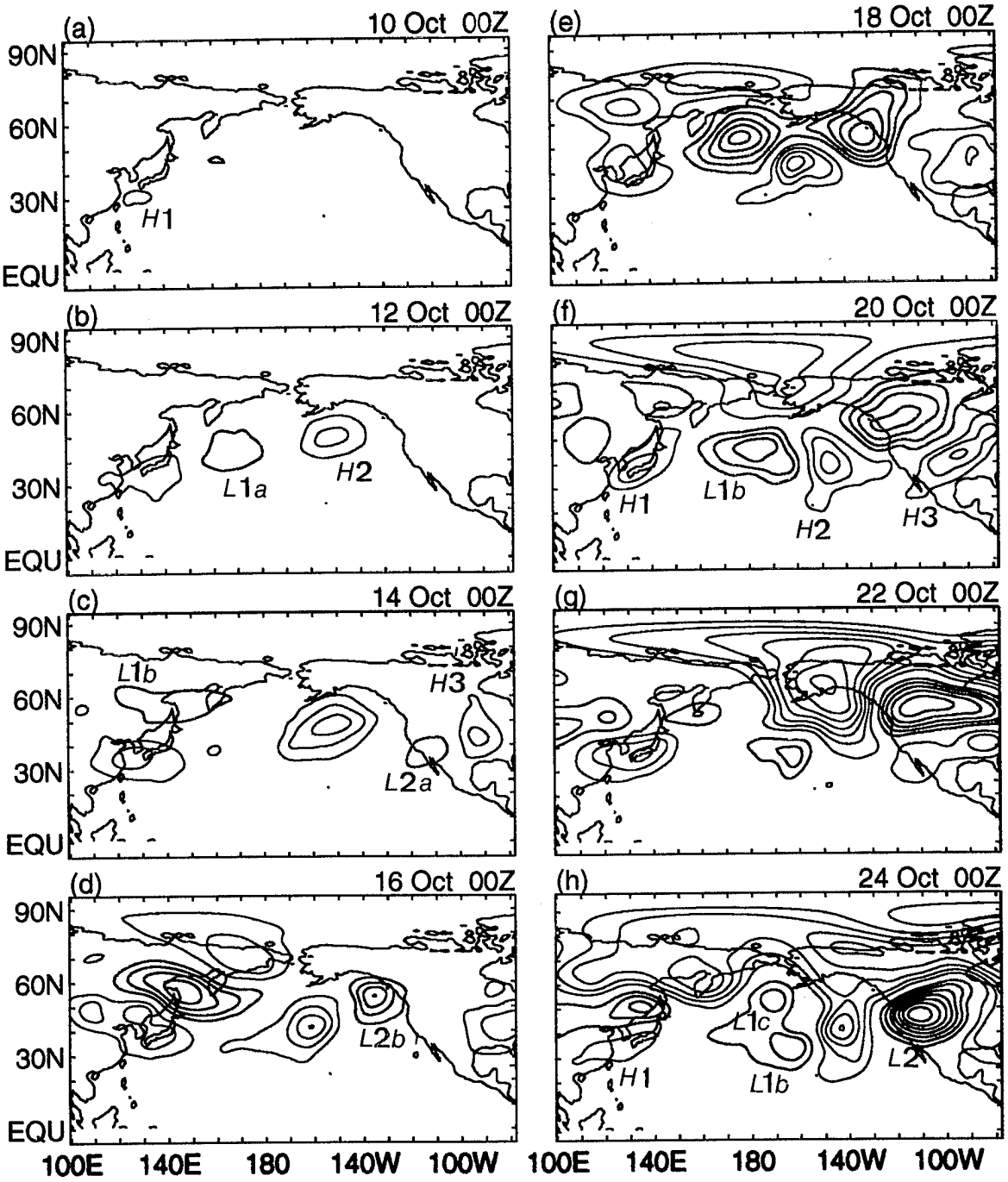

Figure 22. EA differences (POSITIVE - NEGATIVE) in heights at selected times. Red (blue) contours represent positive (negative) height differences; contour interval is 50 gpm. Zero contour omitted.

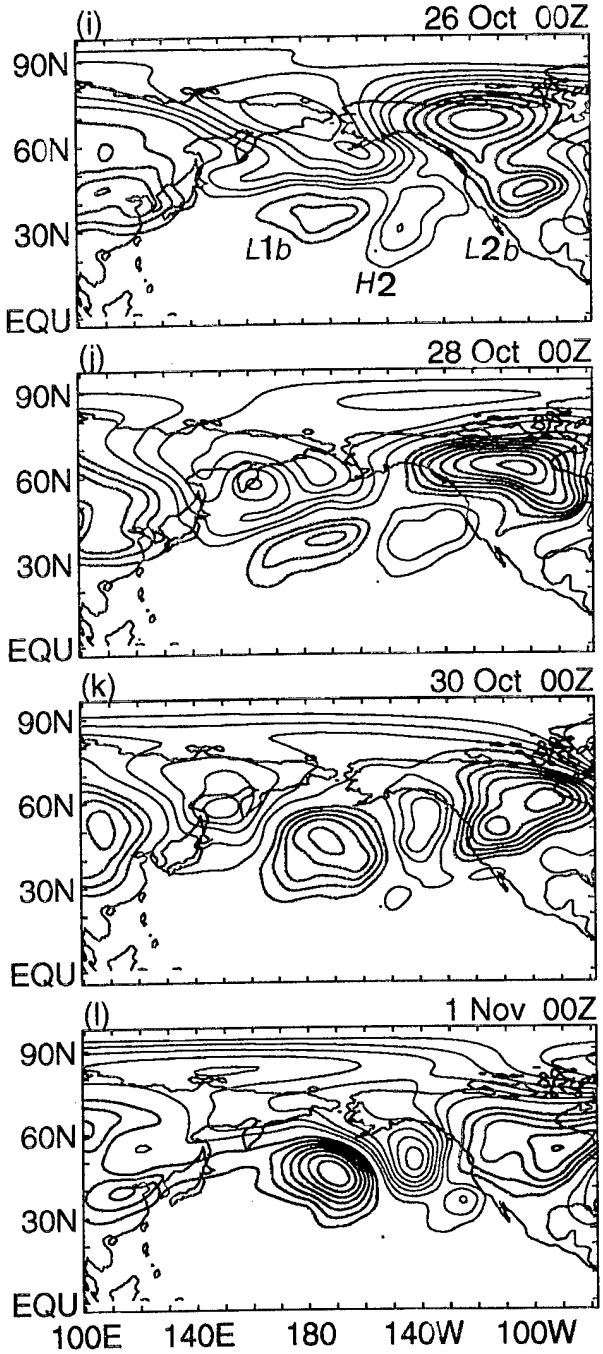

Figure 22. (Continued).

L2, the second major negative difference, which appeared as a very weak low just off the west coast of North America on 13 October 1994 (cf. Figure 22c, d);

H3, the third major positive difference, appeared over central North America on 13 October 1994 (cf. Figure 22c).

H1 formed south of Japan slightly, about 775 km northeast of where the ensemble average POSITIVE runs positioned Seth. H1 then strengthened and expanded to the east-northeast (Figure 22a-e) until 20 October 1994, when it contracted to a central location over southern Japan where it remained for the rest of its existence (Figure 22f-h).

Soon after H1 formed, L1a formed to the east-northeast of H1 (Figure 22b) and moved to the east-northeast, where it was absorbed by L1b.

H2 formed to the east-northeast of L1a and south of Alaska on 11 October 1994 (Figure 22b). Throughout its existence, H2 stayed in the general northeast Pacific-southern Alaska region where its strength increased, reaching over 150 gpm during 14-22 October 1994 (Figure 22c-h).

L2 formed on 13 October 1994 off the west coast of North America but was too weak to appear in Figure 20 until 16 October 1994 (Figure 22 d). It moved slowly northward and eastward into North America, reaching

the Great Lakes region by 2 November. It reached a peak strength of (-) 400 gpm on 00Z, 28 October 1994 (Figure 22j).

H3 first appeared on 13 October 1994 over central North America (cf. Figure 22c). It broadened and slowly moved to the east and slightly to the south (Figure 22c-l). H3 reached a maximum strength of over 200 gpm on the 19 October 1994 (not shown). On 30 October 1994, H3 merged with a higher-latitude height difference and formed a ridge over eastern North America.

L1b, the large, weak low just east of the Sea of Okhotsk on 14 October 1994 (Figure 22c), grew rapidly and eventually absorbed L1a. L1b moved east-southeastward into the central North Pacific during 17-24 October 1994 (Figure 22e-h).

L1c formed over Kamchatka on about 28 October 1994 (Figure 22j). It then deepened rapidly and moved southward into the central North Pacific. By 29 October 1994, it had absorbed L1b and deepened to about (-)250 gpm (Figure 22k). By 2 November, it had deepened to (-)350 gpm (Figure 22l).

2. Conclusion for hypothesis 1

The strong and persistent height differences shown in Figure 22 represent a significant teleconnection response to Seth, which supports Hypothesis 2.

The pattern of highs and lows shown in Figure 22 are also seen in the corresponding ensemble averaged SLP difference fields (not shown). This indicates that the response to Seth is equivalent barotropic, as found in many other teleconnections studies (Tribbia 1991, Woll 1993, Springer 1994). The overall 200 mb height response pattern (Figure 22) is also similar to the northern summer teleconnection response to tropical western Pacific heating anomalies found by Nitta (1987) (Figure 6).

Springer (1994) found that the 200 mb height response to typhoon Robyn first developed in the western part of the NPNA region, along the East Asian jet. He also found that the area in which the largest height differences occurred was located progressively farther to the east, and that eastward propagation speeds of the site at which new height differences formed, and of the area in which the largest height differences occurred, were much faster than the eastward propagation speeds of the height differences themselves. This suggested that the eastward motion of the teleconnection response was dominated by Rossby wave group propagation, occurring at relatively fast eastward speeds. The individual height differences moved at a much slower eastward phase speed. Figure 22 shows similar group and phase propagation results for the response to Seth.

Figure 22 also shows that most of the growth in the individual height differences occurred well after the demise of Seth and far from Seth.

Springer (1994) had a similar finding. This suggests that the growth of the individual height differences was not a simple and direct response to the heating differences associated with Seth and/or to simple Rossby wave energy propagation.

G. HYPOTHESIS 2 - THE JET'S ROLE IN TELECONNECTIONS

Hypothesis 2 proposes that the development of the teleconnection response is strongly influenced by the waveguiding and amplification effects of the midlatitude jet. This can be expressed in terms of the following components:

- the teleconnection response, defined by the 200 mb height differences, has a characteristic relationship to the jet.
- the jet acts as a waveguide for QG wave energy propagation; and
- areas of potential BTI associated with the jet may be important wave energy sources (Woll, 1993).

The jets were identified from the ensemble averaged 200 mb U and V winds from the POSITIVE runs. The jet axes were defined as the regions in which the total wind speed was greater than or equal to 30 m/s. We used the POSITIVE runs to identify the jets because these runs reflect the conditions under which the response to Seth developed.

1. 200 MB Height differences and the jets

Figure 23 is the same as Figure 22 except that the 200 mb jet axes have been superimposed over the ensemble average POSITIVE - NEGATIVE 200 mb height differences.

The first positive height difference, H1, appeared on 9 October 1994 south of Japan and the east Asian jet (Figure 23a). By 10 October 1994, H1 and the jet had shifted to the north, with the jet occurring along the north side of H1.

By 14 October 1994, the jet had strengthened, with H1 just south of the jet and L1b at a similar longitude and just north of the jet. H2 was centered just south of the jet in the central North Pacific. From east Asia eastward to the east coast of North America, the jets arced northward, with large height differences on or just south of the arcs.

This pattern persisted through 18 October 1994 (Figure 23d-e), but with an intensification of the negative height differences which tended to be located on the north sides of the jets (e.g., over the North Pacific on 18 October 1994, Figure 23e).

This pattern of positive differences on the south side of the jet and negative differences on the north side was also seen by Woll (1993) and Springer (1994). However, this pattern is generally less clear in our study after 18 October 1994 (Figure 23f-l), except for the leading edge (i.e., the

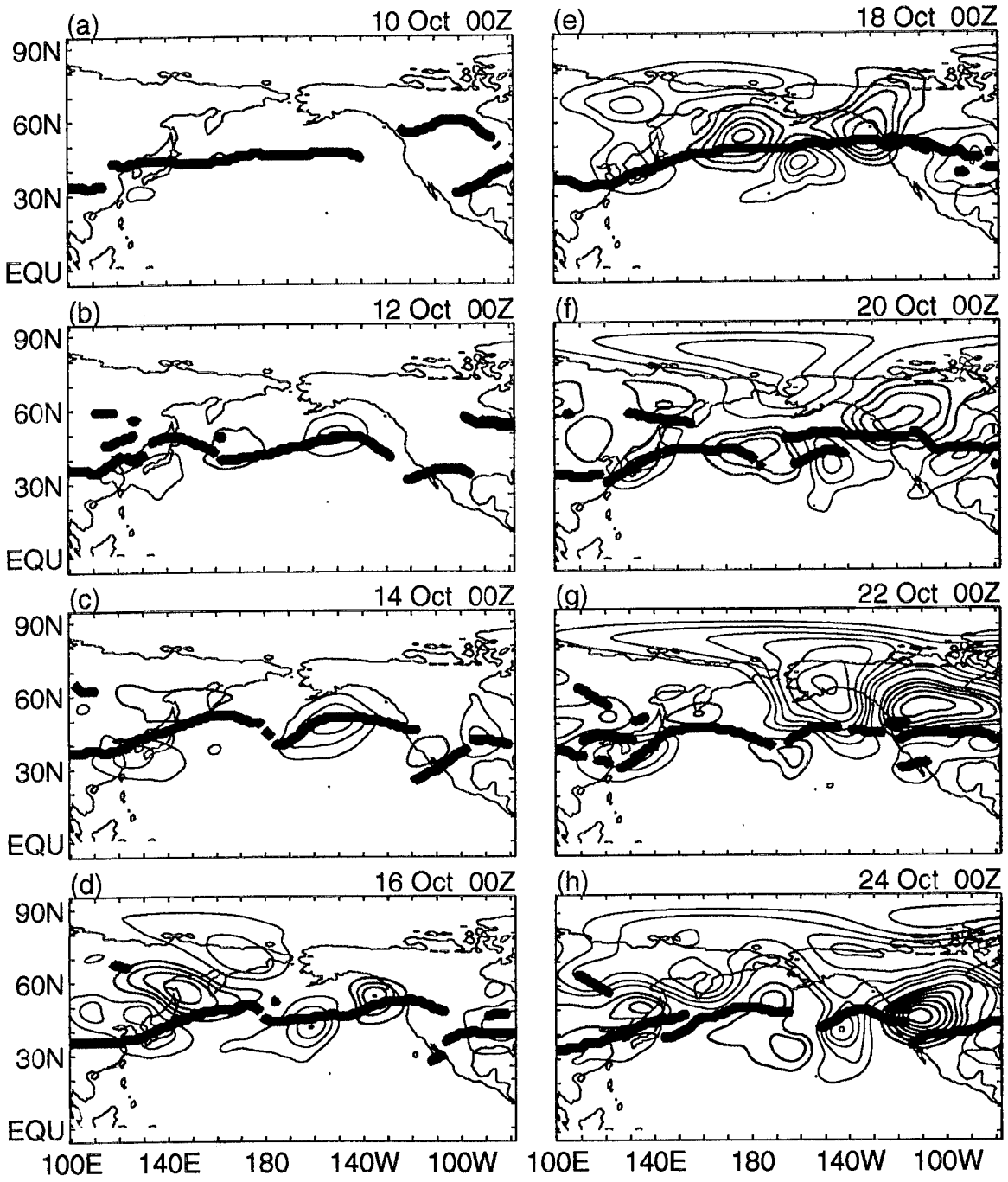

Figure 23. EA differences (POSITIVE - NEGATIVE) in heights at selected times. Red (blue) contours represent positive (negative) height differences; contour interval is 50 gpm. Zero contour omitted. Solid thick lines show jet axes (> 30 m/s).

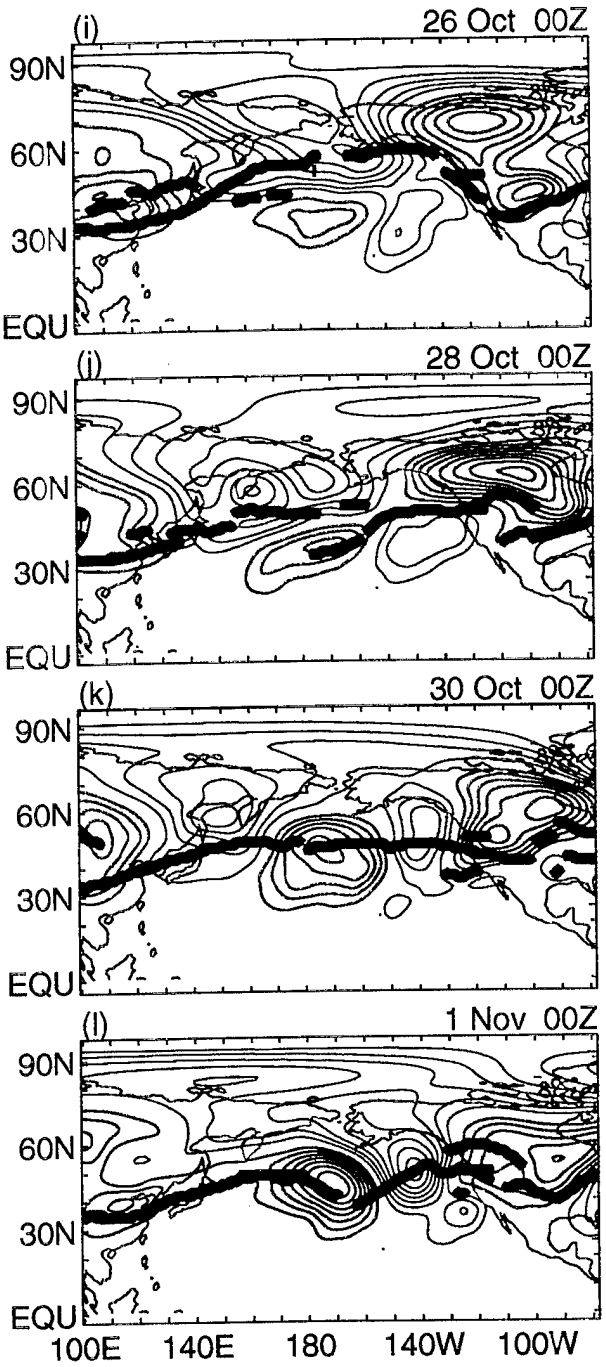

Figure 23. (Continued).

eastern portion) of the response. This response is evident over North America on 20-29 October 1994 (Figure 23f-j).

2. The 200 mb wave energy response

In this section, we analyze the quasi-geostrophic (QG) wave activity flux vectors (Plumb 1985) associated with the 200 mb height response to Seth. Figure 24 shows the wave activity flux vectors calculated from the ensemble average 200 mb height differences in Figure 23 with jet locations superimposed.

The following discussion is based on Figure 24.

10 October 1994: H1 and L1a were still weak, so the wave activity flux vectors were also weak.

12 October 1994: The flux vectors were still relatively weak, with the strongest ones near H1 where they were directed eastward and roughly aligned with the east Asian jet. The divergence of these vectors indicated a wave energy source near H1. The vectors near H2 in the northeast Pacific also pointed eastward and parallel to the jet in that region.

14 October 1994: The strongest vectors were roughly aligned with the local jets. Wave energy sources were indicated by divergent vectors over the central North Pacific, the northeast Pacific along the jet, and over the western and central US near the jet.

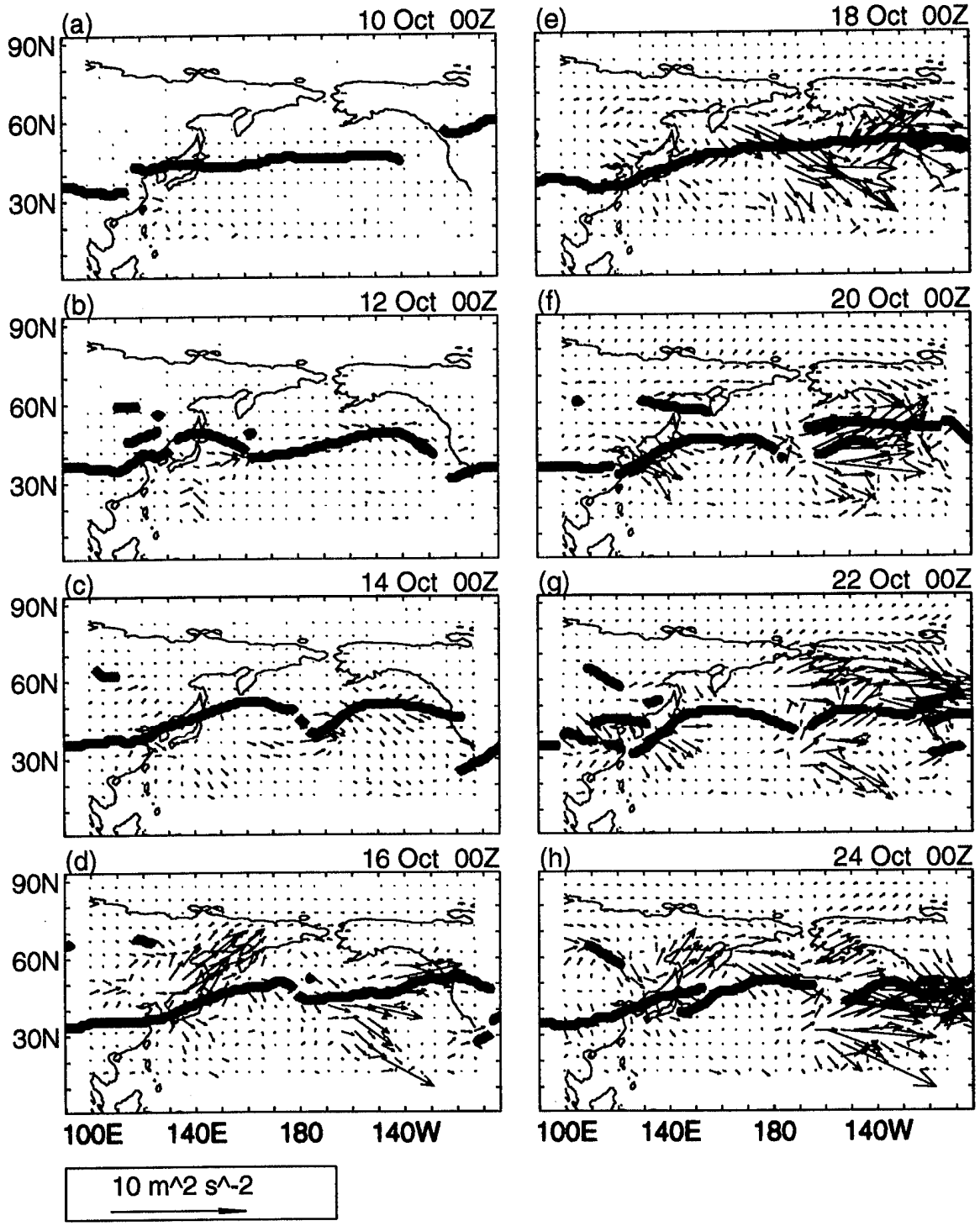

Figure 24. EA differences (POSITIVE - NEGATIVE) in QG wave activity fluxes at selected times. Solid thick lines show jet axes (>30 m/s).

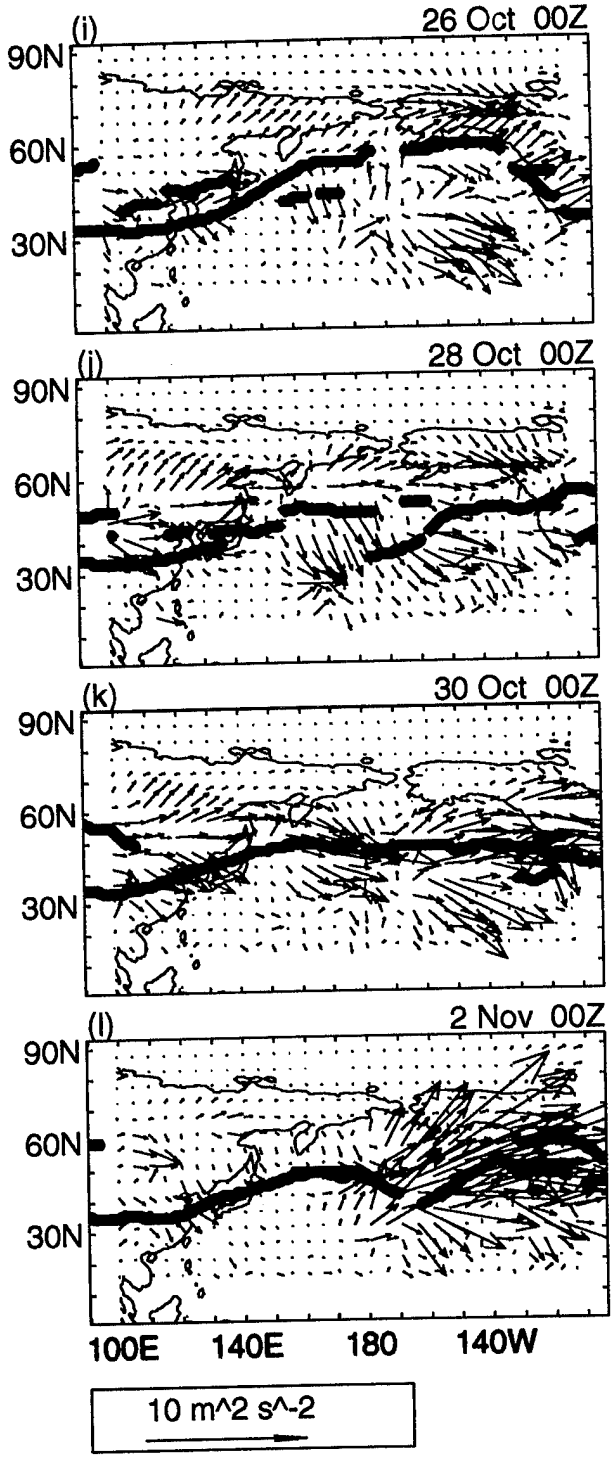

Figure 24. (Continued).

16 October 1994: The magnitude of the vectors increased substantially but they were still roughly parallel to the jets. There were large sources just north of the east Asian jet and near the jet over the North Pacific.

18-24 October 1994: The pattern seen on 16 October 1994 persisted with a general eastward propagation of the strongest source regions (e.g., to the northeast Pacific on 24 October 1994).

26-28 October 1994: The vector patterns were smaller scale but with the major energy sources still associated with the jets.

30 October 1994 - 2 November 1994: The vectors showed relatively large scale patterns with sources associated with the jets. On 2 November 1994, there was a large source just downstream of the east Asian-North Pacific jet, with large poleward and equatorward components of energy propagation in the exit of this jet and along the arcing jet over the northeast Pacific.

In summary, the wave activity flux vectors indicate the energy associated with the response to Seth propagated approximately along the midlatitude jets. The general vicinity of the jets were important sources of energy for the response. Similar results were found by Woll (1993) and Springer (1994). The growth of the height responses through time, with the areas of growth propagating eastward faster than the height responses

themselves (see the discussion of Figure 22), indicates that the energy propagation (see the flux vectors, Figure 24) was faster than the phase propagation.

3. Barotropic instability

The association of the wave energy sources with the jets (Figure 25) suggests that BTI along the jet flanks may play a role in providing energy to the 200 mb height response (Figure 22). Thus, we calculated the Rayleigh-Kuo (Kuo 1949) condition for barotropic instability for the ensemble average POSITIVE - NEGATIVE 200 mb wind (see Chapter II). Figure 25 shows the regions where this condition is met (i.e., $\beta - U_{yy} = 0$).

The areas where the potential for barotropic instability existed were generally along the jet flanks (e.g., Figure 23a-b). However, these regions were very extensive, so that it is difficult to identify a clear and simple association of the energy source regions (Figure 4) with barotropically unstable regions. That is because the sources were always in or near regions of potential instability. But since these regions were so common and extensive, they were equally well associated with energy sink regions and with neutral regions.

4. Conclusion for hypothesis 2

The wave energy fluxes indicate that the response was guided by the jets and received energy from the jets through barotropic instability

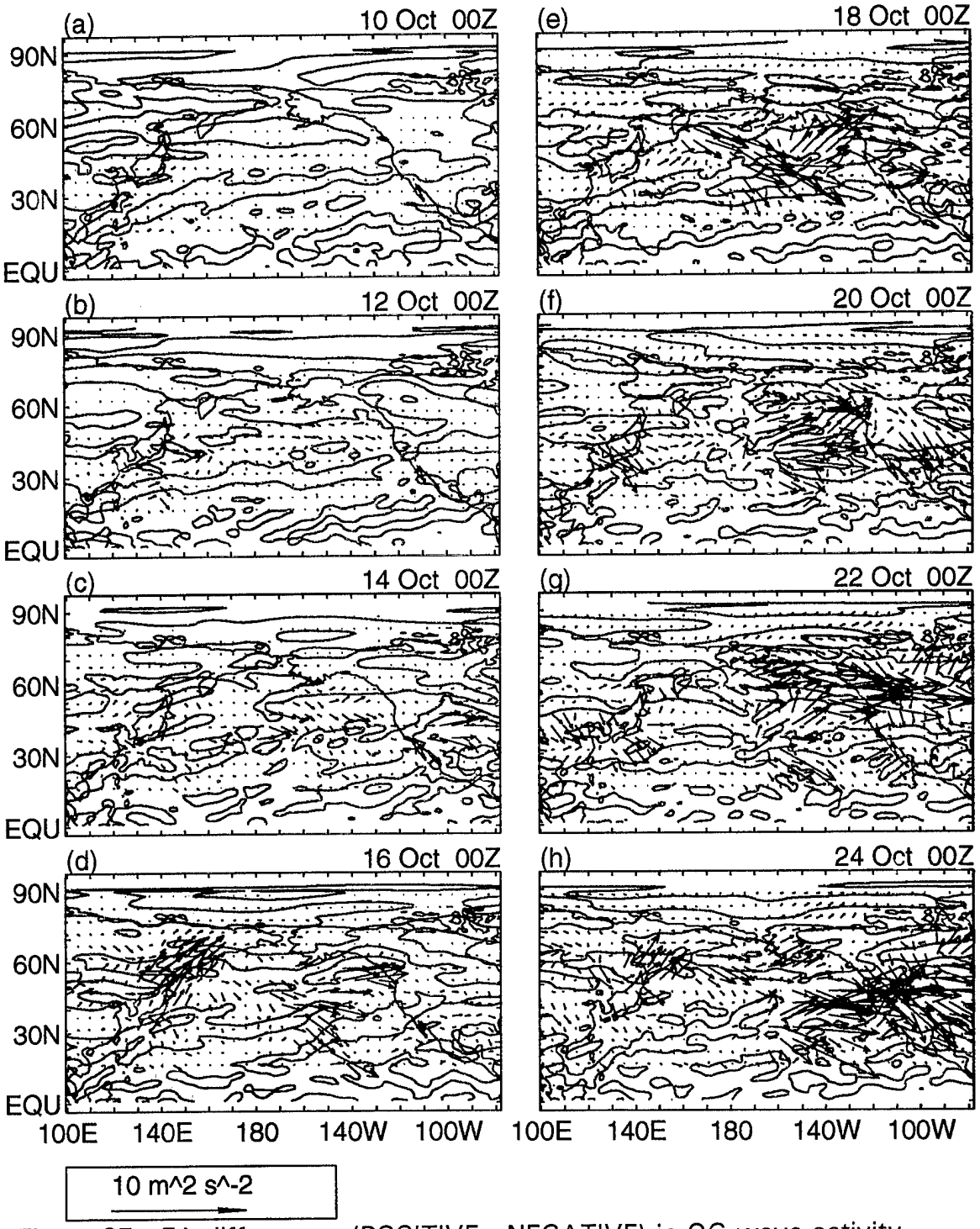

Figure 25. EA differences (POSITIVE - NEGATIVE) in QG wave activity fluxes at selected times. Blue lines indicate area of potential BTI ($\beta - u_{yy} = 0$).

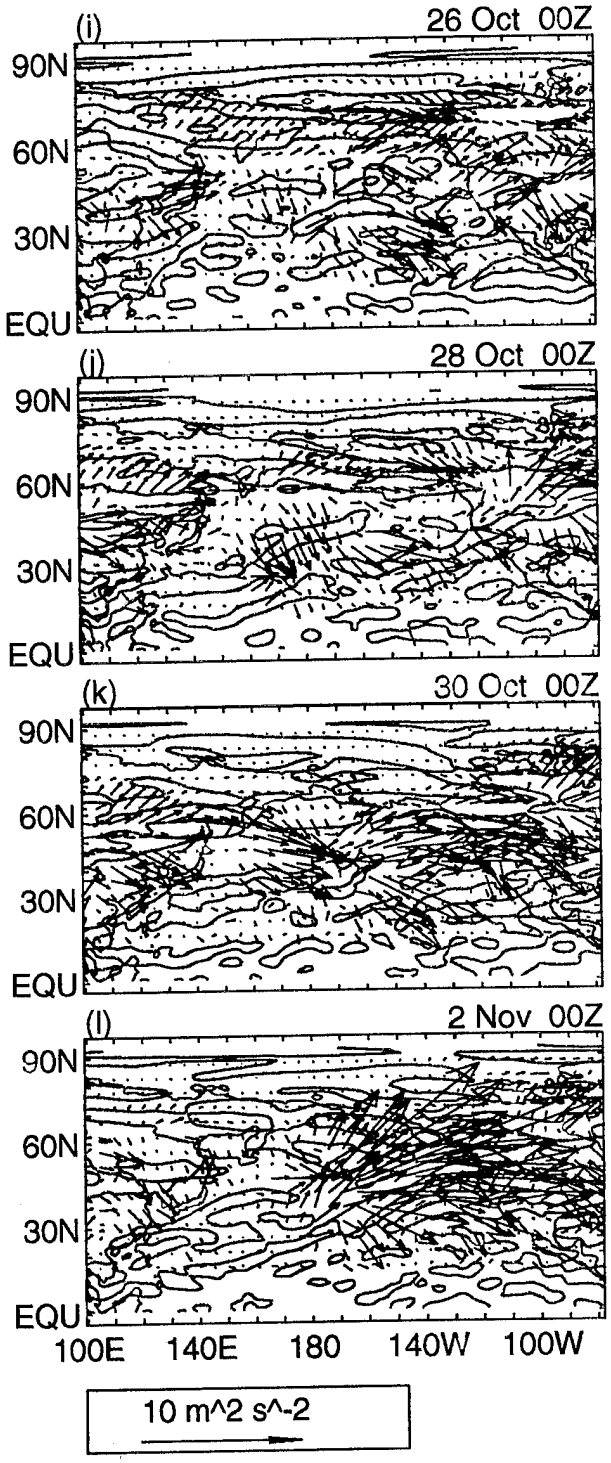

Figure 25. (Continued).

mechanisms. However, a second test, the Rayleigh-Kuo condition for barotropic instability analyses, gave no clear support or challenge to this hypothesis. Thus, this hypothesis is partially supported by these results. The instability analyses from Woll (1993) and Springer (1994) were also somewhat equivocal, but less so than for our results. This equivocation probably reflects the weakness of the Rayleigh-Kuo condition as a diagnostic tool, especially when applied to realistically wavy flows such as ours.

H. HYPOTHESIS 3 - THE ROLE OF ROSSBY WAVE SOURCES IN TELECONNECTIONS

In this section, we investigate the possibility that Rossby wave sources contributed to the teleconnections caused by Seth.

1. The Rossby wave source

The ensemble average POSITIVE - NEGATIVE 200 mb divergence field (Figure 26) shows the upper-level divergence difference that resulted from the presence and location of Seth in the POSITIVE runs. This divergence difference is also a factor in producing the POSITIVE - NEGATIVE differences in the Rossby wave sources (Figure 27). The 200 mb height responses to Seth over the western North Pacific are shown in Figure 28. Comparisons of Figures 26-28 give an indication of how Seth and its associated Rossby wave sources may have been related to the initiation of

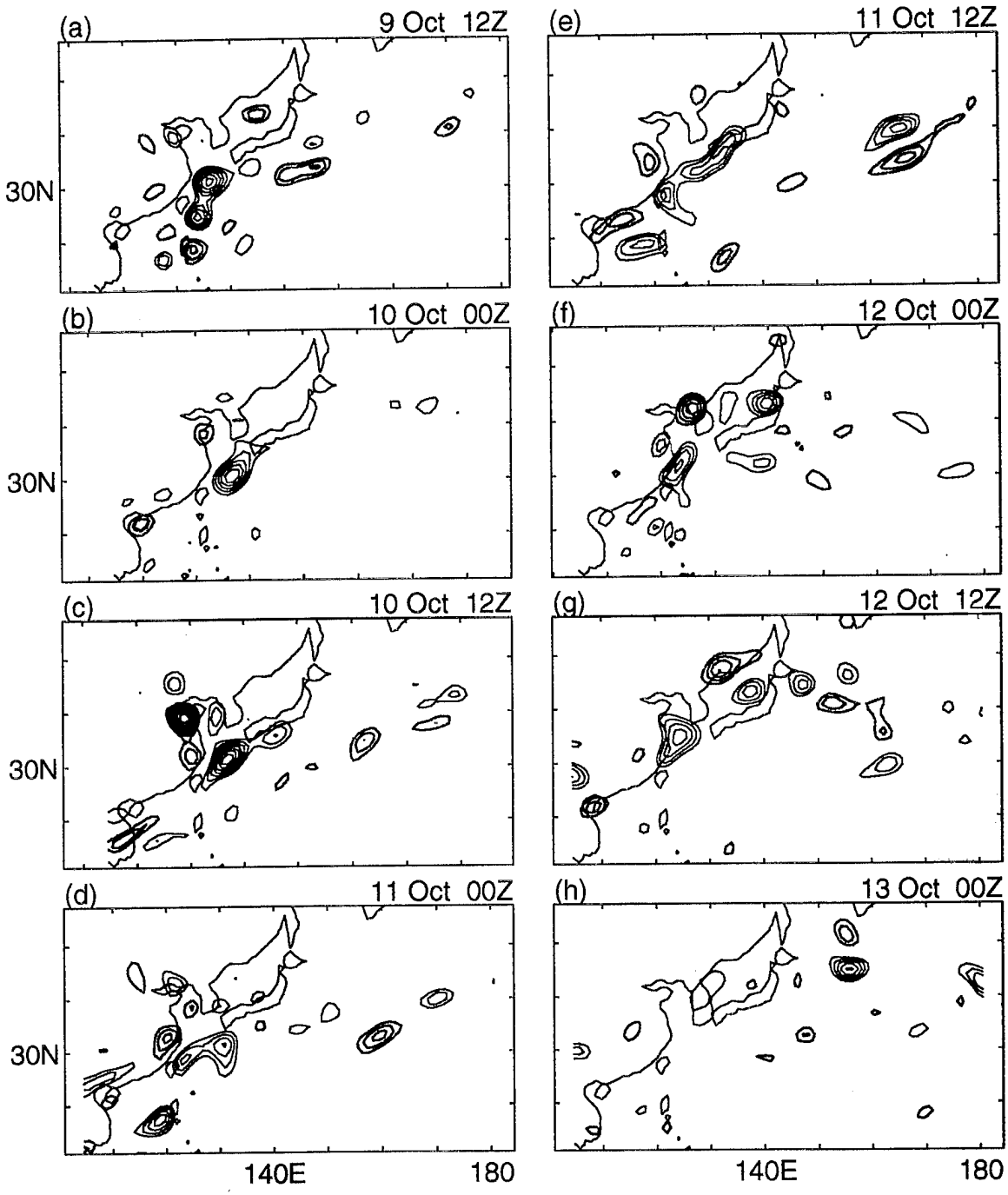

Figure 26. EA differences (POSITIVE - NEGATIVE) in 200 mb divergence at selected times. Red (blue) contours represent positive (negative) divergence differences; contour interval is 5 x 10^{-6} s^{-1}.

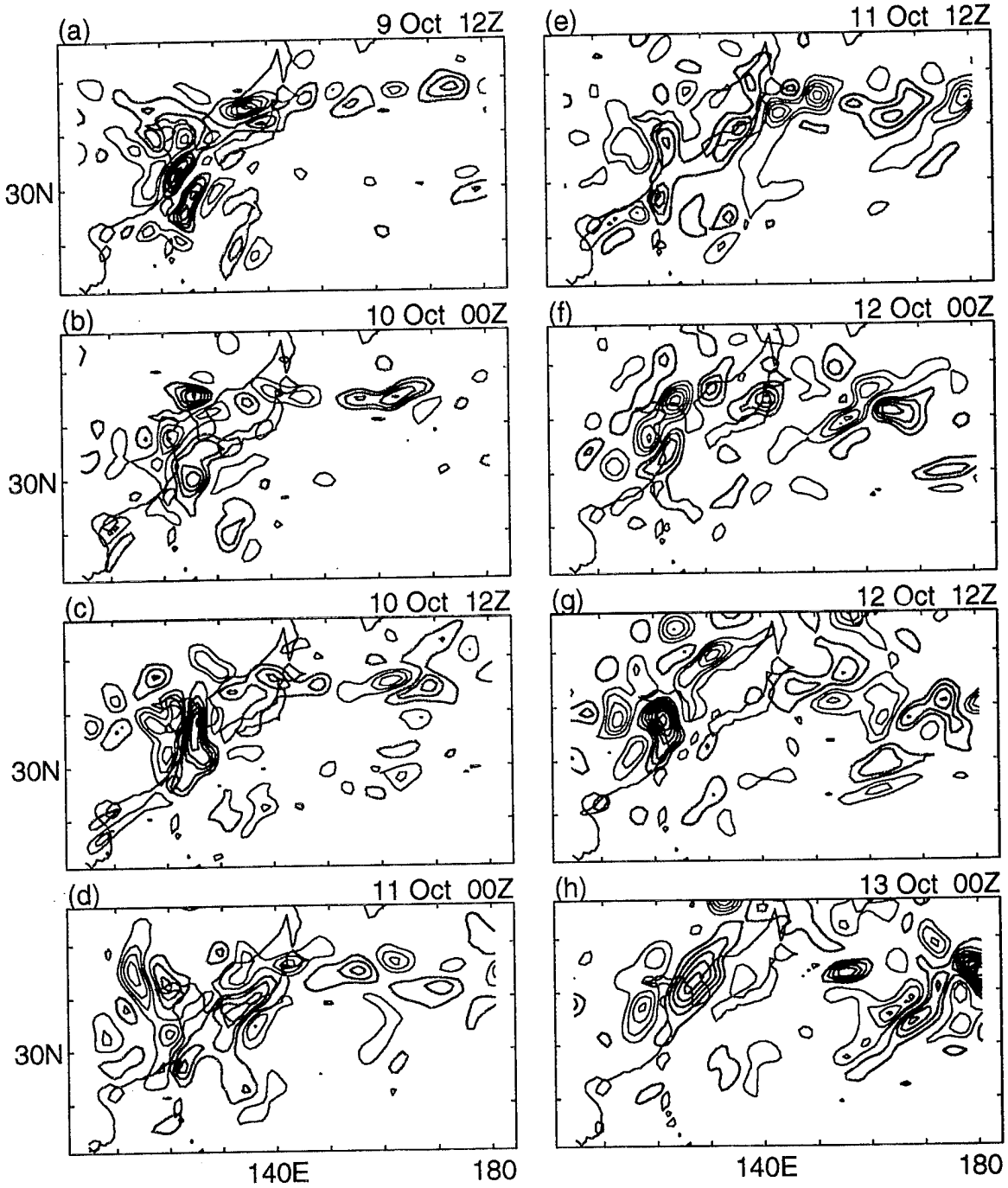

Figure 27. EA differences (POSITIVE - NEGATIVE) in 200 mb Rossby wave sources at selected times. Red (blue) contours represent positive (negative) source differences; minimum contour is .05 x 10^{-8} s^{-2}; contour interval is .05 x 10^{-8} s^{-2}.

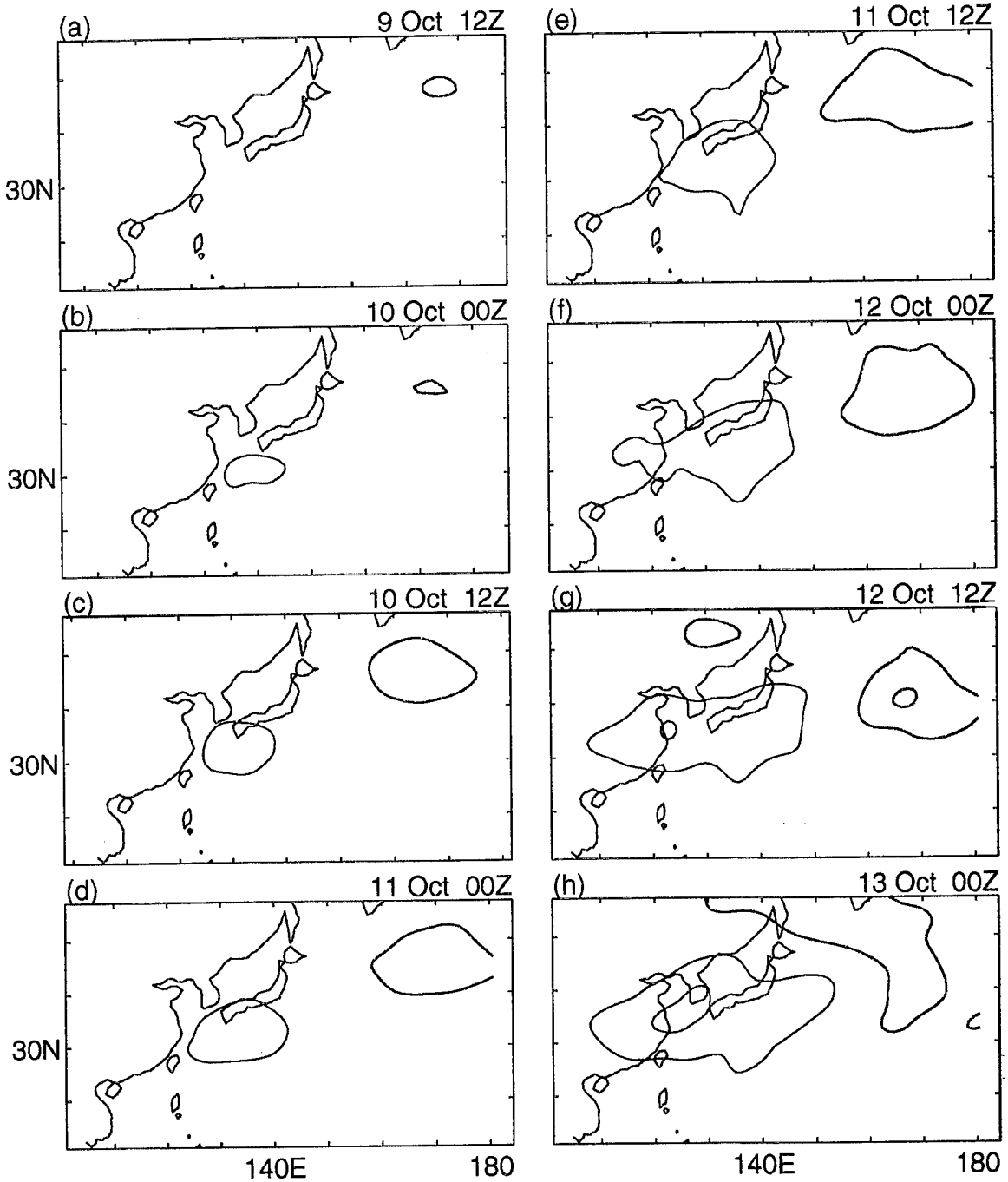

Figure 28. EA differences (POSITIVE - NEGATIVE) in heights at selected times to correspond with the times shown in subsequent plots. Red (blue) contours represent positive (negative) height differences; contour interval is 50 gpm. Zero contour omitted.

the 200 mb height response. The following description of these fields refers to these three figures.

12Z, 9 October 1994: Seth was just east of Taiwan, there was a negative source difference region east and north of Taiwan, and a weak positive height response just northeast of Taiwan (too weak to show up in Figure 28a).

00Z, 10 October 1994: Seth was located east and north of Taiwan, there was a negative source difference region just north of that which extended northward to Korea and southern Japan. The height response was collocated with the negative source.

12Z, 10 October 1994: Seth was located between Taiwan and Japan, with the negative source difference and the height response at and to the north of this area.

00Z, 11 October 1994 - 00Z, 13 October 1994: Similar relationships between the locations of Seth, the negative Rossby wave source difference, and the height response persisted through this period, as Seth travelled north and northeastward over the Sea of Japan.

The positive height difference corresponds to a negative vorticity difference which is consistent with a negative Rossby wave source difference. Thus, the collocation of patterns in Figures 26-28 suggest that the height response (figures 22 and 28) may have been initiated by the

Rossby wave source mechanism. That is, the upper-level divergent wind associated with the occurrence of Seth in the POSITIVE runs may have generated a Rossby wave response through the advection of absolute vorticity by the divergent wind and through vortex stretching.

2. The Rossby wave source components

To examine this possibility further, we calculated the ensemble average POSITIVE - NEGATIVE differences in this advection term (ADVDIV, Figure 29) and the stretching term (Figure 30). The corresponding differences in the divergent wind, with jets overlaid, are shown in Figure 31. These wind differences and jets give a rough indication of the areas in which the advection term was strong. The advection term (Figure 29) and stretching term (Figure 30) had the same magnitude in the general vicinity of Seth (Figure 26). But the stretching term was generally about twice as large in the area of the negative source (Figure 27) previously identified with the initiation of the height response near southern Japan (Figure 28). This suggests that the major initiation was caused by the vortex stretching associated directly with Seth, but that the advection by the divergent wind was also important in this initiation.

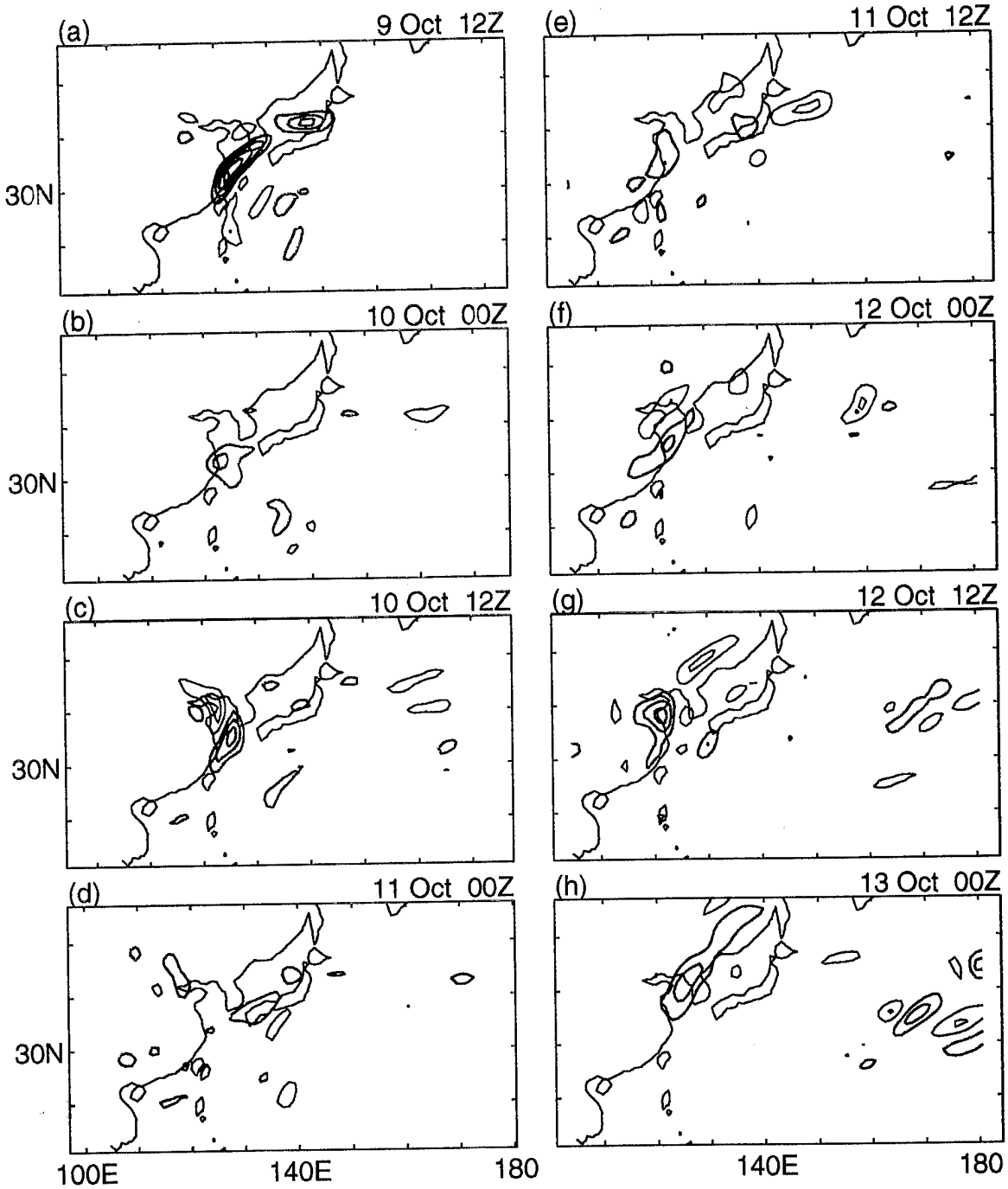

Figure 29. EA differences (POSITIVE - NEGATIVE) in 200 mb Rossby wave source ADVDIV component at selected times. Red (blue) contours represent positive (negative) ADVDIV differences; minimum contour is .05 x 10^{-8} s^{-2}; contour interval is .05 x 10^{-8} s^{-2}.

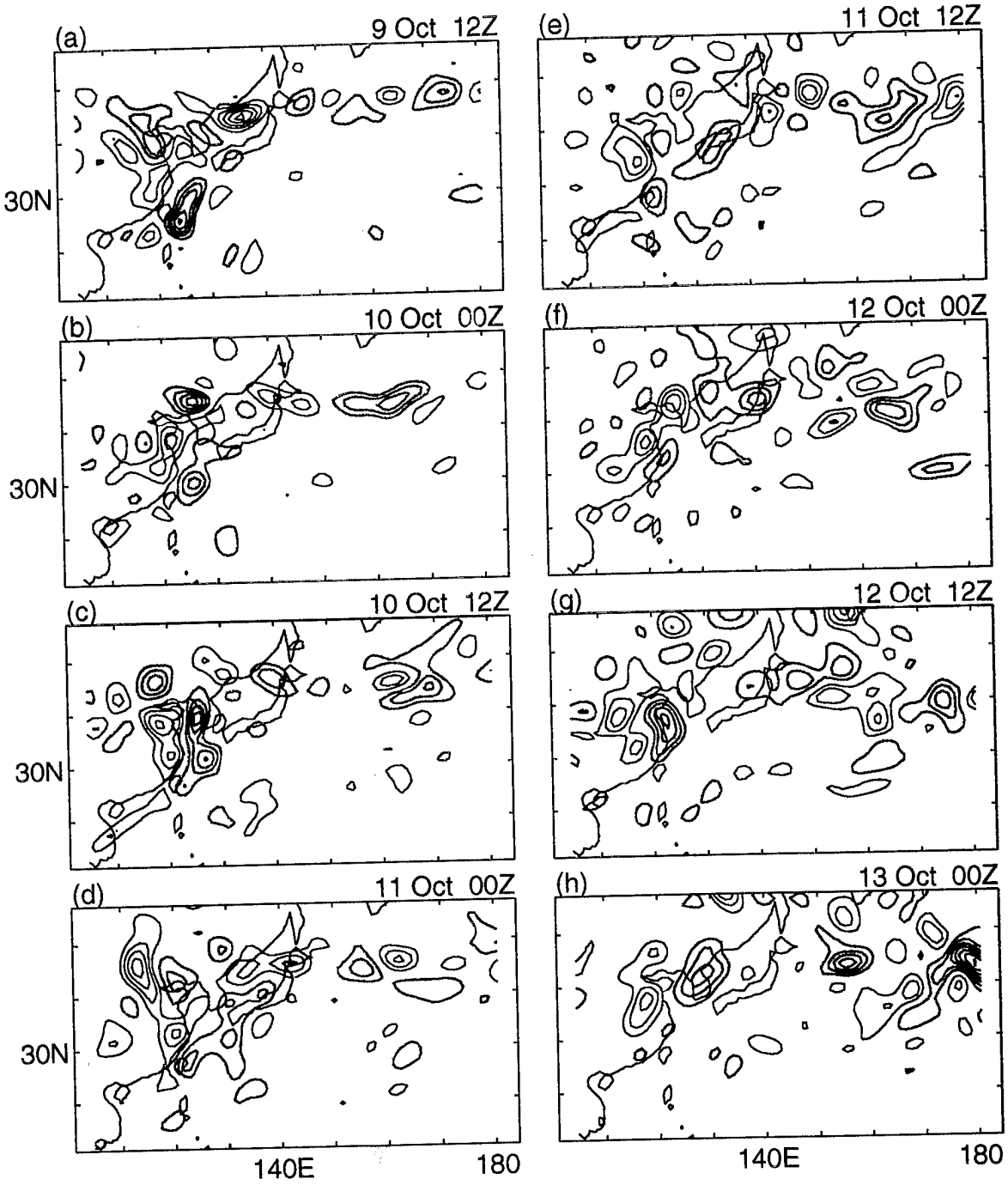

Figure 30. EA differences (POSITIVE - NEGATIVE) in 200 mb Rossby wave source stretching component at selected times. Red (blue) contours represent positive (negative) stretching differences; minimum contour is .05 x 10^{-8} s^{-2}; contour interval is .05 x 10^{-8} s^{-2}.

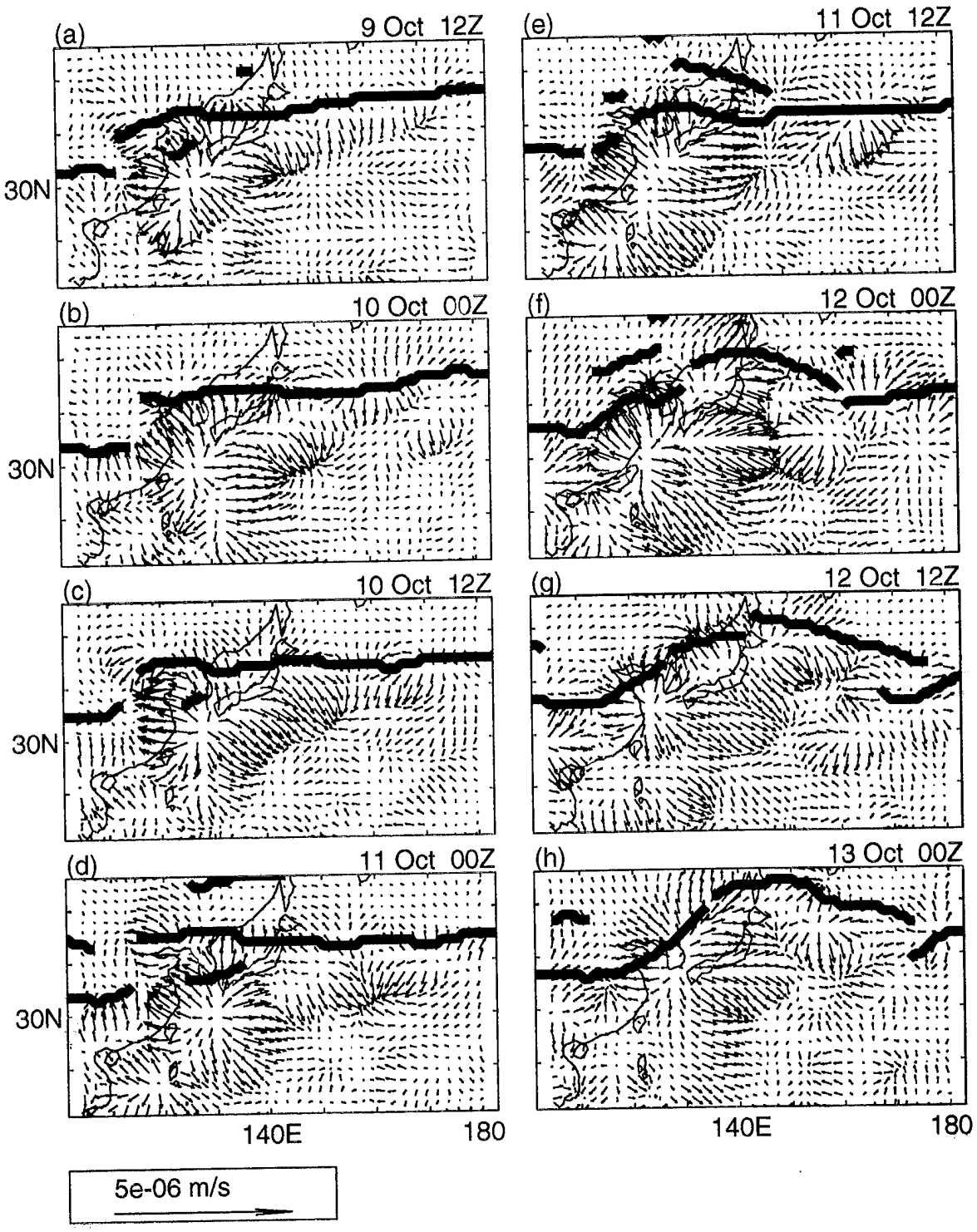

Figure 31. EA differences (POSITIVE - NEGATIVE) in 200 mb divergent winds. Solid thick lines show jet axes (> 30 m/s).

3. Comparison of the Rossby wave sources for Yuri, Robyn and Seth

The Rossby wave source results for Seth show that this wave generation process played a role very similar to that seen in the development of the wave responses to Yuri and Robyn (Springer 1994). Comparisons between the Rossby wave source differences can be made by referring to Springer (1994). The following is a list of figure numbers that refer to the Rossby wave source and 200 mb height difference figures for Yuri, Robyn, and Seth.

	Spinger (1994)		
	Yuri	Robyn	Seth
Figure numbers for Rossby wave source:	36	42	26
Figure numbers for 200 mb height differences:	37	43	25

For all three storms, negative source difference features occurred near and especially to the north of the storm, along the south flank of the east Asian jet. The initial 200 mb height differences were positive and developed over these negative source differences. The sign of this initial wave response was consistent with the sign of the source difference. That is, a negative source corresponded to a height response with negative vorticity. This suggests that the phasing of the wave response was governed, at least initially, by the sign of S. In turn, the sign of S was

determined by the sign of the divergent wind and the sign of the relative vorticity gradient along the jet.

Some differences between Seth and Yuri/Robyn are noteworthy. For Yuri and Robyn, the advection term was the larger term in the Rossby wave source, while in Seth the vortex stretching term was larger. The Yuri and Robyn Rossby wave sources were stronger and better defined than for Seth.

4. Conclusion for hypothesis 3

The association of a negative Rossby wave source with the initial positive height response is consistent with the wave response to Seth being initiated by the advection and stretching processes. Thus, hypothesis 3 is supported by our results.

IV. CONCLUSIONS

A. SUMMARY

The purpose of our study was to examine the remote extratropical response to a single western Pacific typhoon. We followed the methods used in Woll (1993) and Springer (1994), using the NOGAPS global data assimilation, with tropical cyclone bogusing, and the NOGAPS numerical weather prediction model to simulate the atmosphere with and without typhoon Seth. To ensure the validity and applicability of our results for Seth, we applied the four prerequisites (see the beginning of Chapter III) and three hypotheses (see the end of Chapter I) used in Woll (1993) for typhoon Yuri and in Springer (1994) for typhoon Robyn.

The prerequisite tests gave the following results.

Prerequisite 1: The tropical cyclone bogusing procedures had a large impact on the model's initial conditions only near the initial location of Seth, with Seth being clearly present in the POSITIVE runs and effectively eliminated from the NEGATIVE runs.

Prerequisite 2: The forecast model maintained a reasonable representation of Seth in all the POSITIVE runs. The POSITIVE Forecast 1 run was the least successful in simulating Seth, while the POSITIVE Forecast 3 run was most successful. In all the NEGATIVE runs, Seth was absent.

Prerequisite 3: The model runs, especially the POSITIVE runs, gave a good representation of the monthly mean 200 mb circulation for October 1994.

Prerequisite 4: For most of the ensemble averaging period, the large-scale, low-frequency features of the 200 mb circulation were similar in all the POSITIVE runs. The same was true for all the NEGATIVE runs. Thus, the ensemble averaging process gave a good representation of the individual runs.

These results indicate that the data assimilation and model fields satisfied the prerequisites. The tests of the hypotheses gave the following results.

Hypothesis 1: The model's 200 mb height responses showed that Seth initiated a strong teleconnection across the NPNA region. These responses were strong, persisted for more than a week, and showed distinct Rossby wave train characteristics, with eastward group velocities exceeding relatively slow eastward phase velocities.

Hypothesis 2: The initiation and development of the teleconnection response was strongly influenced by the interactions of Seth, and the wave response to Seth, with the east Asian - North Pacific jet. The jet acted as a guide for the wave energy. Areas of barotropic instability along the jet may have provided energy to the wave response. Thus, the jet appears to have

guided and amplified the response to Seth.

Hypothesis 3: The wave response was apparently initiated by the induction of Rossby waves as divergent flow from Seth crossed the jet's region of high absolute vorticity gradient.

These results give substantial support for the three hypotheses.

B. COMPARISONS WITH OBSERVED ANOMALIES

The model responses to Seth are very similar to those from observational studies (e.g., Harr and Elsberry 1995, Nitta 1987, and Kousky 1994, which are represented by Figures 1, 6, and 32, respectively, in this study). Comparisons of the model's 200 mb height response to Seth (e.g., Figure 22h, k) and the observed 200 mb streamfunction anomaly field for October 1994 (Figure 32) show a number of similarities in the NPNA region. In particular, both the model response and the observed anomalies are negative over much of China, positive over northeastern Asia, negative over the central North Pacific, positive over the northeastern Pacific, negative over western North America, and positive over eastern North America. This suggests that the teleconnection mechanisms represented by the model response to Seth may have been important in the real atmosphere during October 1994.

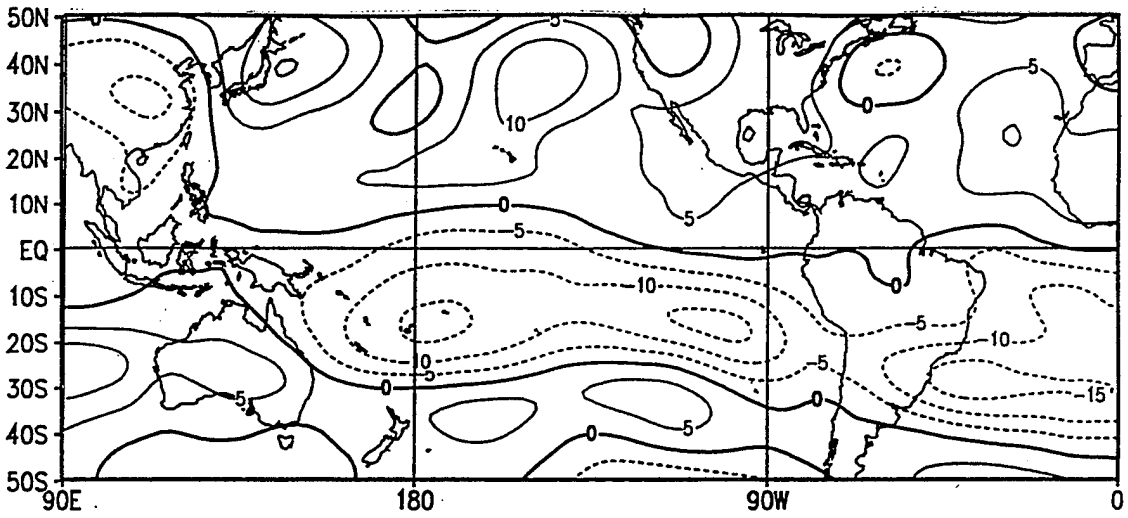

Figure 32. Anomalous 200 mb stream function for October 1994. Contour interval is 5 x 10^6 m^2 s^{-1}. Negative (positive) values are indicated by dashed (solid) lines and the zero line is indicated by the heavy solid line. Positive (negative) anomalies correspond to positive (negative) geopotential height anomalies in the northern hemisphere and to negative (positive) height anomalies in the southern hemisphere. (from Kousky 1994).

C. IMPLICATIONS FOR EXTENDED-RANGE FORECASTING

This study, along with the Woll (1993) and Springer (1994) studies, indicates that strong interactions may occur between tropical cyclones over the western north Pacific and the east Asian - North Pacific jet. These interactions may lead to strong and persistent downstream impacts over the NPNA region. These impacts include significant alterations in the east Asian - North Pacific jet itself and in the jet flow farther to the east, especially in the NPNA region. Since the jets act as the steering flow for midlatitude synoptic weather systems, it appears that tropical cyclones may have a significant impact on midlatitude synoptic weather far from the tropical storm's location. Thus, a better understanding of how tropical cyclones interact with jets, and which tropical cyclone and jet situations are most likely to lead to remote impacts, could help improve extended-range midlatitude weather forecasts.

To illustrate these midlatitude weather implications, Figure 33 shows schematically the ensemble average east Asian - North Pacific jet near the ends of the POSITIVE and NEGATIVE runs. Note the relatively zonal jet that developed over the NPNA region when Seth was present (Figure 33a) and the much more diffluent flow over the eastern North Pacific and North American region when Seth was absent (Figure 33b). These two different jet patterns represent distinctly different synoptic weather patterns, with the

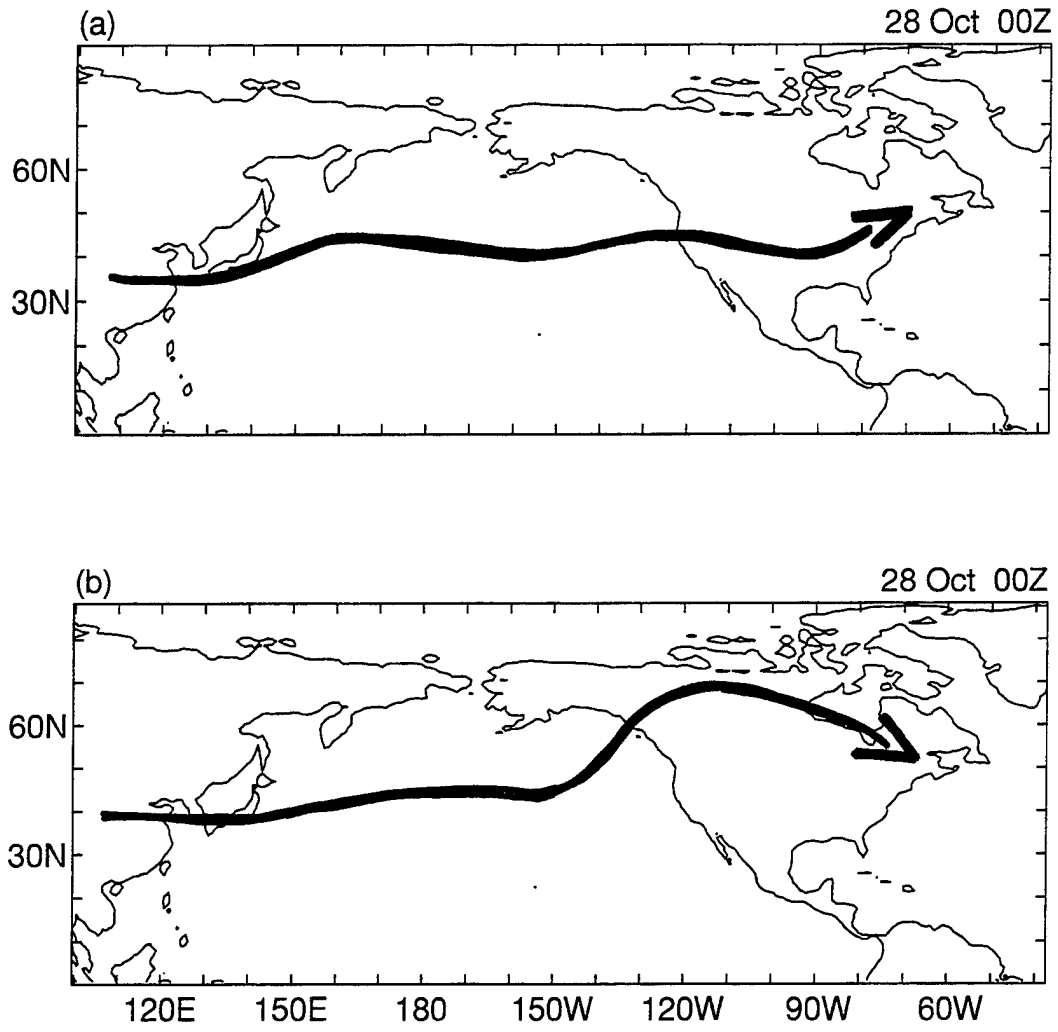

Figure 33. Schematic of the ensemble average 200 mb jet after about 2.5 weeks of the: (a) POSITIVE runs, (b) NEGATIVE runs.

differences being due to the occurrence of Seth in the tropical western Pacific two to three weeks earlier.

D. RECOMMENDATIONS FOR FUTURE WORK

1. Further analysis of Seth results

Prerequisite 2 required that the model accurately forecast the typhoon track and intensity. This study evaluated the models typhoon intensity by converting the JTWC Maximum Sustained Surface Winds to estimated minimum sea level pressure using the Alkinson and Holliday (1997) equivalent minimum SLP method. A more accurate method might involve using the radius of maximum winds, as is done operationally at JTWC.

The differences between the individual POSITIVE runs and between the individual NEGATIVE runs made the use of the ensemble average procedure somewhat problematic. In particular, the ensemble average response may give a picture of the model response that is too weak or that distorts some aspects of the wave initiation, guiding, or amplification. These possibilities led us to conduct a preliminary investigation of the responses found in individual model run differences. For this, we chose the F3 POSITIVE - NEGATIVE run difference, since the F3 POSITIVE gave the best simulation of Seth. To produce a relatively smooth response from which to calculate derivative quantities (e.g., the Rossby wave source, the wave activity flux), we time averaged the F3 height response to produce a

48-hour running time mean response (Figure 34). Thus, for example, the response at 00Z, 22 October 1994 is the average of the responses at: 00Z, 21 October; 12Z, 21 October; 00Z, 22 October; 12Z 22 October; 00Z, 23 October; and 12Z, 23 October. This time averaging makes the response in Figure 34 slightly smoother but has no effect on the basic pattern of strong and persistent positive and negative height responses across the NPNA region.

These responses are very similar to the ensemble average responses (compare Figures 22 and 34) and to the results in previous studies (e.g., Nitta 1987, Kousky 1994, Malsick 1995). However, there are some significant differences. In particular, the F3 responses are much larger and the overall arcing and zonal patterns are more pronounced. For example, during 18 October-2 November (Figure 34e-l), the F3 response shows a much more clear arcing pattern over the NPNA region. This pattern is especially distinct on 20 October (Figure 34f) and indicates a strong wave activity flux arcing out of the tropics and into the extratropics. These time averaged responses suggest that the identification of the teleconnection mechanisms involved in the response to Seth may be aided by a further analysis of the differences between individual pairs of POSITIVE and NEGATIVE runs.

In addition, more analysis of the significance of the model responses

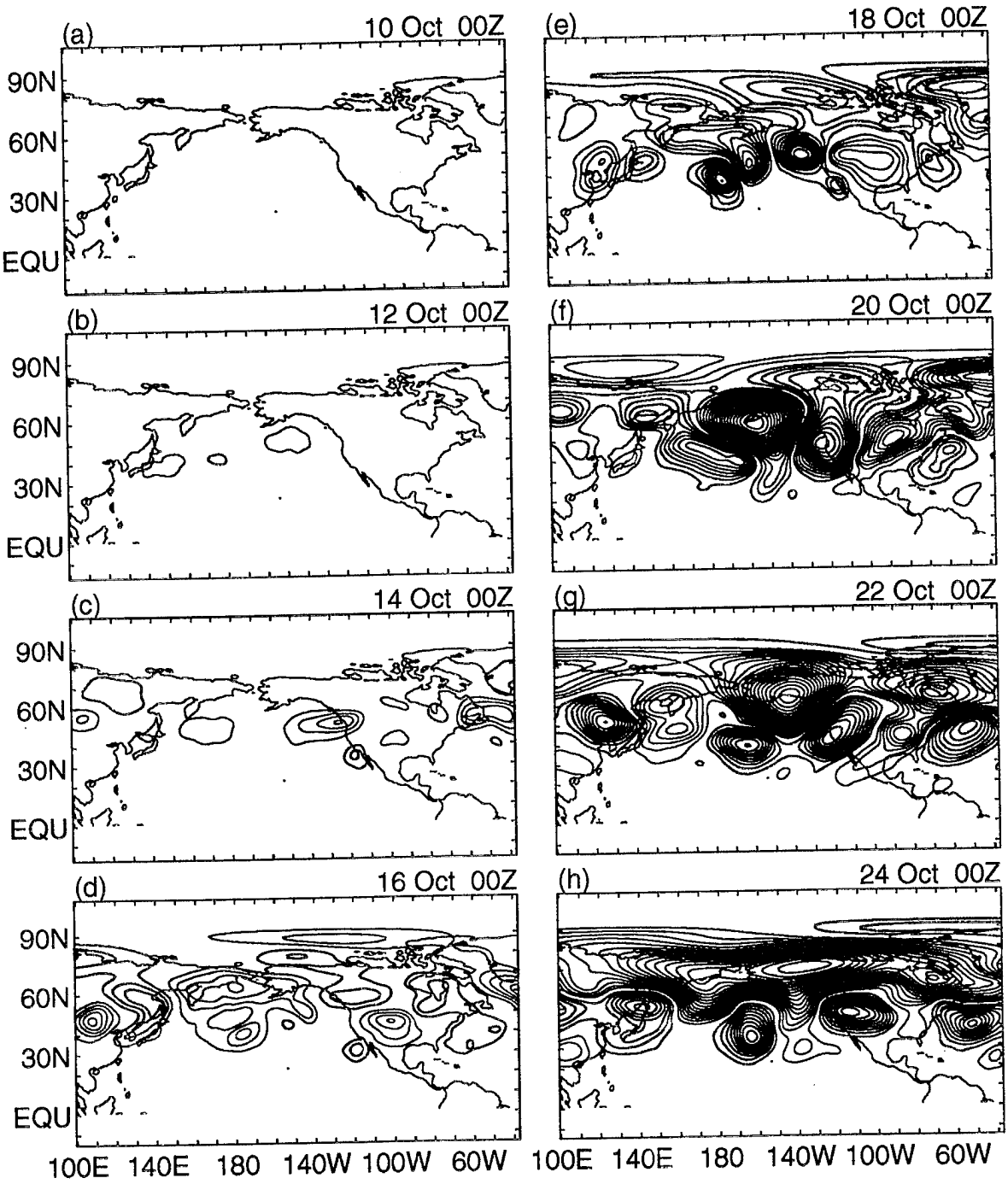

Figure 34. Differences in 200 mb geopotential heights (F3 POSITIVE run - F3 NEGATIVE run). Fields shown are the 48-hour running time mean differences. Contour Interval is 50 gpm. Zero contour omitted.

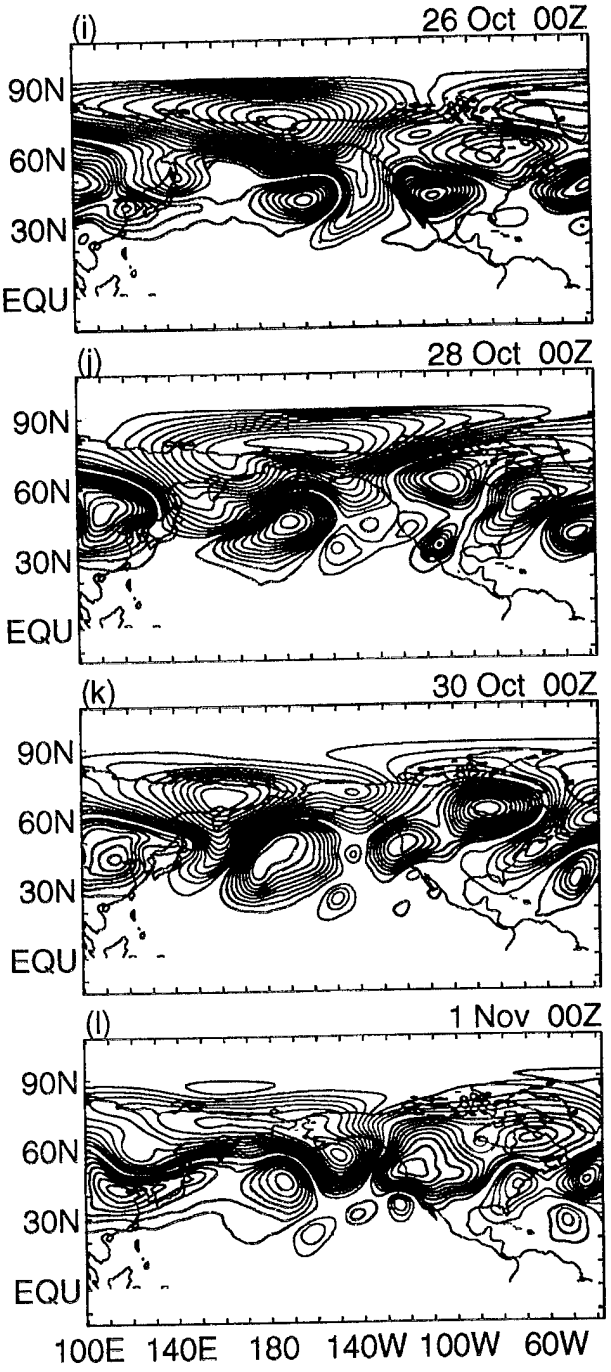

Figure 34. (Continued).

would be helpful. This might include an estimate of the model's characteristic variability in the NPNA region during October, and a comparison of that variability with the magnitude and location of the major response features.

The model fields should also be further verified by comparisons with analyzed fields. This would include applying the diagnostic tools, such as the wave activity flux and the Rossby wave source calculations, to the October 1994 analyzed fields (e.g., to the 200 mb height anomalies). These comparisons would help answer questions such as: Are the POSITIVE runs more accurate than the NEGATIVE runs? How do the inaccuracies of both sets of runs compare with the response patterns? How relevant is the model's response to what actually happened in October 1994 or what might be expected from cases similar to Seth's?

2. **Additional case studies**

Several key features of the teleconnection mechanisms identified in this study occur on relatively small space scales (e.g., the divergent outflow from the typhoon, the initiation of the Rossby wave response, some aspects of the wave amplification and wave guiding). Thus, it would be helpful to use a regional forecast model in tandem with NOGAPS. The Navy Operational Regional Atmospheric Prediction System (NORAPS), or it's successor, the Coupled Ocean Atmospheric Mesoscale Prediction System

(COAMPS), are two such regional models that might be linked to NOGAPS. For example, this linkage might occur by using NOGAPS forecast fields as the initial conditions for NORAPS runs.

This study and those by Woll (1993) and Springer (1994) used similar procedures and models. Additional case studies using different models or blends of models would be useful. Some possible options are listed below.

Different operational data assimilation and forecast models have different characteristics, such as different biases and systematic errors that can become especially significant during extended-range forecasts. Thus, it would be useful to rerun the Yuri, Robyn, and/or Seth POSITIVE and NEGATIVE forecasts using different models and compare the results with those from Woll (1993), Springer (1994), and/or this study. This comparison would help clarify the sensitivity of the results to the model.

Tropical cyclones often occur simultaneously. Thus, it would be helpful to examine the teleconnection response to two or more simultaneous tropical cyclones. It would be especially interesting to determine if the responses to the different storms interfere, constructively or destructively, with each other.

Additional case studies should be careful to avoid situations in which the model has difficulty forecasting the tropical cyclone's intensity and approach toward the jet. These two features of the storm, especially the

approach, seem to be critical in initiating the response to the storm. Thus, a useful simulation of the teleconnection response requires that at least this initial portion of the storm's development be relatively well forecast.

E. INTERNET MOVIES

Computer movies of the teleconnection responses generated by typhoons Yuri (Woll 1993), Robyn (Springer 1994), and Seth (this study) can be viewed on the Internet. These movies can be accessed via the Naval Postgraduate School home page at http://www.met.nps.navy.mil/. Under the research topics heading, select "Teleconnections" and then follow the instructions.

Readers of this study are encouraged to ask questions or offer their comments by sending e-mail to Professor Tom Murphree at: murphree@osprey.met.nps.navy.mil.

This page intentionally blank.

LIST OF REFERENCES

Atkinson, G.D. and C.R. Holliday, 1977: Tropical cyclone minimum sea-level pressure and maximum sustained wind relationship for the western North Pacific. *Mon. Wea. Rev.,* **105,** 421-427.

Bjerknes, J., 1972: Large-scale atmospheric response to the 1964-1965 Pacific equatorial warming. *J. Phys. Oceanogr.,* **2,** 212-217.

Branstator, G., 1983: Horizontal energy propagation in a barotropic atmosphere with meridional and zonal structure. *J. Atmos. Sci.* **40**, 1689-1708.

Carlson, T., 1991: *Mid-Latitude Weather Systems*. Cambridge Univ. Press. 507 pp.

Chang, C., and K. Lum, 1985: Tropical-midlatitude interactions over Asia and the western Pacific Ocean during the 1983/84 northern winter. *Mon. Wea. Rev.*, **113**, 1345-1358.

Glantz, M. H., R. W. Katz, and N. Nicholls, editors, 1991: *Teleconnections Linking Worldwide Climate Anomalies: Scientific Basis and Societal Impacts.* Cambridge University, 535 pp.

Goerss, J., and R. Jeffries, 1994: Assimilation of tropical cyclone observations into the Navy Operational Global Atmospheric Prediction System. Submitted to *Mon. Wea. Rev.*

Harr, P., and R. Elsberry, 1991: Tropical cyclone track characteristics as a function of large-scale circulation anomalies. *Mon. Wea. Rev.,* **119,** 1448-1468.

Harr, P., and R. Elsberry, 1995: Large-scale circulation variability over the tropical western Pacific. Part I and II. *Mon. Wea. Rev.,* **123,** 1225-1245.

Hogan, T., and T. Rosmond, 1991: The description of the Navy Operational Global Atmospheric Prediction System's spectral forecast model. *Mon. Wea. Rev.,* **119,** 1786-1815.

Hurrell, J., and D. Vincent, 1990: Relationship between tropical heating and subtropical westerly maxima in the southern Hemisphere during SOP-1, FGGE. *J. Climate*, **3**, 751-768.

Kousky, V.E, editor, 1994: *Climate Diagnostics Bulletin, October 1994.* Climate Analysis Center, National Meteorlogical Center, Washington, D.C., No. 94/10, 77 pp.

Kuo, H.-L., 1949: Dynamic instability of two-dimensional nondivergent flow in a barotropic atmosphere. *J. Meteor.*, **6**, 105-122.

Kurihara, K. and T. Tsuyuki, 1987: Development of the barotropic high around Japan and its association with Rossby wave-like propagations over the North Pacific: Analysis of August 1984. *J. Meteor. Soc. Japan,* **65**, 237-246.

Malsick, M., 1995: *The dynamics of teleconnections induced by short term tropical forcing.* Master's Thesis, Naval Postgraduate School, Monterey, California, September 1995.

Nitta, T., 1987: Convective activities in the tropical western pacific and their impact on the northern hemisphere summer circulation. *J. Meteor. Soc. Japan,* **65**, 373-390.

Plumb, R., 1985: On the three-dimensional propagation of stationary waves. *J. Atmos. Sci.,* **42**, 217-229.

Sardeshmukh, P., and B. Hoskins, 1988: The generation of global rotational flow by idealized tropical divergence. *J. Atmos. Sci.,* **45**, 1228-1251.

Simmons, A. J., J. M. Wallace, and G. Branstator, 1983: Raortropic propagation and instability, and atmospheric teleconnection patterns. *J. Atmos. Sci.*, **40**, 1363-1392.

Springer, C., 1994: *Short Term Teleconnections Associated with Western Pacific Tropical Cyclones.* Master's Thesis, Naval Postgraduate School, Monterey, California, June 1994.

Tribbia, J. J., 1991: The rudimentary theory of atmsopheric teleconnections associated with ENSO. *Teleconnections Linking Worldwide Climate Anomalies: Scientific Basis and Societal Impact.* Glantz, M. H., R. W. Katz and N. Nicholls, editors. Cambridge Univ Press. 535 pp.

Wallace, J. M., and D. S. Gutzler, 1981: Teleconnections in the geopotential height field during the northern hemisphere winter. *Mon. Wea. Rev.*, **109**, 784-812.

Woll, S., 1993: *Short Term Teleconnections Associated with an Individual Tropical Cyclone.* Master's Thesis, Naval Postgraduate School, Monterey, California, December 1993.

This page intentionally blank.

INITIAL DISTRIBUTION LIST

		No. of Copies
1.	Defense Technical Information Center Cameron Station Alexandria VA 22304-6145	2
2.	Librarian Code 52 Naval Postgraduate School 411 Dyer Rd Rm 104 Monterey CA 93943-5101	2
3.	Oceanography Department Code OC/CO Naval Postgraduate School 833 Dyer Rd Rm 331 Monterey CA 93943-5122	1
4.	Meteorology Department Code MR/HY Naval Postgraduate School 589 Dyer Rd Rm 252 Monterey CA 93943-5114	1
5.	Dr. Tom Murphree Code MR/ME Naval Postgraduate School 589 Dyer Rd Rm 252 Monterey CA 93943-5114	5
6.	LCDR. Craig E. Jakus, USN HSL - 45 P.O. BOX 357128 San Diego, Ca. 92135-7128	1
7.	Director Naval Oceanography Division Naval Observatory 34th and Massachusetts Avenue NW Washington DC 20390	1

8. Commander
Naval Oceanography Command
Stennis Space Center
MS 39529-5000
1

9. Commanding Officer
Naval Oceanographic Office
Stennis Space Center
MS 39529-5001
1

10. Commanding Officer
Fleet Numerical Oceanography Center
7 Grace Hopper Ave Stop 4
Monterey CA 93943-0001-0120
1

11. Commanding Officer
Naval Oceanographic and Atmospheric
Research Laboratory
Stennis Space Center
MS 39529-5004
1

12. Superintendent
Naval Research Laboratory
7 Grace Hopper Way Stop 2
Monterey CA 93943-5502
1

13. Chairman
Oceanography Department
U.S. Naval Academy
Annapolis MD 21402
1

14. Chief of Naval Research
800 N. Quincy Street
Arlington VA 22217
1

15. Office of Naval Research (Code 420)
Naval Ocean Research and Development
Activity
800 N. Quincy Street
Arlington VA 22217
1

16. Scientific Liaison Office — 1
Office of Naval Research
Scripps Institution of Oceanography
La Jolla CA 92037

17. Library — 1
Scripps Institution of Oceanography
P.O. Box 2367
La Jolla CA 92037

18. Commander — 1
Oceanographic Systems Pacific
Box 1390
Pearl Harbor HI 96860

19. Director, Pacific Marine Center — 1
(N/MOP)
National Ocean Service, NOAA
1801 Fairview Avenue East
Seattle WA 98102

20. Director, Atlantic Marine Center — 1
(N/MOA)
National Ocean Service, NOAA
439 W. York Street
Norfolk VA 23510

21. Commander (Air-370) — 1
Naval Air Systems Command
Washington DC 20360

22. Chief, Ocean Services Division — 1
National Oceanic and Atmospheric
Administration
8060 Thirteenth Street
Silver Springs MD 20910

23. Commander, International Ice Patrol — 1
Avery Point
Groton CT 06340

24. Commanding Officer — 1
U.S. Coast Guard Research and
Development Center
Avery Point
Groton CT 06340-6096

25. NOAA Library — 1
7600 Sand Point Way NE
Building 3
Seattle WA 98115

26. Dr. Ronald Gelaro — 1
Naval Research Laboratory
7 Grace Hopper Ave Stop 2
Monterey CA 93943-5502

27. Director Naval Meteorology and Oceanography Division — 1
Naval Observatory
34th and Massachusetts Avenue NW
Washington, DC 20390

28. Commander — 1
Naval Meteorology and Oceanography Command
Stennis Space Center
MS 39529-5000

29. Dr. James Goerss — 1
Naval Research Laboratory
7 Grace Hopper Way Stop 2
Monterey, CA 93943-5502

30. Dr. Carolyn Reynolds — 1
Naval Research Laboratory
7 Grace Hopper Way Stop 2
Monterey, CA 93943-5502

31. Mr. Robin Brody — 1
Naval Research Laboratory
7 Grace Hopper Way Stop 2
Monterey, CA 93943-5502

32. Mr. Steve Payne — 1
Naval Research Laboratory
7 Grace Hopper Way Stop 2
Monterey, CA 93943-5502

33. Dr. Simon Chang — 1
Naval Research Laboratory
7 Grace Hopper Way Stop 2
Monterey, CA 93943-5502

34. Dr. Patrick Harr — 1
Code MR/HR
Naval Postgraduate School
589 Dyer Road Room 244
Monterey, CA 93943-5114

35. Dr. Huug M. van den Dool — 1
Chief, Prediction Branch
Climate Prediction Center
National Meteorological Center
W/NMC51
5200 Auth Road
Washington, DC 20233